INSTITUTO SUPERIOR TÉCNICO
Universidade Técnica de Lisboa

Intra-cardiac Impedance Reography correlated with Pulse Oximetry and EASI-ECG Lead System

Wireless Sensor Network for Biomedical Applications

Bruno Miguel Gil Rosa

Dissertação para obtenção do Grau de Mestre em

Mestrado Integrado em Eng.ª Biomédica

Júri

Presidente: Prof. Dr. Fernando Lopes da Silva

Orientador: Prof. Dr. Raul Daniel Lavado Carneiro Martins

Vogais: Prof. Dr. Luis Silva Carvalho

Prof.ª Dr.ª Maria Isabel Rocha

Prof. Dr. Fernando Tim Tim Janeiro

Novembro 2008

Acknowledgements

First of all, I would like to express my deepest thanks to all my family for all the emotional and financial support that they have given to me throughout these five years of graduation. They have made my transition to a graduated student in a more comfortable way that it might have otherwise been.

I would like to thank my thesis advisors, Prof. Raul Carneiro Martins, Prof. Dr. Luis Silva Carvalho and Prof.ª Dr.ª Maria Isabel Rocha, for giving me the opportunity to develop my Masters Project in an area that have always played a fascinating role in my life since I was a little boy and started to make my first electronic experiences with the help of my father. With the support of my advisors I have reached a superior technical knowledge which had guided me to do something that I expect to contribute for the good of the medical community.

I would also like to give special recognition to Eng.ers Armando Fernandes, Nuno Brás and João Branco, work colleagues at Instituto de Telecomunicações – Pólo de Lisboa. I have appreciated all the technical guidance and suggestions they have provided to help improving my work.

Finally and with similar importance, I would like to thank all the friends I made during my biomedical engineering course at Instituto Superior Técnico. They are so many that I can't name them but, in recompense, this thesis is dedicated to them all, from A to Z. I hope not to have disappointed them.

Abstract

The goal of the present work is to develop an integrated wireless network consisting of biomedical sensors for acquisition of physiological variables such as: electric potentials generated by the heart and recorded at the thorax surface, pulse oximetry at the level of the finger and measurement of biological tissues' impedance by reography.

In order to achieve this objective, the author needed to study, amongst others, the physiological bases behind the selective absorption of light by the hemoglobin molecule at different wavelengths; the established impedance models for biological tissues and their frequency dependence of the current waveform that crosses them; and also to study the electrocardiogram signals. Following this stage, all the electronic devices involved in capturing and conditioning the different kinds of signals were built, performing the digitalization and transmission in communication packets between the sensor node and the remote recording one. The project also includes a graphical interface for visualization of the acquired signals as well as some physiological parameters resulting from the application of digital processing algorithms like the computation of blood oxygen saturation level and cardiac frequency.

The present work was developed at Instituto de Telecomunicações as part of IST in a partnership with Instituto de Fisiologia from FMUL and it can have practical applications in healthcare monitoring units, eliminating the need for using physical connections between the patient and the recording equipment.

Keywords: Electrocardiogram, Pulse Oximetry, Biological Conductivity, Reography, Embedded Systems, Wireless Transmission, Digital Signal Conditioning.

Resumo

O objectivo do presente trabalho é desenvolver uma rede integrada de sensores biomédicos com comunicação sem fios para aquisição de variáveis fisiológicas tais como: potenciais eléctricos gerados pelo coração e medidos à superfície do tórax, oximetria pulsada ao nível do dedo e a medição da impedância dos tecidos biológicos por reografia.

Para atingir este objectivo, o autor necessitou de estudar, entre outros, as bases fisiológicas por detrás da absorção selectiva de luz pela molécula de hemoglobina a diferentes comprimentos de onda; os modelos estabelecidos de impedância para os tecidos biológicos e dependentes da frequência da onda de corrente que os atravessa; e ainda estudar os sinais do electrocardiograma. Seguidamente, todos os dispositivos electrónicos envolvidos na captura e acondicionamento dos diferentes tipos de sinais foram construídos, procedendo ainda à sua digitalização e transmissão em pacotes de comunicação entre o nodo sensor e o nodo central de registo remoto. O projecto inclui ainda um interface gráfico para visualização dos sinais adquiridos bem como alguns parâmetros fisiológicos resultantes da aplicação de algoritmos de processamento digital do sinal, tais como, o nível de saturação em oxigénio do sangue e a frequência cardíaca.

Este trabalho foi desenvolvido no Instituto de Telecomunicações do IST em parceria com o Instituto de Fisiologia da FMUL e poderá ter aplicações práticas em unidades hospitalares de monitorização eliminando a necessidade de ligações físicas entre o paciente e o equipamento de registo.

Palavras-chave: Electrocardiograma, Oximetria Pulsada, Condutividade Biológica, Reografia, Sistemas Embebidos, Transmissão sem Fios, Condicionamento Digital de Sinais.

Index

List of Figures

List of Tables

List of Acronyms

AC	Alternating Current
ACK	Acknowledged Message
ADC	Analog to Digital Converter
AFG	Application Framework
ALU	Arithmetic Logic Unit
APL	Application Layer
APS	Support Sub-Layer
ASCII	American Standard Code for Information Interchange
BPS	Bits *Per* Second
BPSK	Binary Phase Shift Keying
CISC	Complex Instruction Set Computer
CMOS	Complementary Metal Oxide Semiconductor
CMRR	Common-Mode Rejection Ratio
COM	Communication Port
CPU	Central Processing Unit
DC	Direct Current
EEPROM	Electrically-Erasable Programmable Read-Only Memory
EPROM	Erasable Programmable Read-Only Memory
FCY	Instruction Cycle Frequency
FET	Field-Effect Transistor
FIFO	First-In First-Out
FIR	Finite Impulse Response
FOSC	Oscillation Frequency
FWHM	Full Width at Half Maximum
I/O	Input/Output
I2C	Inter-Integrated Circuit
IC	Integrated Circuit
ID	Identification Number
IEEE	Institute of Electrical and Electronics Engineers
IF	Interruption Flag
IIR	Infinite Impulse Response
IR	Infrared
ISM	Industrial Scientific and Medical
LASER	Light Amplification by Stimulated Emission of Radiation
LED	Light Emitting Diode
LSB	Least Significant Bit
MAC	Median Access Layer
MCU	Microcontroller Unit
MIPS	Million Instructions *Per* Second
MSB	Most Significant Bit
NACK	Not-Acknowledged Message
NWK	Network Layer
OP AMP	Operational Amplifier
O-QPSK	Offset Quadrature Phase Shift Keying
PAN	Personal Area Network
PC	Personal Computer
PCB	Printed Circuit Board
PDA	Personal Digital Assistant
PHY	Physical Layer
PIC	Peripheral Interface Controller
RAM	Random Access Memory
RC	Resistor-Capacitor Circuit
RF	Radio Frequency
RISC	Reduced Instruction Set Computer
RMS	Root Mean Square
ROM	Read-Only Memory

SPI	Serial Peripheral Interface
TTL	Transistor-Transistor Logic
UART	Universal Asynchronous Receiver Transmitter
USB	Universal Serial Bus
ZC	ZigBee Coordinator Device
ZDO	ZigBee Device Object
ZED	ZigBee End Device
ZR	ZigBee Router Device

In memory of

Prof. Dr. Luis Silva Carvalho

Chapter 1

Introduction

"Only one who devotes himself to a cause with his whole strength and soul can be a true master. For this reason mastery demands all of a person."

Albert Einstein

The first chapter of this report deals with all the context and motivation issues behind the choice of a thesis of this kind and, in the end, it briefly describes the fundamental technical steps followed by the author in his quest to achieve the projected objectives from the very beginning till obtaining the first valid results.

1.1. Context and Motivation.

The main goal of the present work is to build an integrated wireless network consisting of biomedical sensors that are able to capture and transmit relevant data from the human body which by itself constitutes a step forward in what concerns the classical process of recording the human physiological variables. It is a very challenging and motivating task to build a system like this which also has the ability to expand itself and incorporate new sensor nodes at anytime, thus, increasing the quantity of physiological variables recorded inside the network. The available data can then be intersected and physiological aspects revealed this way can be correlated.

The building of an integrated recording system where all the communications between the sensors and the recording node exclude any possibility of using physical wire connections certainly will constitute an even better aspect in preventing the occurrence of electrical shock events to the patient derived from a fault of the equipment which is typically fed by high voltage power lines.

Placing the sensors quick and easily without the need to care about if all wire connections are twisted or broken can make all the difference in healthcare units. The capacitive coupling effects and the electronic noise are also minimized because the analog signal of interest is locally converted to its binary form which allows only two distinctive voltage levels – on and off. So, only strong electromagnetic fields can affect the carrying waves and damage decisively the coded voltages.

Typical measurement systems include several electronic stages as represented in *fig. 1.1*. The physiological process of interest is converted into an electric signal by the input

transducer [1]. Some analog signal processing is usually performed, often including amplification and filtering. Analog-to-digital conversion, signal storage and digital processing constitute to some extent the digital block for every biomedical sensor.

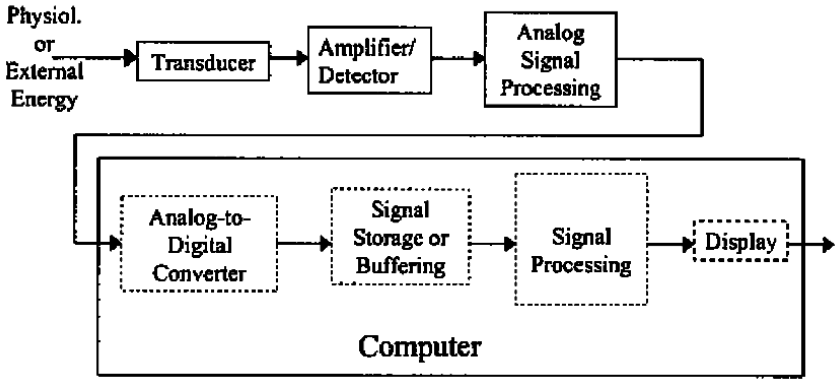

Figure 1.1 – Schematic representation of a typical biomedical measurement system [1].

The transducer is often the most critical element in the system since it constitutes the interface between the patient and the rest of the electronic device. The type of biotransducer used dictates most of the first analog stages of the block diagram. The energy that is converted by the input transducer may be generated by the physiological process itself as the case of ECG biopotentials, indirectly related to the physiological process as pulse oximetry or produced by an external source as the case of impedance reography. So, the first stages in developing biomedical sensors are quite different and attention must be paid to the physiological variables involved in each measurement device.

1.1.1. Electrocardiogram (ECG).

The history of electrocardiography starts at the middle of the 19th century when Ludwig Hoffa first described unregulated actions of the ventricles: he showed that a single electrical pulse can induce ventricular fibrillation.

Some years latter, in 1878, British physiologists John Burden Sanderson and Fredrick Page recorded the heart's electrical current with a capillary electrometer that revealed the existence of two phases in the recordings, later called QRS and T.

At the end of the century, Willem Einthoven started to improve the classical capillary electrometer building the first electrocardiograph machine by means of a spring galvanometer. He also introduced the term *electrocardiogram* (abbreviated to EKG or ECG) at a meeting of the Dutch Medical Association [2].

Meanwhile important clinical findings have shown the potential of the electrocardiograph recordings: Jean-Louis Prevort and Frederic Batelli discovered that large electrical voltages applied across an animal's heart can stop ventricular fibrillation; by its turn, Arthur Cushny

published the first case report of atrial fibrillation. Nicolai and Simmons reported on the changes to the electrocardiogram during *angina pectoris*, commonly referred to chest pain.

In 1912, Einthoven described an equilateral triangle formed by his standard leads I, II and III latter called “Einthoven’s Triangle” which has guided him to win the Nobel Prize for inventing the ECG twelve years later.

In 1928 Ernestine and Levine reported the use of vacuum tubes to amplify the electrocardiogram instead of the mechanical amplification performed by string galvanometers. In the same year, Frank Sanborn’s company converted the table ECG machine model into the first portable version, powered by a low voltage battery. Soon after, the production of portable electrocardiographs has started: one of the first electrocardiograph devices available in Europe was developed by Siemens and Halske in Germany in 1934.

A further significant step was made after the invention of the cathode ray tube which allowed the manufacturing of cathode ray oscilloscopes. It improved considerably the physical characteristics of ECG recording and new domains for electrocardiographic research such as vectorcardiography were opened. Another fundamental breakthrough for wide application of ECG in clinics was the development of pen-writing (direct-writing) instruments.

Finally, the introduction of computers into electrocardiography write-out systems soon replaced all the conventional ECG recording systems. At this point, recording time dependent signals without distortion is not anymore a major problem.

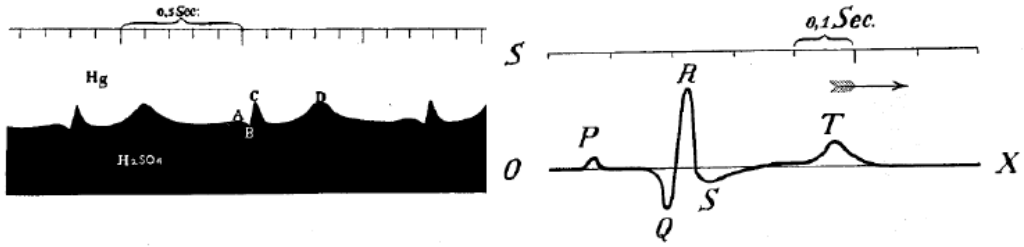

Figure 1.2 – Electrocardiograph recording derived from capillary electrometer with the notations introduced by Einthoven [2].

1.1.2. Pulse Oximetry.

The first attempts to build pulse oximeters occurred in the 1930s and 40s by Carl Mathes (Germany) and Glen Millikan (England). In 1935, Mathes built the first device to continuously measure blood oxygen saturation *in vivo* by transilluminating tissue [3]. In the early 1940s, Millikan used the term “oximeter” to describe a lightweight earpiece to detect the oxygen saturation of hemoglobin for use in aviation research to investigate high altitude hypoxic problems.

In the late 1940s, Dr. Earl Wood introduced oximeters in the clinical setting but all of these instruments were difficult to set up and calibrate at that time.

In 1964, a surgeon Robert Shaw built a self-calibrating ear oximeter which was marketed by *Hewlett Packard*® in 1970 for use in physiology and cardiac catheterization laboratories [4]. The first commercial self-calibrating oximeter was an earlobe mounted sensor with a fiber optic light source and a heat element to improve local perfusion.

Figure 1.3 – Commercial pulse oximeter incorporating the emission and detection spring and the recording equipment [3].

The year 1972 recorded the greatest step forward in monitoring oxygenation levels. Until then, in order to isolate the pulsatile or arterial element of the blood, oximeters relied on compression and heating the earlobe to remove signals arising from venous interference. Aoyagi was the first to recognize that signals measured at two different wavelengths of light could be accurately related to oxygen levels in arterial blood [3].

Contemporary pulse oximeters use Aoyagi's theory with two light-emitting diodes (LED) which can generate large amounts of narrowband light which improve the signal quality and one or more photodetectors to sense them.

1.1.3. Bioimpedance Reography.

Reography is also known as Electrical Impedance Plethysmography. The designation is more used in Anglo-Saxon countries like USA and it is based upon the fact that blood volume changes within the territory crossed by the electrical current constitute the main factor in obtaining the recordings. According to some experts in the topic, this is not the only factor to account for the recordings and, in some situations, it can only be a secondary factor. Thus the term Plethysmography seems to be abusive although it is widely used.

The first publications concerning impedance plethysmography date back to the 1930s and 1940s. In 1932 Atzler and Lehmann observed changes in the capacitance between two parallel plates kept across the human chest. These changes were observed to be synchronous with the activity of the heart. The technique as it exists today was first introduced by Jan Nyboer and co-workers in 1940 [5].

The method reached clinical value about 20 years ago based on the research work by Kinnen, Kubicek *et al* [6]. A related method, integral reography, for measuring the cardiac output

was developed by Tišĉ Enko and co-workers in 1973. The method has, however, hardly been used outside the Soviet Union.

All these methods are based upon the placement of electrodes at the surface of the body while performing bioimpedance measurements inside body tissues as blood vessels and the heart constitutes a more subtle technique.

In 1980, a Portuguese researcher, Luís O. D. Amado, working at Instituto de Fisiologia as part of Faculdade de Medicina da Universidade de Lisboa, published his doctoral dissertation under the topic of “Reografia Intracardíaca” (Intra-cardiac reography) where he described that the volume of the four cardiac chambers could be rigorously measured with the reography method and using intracavitary catheters [7]. He also identified the major problems associated with this technique, in particular the weak capacity of the method in determining the absolute volume due to external factors like the geometry of the cardiac walls.

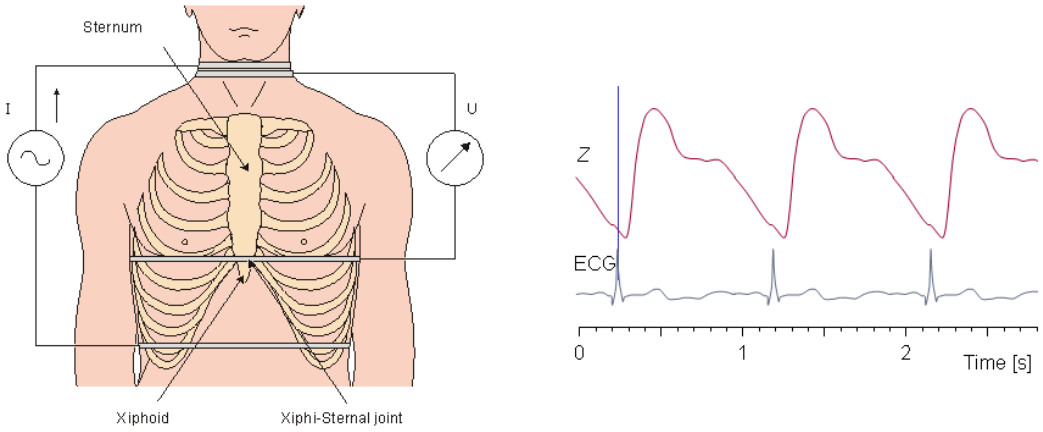

Figure 1.4 – Placement of the surface electrodes in the thorax and impedance curve recorded and correlated with ECG. Translated from [8] with modifications.

1.2. Fundamental Stages.

The present work was developed from February 2008 to September of the same year, throughout an intense journey of seven months.

In the very beginning, the author started to familiarize himself with the basic physiologic concepts that support pulse oximetry. It was at that time that the two wavelengths of the excitation pulses were established and the race for selecting the best electronic devices involved in the both photoemission and detection has started. After that, an elementary excitation circuit was designed, whose digital interface with MATLAB® was ensured by a commercial data acquisition device. In the software application, the first signal processing algorithms involved in pulse oximetry were successfully tested.

As soon as the analog circuit for the oximeter was fully operational, the main attention has turned on how to build its digital part. For this effect, two fundamental devices were selected: an analog-to-digital converter and a microcontroller. The resolution of the ADC was established to be 16 bits while the first microcontroller available to be programmed was an 8-bit PICmicro® MCU with USB module incorporated. The C program for the microcontroller was built and tested inside the MPLAB® IDE.

Meanwhile, it came into sight the possibility to develop an additional electronic device together with Instituto de Fisiologia from Faculdade de Medicina da Universidade de Lisboa, under the topic of "Intra-cardiac Impedance Reography". The technical requirements of such an ambitious project in what concerns the development of a device fully capable of performing arithmetic operations, has lead to the migration from an 8-bit microcontroller to an equivalent with a 16-bit architecture and superior performance and available memory. This change implied a restructuring of the microcontroller's C code with all the implemented subroutines to pass from an 8-bit (char) to a 16-bit (integer) data type.

The reography device has also lead to the use of the digital-to-analog conversion process and high speed communication interfaces between the electronic components. The building process was divided in two fundamental stages: the construction of a 20 kHz sine-wave generator circuit and an acquisition one with high sample rate and processing capability inside the memory of the microcontroller.

This advance in terms of technological knowledge has lead to the substitution of the digital part of the oximetry circuit by a 16-bit microcontroller. At this point, the clustering algorithm was implemented inside its memory and the results were transferred from the microcontroller to a personal computer through USB connection.

Soon after obtaining the first oximetry curves, the author started to look for technical solutions that would implement the ZigBee protocol, that is, electronic devices such as radio frequency transceivers that communicate in the frequency bands defined by the ZigBee wireless protocol. After spent some time training with the software available to program the selected RF transceivers, the first "physical" wireless network capable of routing messages between the nodes was established. To optimize the system and to have a better idea how it would work in collecting and broadcasting biomedical data, the third electronic device for this project was designed – an ECG recording device based on the EASI lead positions. The device needs only to acquire data samples at defined periods of time and send them from the sensor node to the recording one. So, this simplest prototype was the best one to test the transmission packets. The first fully operational device mounted in the breadboard was therefore the ECG prototype, followed by the pulse oximetry one and finally the reography device. The results of both devices were recorded and are presented in this report. For reography, one last operation was required: the calibration stage.

Finally, all the devices built in breadboard were passed to their PCB versions, using the EAGLE® application software.

Chapter 2

Microcontroller Unit

A microcontroller is an electronic device constituted by a set of digital logic circuits integrated on a single silicon chip whose functionality is specified by the program stored inside its memory. Microcontrollers differ from microprocessors in many ways: in order for a microprocessor to be used, it is necessary to add several external components such as memory and components for data sending and receiving. By its side, a microcontroller is designed to have it all; no external components are needed for its application because all necessary peripherals are already built into it. So, it is not wrong to say that a microprocessor is only a Central Processing Unit, while a microcontroller is a CPU plus some memory and peripheral modules attached to the processing unit, as shown in *fig. 2.1.*

An alternative view is that a microcontroller is a *state machine* whose logic states are defined by the program allocated on its memory. The big advantage is that all the device's structure and operation can be changed in the program with very little, if any, circuit hardware modifications.

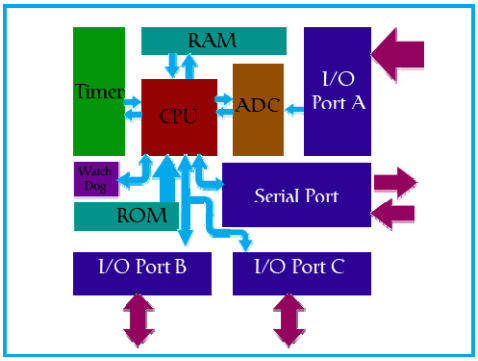

Figure 2.1 – Functional block diagram of a microcontroller [9].

Some of the most important modules built inside a microcontroller are:

- Memory Unit;
- CPU Module;
- Bus;
- Timer Unit;
- Watchdog Module;
- Serial Communication Block;
- Input-Output (I/O) Module.

The Bus represents a group of 8, 16 or more wires depending on the microcontroller's architecture: 8-bit, 16-bit, 32-bit and so on. There exist two types of buses: address and data buses or paths. The first one serves to transmit addresses from the CPU and the second one to connect all the internal blocks inside the microcontroller.

The Timer Unit is responsible for generating signals in regular time intervals which control the program execution and CPU computations. The basic unit of the timer is a free-run counter which is in fact a register whose numeric value increments by one in each time interval.

The Watchdog Module controls the flawless functioning of the microcontroller: whenever it stops working correctly, the watchdog resets it in order to get the program out of being stuck.

The Serial Communication Block is used to communicate with other devices which are external to the microcontroller. This interface can follow several communication protocols such as UART, SPI or I2C.

The I/O Module act like a memory location register: simply written into or read from it, the act is reflected on the voltage levels of the microcontroller's pins or ports. There are three types of ports: input, output or bidirectional ports. When working with ports, it is only necessary to choose which particular port we need to work with and then send data or take it from the port.

2.1. Microcontroller's Architecture.

The microcontrollers with RISC architecture have two different kinds of memory: one is used for program storage while the other is used for data storage. RISC stands for Reduced Instruction Set Computer and has its roots in the Harvard architecture in opposition to the Von Neumann's. Microcontrollers with Von Neumann's architecture are also called "CISC microcontrollers" or Complex Instruction Set Computer. The difference between these two architectures is in the type of memory used. The Von Neumann's architecture uses only one memory for program and data storage. This provides a great flexibility in what concerns with memory allocation because all the instructions and data are within the same physical interface. A schematic representation of the block diagram of the two architectures is shown in *fig. 2.2*.

The Harvard architecture defines two separate memories:

- ROM memory which stands for Read Only Memory is used to store all the program instructions. It is a non-volatile type of memory that does not lose its contents in the case of a fault from power supply. It can be further divided into EPROM which can be erased using ultraviolet light in a 15 minutes time interval and EEPROM, which constitutes a particularly attractive memory technology option as it can be quickly and easily reprogrammed. Newer advanced Flash memories used in microcontrollers nowadays are derived from older versions of the EEPROM.
- RAM memory which stands for Random Access Memory is used to store data. It is a memory for direct read/write access and belongs to the volatile type of memories.

The advantage of using RISC microcontrollers instead of CISC ones is that they have a faster performance due to the fact that the search for a new instruction occurs at the same time as data transfer.

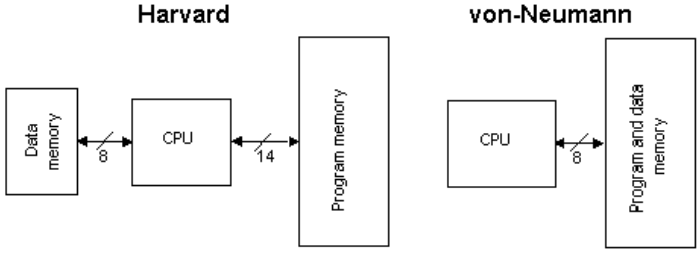

Figure 2.2 – Schematic representation of the two different microcontroller's architecture [10].

The Central Processing Unit has a role of connective element between other blocks in the microcontroller. It coordinates the work of other blocks and executes the user program. Internally, a CPU consists of a series of modules like:

- An Arithmetic Logic Unit, ALU.
- One or more working registers for temporary storage during computations. A register is a small block of memory where data is stored and whose size in bits reflects the internal architecture of the microcontroller.
- Program memory (ROM) and data memory (RAM);
- Program Counter.
- An instruction register with instruction decoder.
- The Control Unit.
- A stack.

The ALU is responsible for performing all arithmetic operations like addition, subtraction and Boolean Logic operations, including bit shifting. Multiplication and division are usually performed by repeated use of addition or subtraction, but some devices have already hardware multiplexers for these operations. The working registers are used by the ALU as temporary memory locations for holding intermediate results of arithmetic computations.

The program memory is an area inside the memory of the microcontroller where actual sequence of instructions which make up the program is stored. Data memory is where data such as the value of constants are kept for use by the program during its execution.

The program counter is a register used to store the address of the next instruction to be executed. Since the program consists of instructions stored sequentially in program memory, the address of the next instruction is obtained by simply increment the number, that is, the address contained in the program counter, *vid. fig. 2.3*.

The instruction register contains the actual binary instruction that needs to be executed. The instruction decoder takes the binary instruction and decodes it to determine what operation must be performed and which data it must use.

The control unit controls the timing and sequencing of all operations necessary to correctly schedule and execute instructions. While an instruction is executing, the next one is fetched from the program memory and placed in the instruction register with help from the program counter. The instruction decoder then decodes the instruction and it is executed when the next execution cycle occurs.

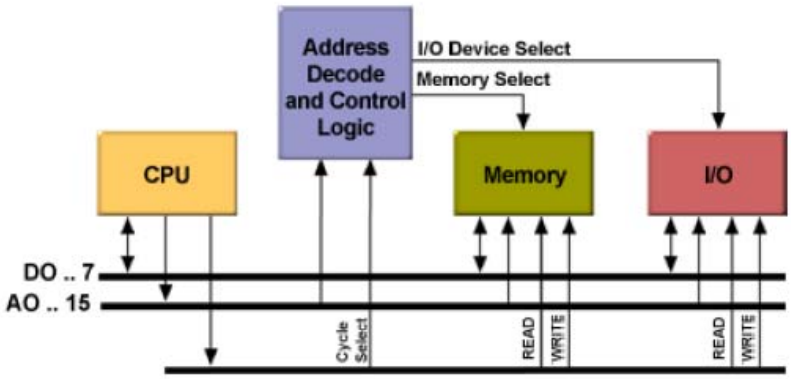

Figure 2.3 – Different paths presented in a microcontroller: data bus, address bus and control bus [11].

The stack is an area of memory used to keep track of the contents of the program counter when subroutines are called [10]. When data is written or pushed to the stack it is stored at the top of the stack. When data is removed from the top, the stack is said to be popped. A subroutine is a block of program code that performs an operation or a response to external interruptions that the main program needs to do a number of times. Instead of repeatedly inserting the block of code at each position of the main program where it is needed, the subroutine is called when required. When this happens, the actual address is pushed onto the top of the stack.

A convenient time base must be used to synchronize all the necessary events (logical state changes) that take place during the execution of a microcontroller program. So, a fixed frequency oscillator circuit must supply the microcontroller with a square wave signal.

A crystal is commonly used to accurately control the oscillator frequency. Another oscillators use RC circuits as well as external clock sources, *vid. fig. 2.4*. The time base signal is referred to as the clock signal and the data and instructions are clocked through the system.

The program instruction cycle is obtained from the division of the oscillator frequency by a pre-scalar integer whose final value can never reach the frequency of the oscillator circuit. In the microcontrollers that experience the best processing performances, the program instruction cycle can only be half the oscillator frequency.

Before an instruction can be executed, it must first be fetched from the instruction register. To maximize the speed of instruction execution, the next instruction is fetched at the same time that the current one is executing. This time overlapping of the fetch and execute cycles is called *pipelining*.

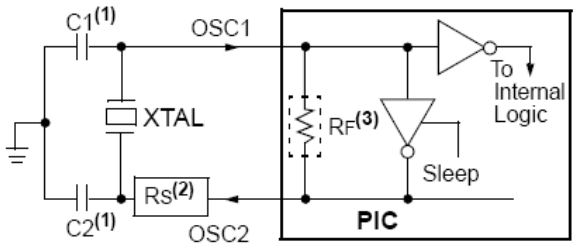

Figure 2.4 – HS oscillator consisting of a crystal (XTAL) and two resonant capacitors (C_1 and C_2) [12].

2.2. Microcontroller's Programming Language.

Each microcontroller's instruction consists of a binary code (or multiple binary codes) that make up what is know as *machine code*. Each microcontroller has its specific machine instructions [13, 14].

It is very difficult for humans to remember a set of binary instructions, so a mnemonic system is used to refer to them. The mnemonic set that programmers use to remember and manipulate the microcontroller program instructions is called the *assembly* language instruction set. For example, instead of writing 10110101110101 to tell the microcontroller to move a byte of data to a specific location, the assembly language instruction *movf* is used. So, the simplest method of writing a program for a microcontroller is to write in assembly language. Another program running on a computer, called an *assembler*, is then used to convert the language program into a set of binary machine code instructions.

The Assembly belongs to lower level programming languages that are programmed slowly, but take up the best amount of space in memory and give the best results when the speed of program execution is concerned. Languages such as *C* and *Basic* are easier to be written, easier to understand but, they are slower in executing.

A variable defined in C is an address of a specific memory location inside RAM and must be declared before it is used in the code. All constants however are stored inside ROM.

A program written in C needs to be converter in assembly language. This is achieved by using a *compiler* that maps the C code to the native assembly instruction set of the microcontroller [15, 16, 17].

After the program is written, it can be transferred to the microcontroller program memory. As soon as the microcontroller receives supply, it will perform a small check up – boot loading mode – and then it will look up for the beginning of the program and start executing it.

One way to look inside a computation system is to analyse the several transactions that take place from the high level code to the electrical signals that constitute in fact the single way of communication used by the hardware. This is shown in *fig. 2.5* for an increment operation.

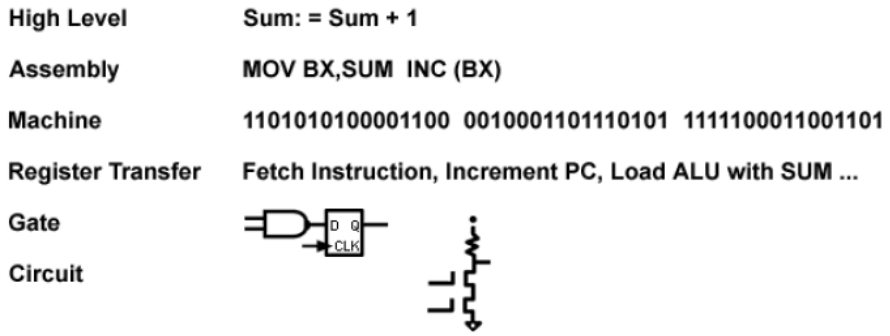

Figure 2.5 – Sequence of events that take place inside the microcontroller from high level programming command to the electronic action coded [11].

In digital electronic circuits the way of representing a binary set of states is using a positive and a zero voltage. Circuits implemented using TTL technology use 5V to represent the binary value 1 and 0V to represent 0. To provide some robustness to the representation, voltages above 3.5V will represent a logical 1 and those below 1.5V to represent a logical 0. In many microcontroller devices it is the power supply range that determines the upper and lower level for the TTL signals.

2.3. Selected PIC Microcontroller Device.

The PIC24FJ64GA002 is a general purpose microcontroller unit from *Microchip*® whose pin diagram is shown in *fig. 2.6*. It belongs to the 16-bit family of PICmicro® MCUs with a broad peripheral feature and enhanced computational performance [18]. It has several convenient built-in modules such as UART and SPI which can operate in parallel with the microcontroller's CPU, saving CPU instruction cycles.

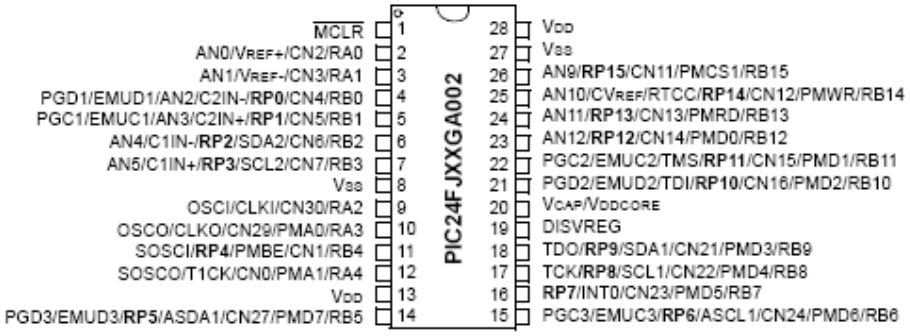

Figure 2.6 – PIC24FJ64GA002 pin diagram [18].

The two different kinds of memory present on the PIC24FJGA002 are a 64 kB program memory (ROM) and an 8 MB data memory (RAM), so, it has RISC architecture. Other important technical issues that make the microcontroller so attractive are the following ones [18]:

- 16-bit data and 24-bit address paths with the ability to move information between data and memory spaces. The 16-bit data bus architecture allows it to be connected to 16-bit analog-to-digital devices with no missing codes in the communication.
- a 16-element working register array with built-in software stack support;
- a 17x17 hardware multiplexer with support for integer math;
- hardware support for 32 by 16-bit division;
- an instruction set that supports multiple addressing modes and it is optimized for high-level languages such as C;
- operation performance up to 16 MIPS;
- inclusion of special interruption subroutines that the PIC has to attend;
- the instruction cycle frequency is half the oscillation frequency;
- 3.3 V supply operation.

Each single-word instruction of the PIC MCU is a 24-bit word divided into an 8-bit *opcode* (operational code), which specifies the instruction type and one or more operands which further specify the operation of the instruction.

The commercial software available for programming the PIC MCUs from Microchip is the MPLAB® IDE which is an integrated development environment where the user or designer can write its own program in assembly language. This software also includes a *simulator* program which accurately mimics the behaviour of a given microcontroller device in several control situations, enabling the designer to execute and debug an assembly language program for a PIC microcontroller, testing the device easily and making notes of the changes required.

For those designers more used to work with high level programming languages, Microchip has also available one C compiler for the 16-bit family of MCUs - the MPLAB® C30 Compiler – which works inside the MPLAB® IDE [13]. All the programs developed within this project were written in C due not only to the fact that C represents a more attractive programming language but also because the author has already experienced C programming language during its graduation.

Finally, to transfer the program from the computer terminal to the microcontroller it was used the MPLAB® ICD2 In-Circuit Debugger connected *via* USB in the computer's side (*vid. fig. 2.6*) and a 5 –wire connection to the microcontroller, through an RJ11 connector. The pins of the PIC used for program loading were the power supply (VDD), ground (VSS), $\overline{MCLR}$, PGD and PGC ones. Once the program is successfully built and the Configuration Bits of the device are correctly programmed, the microcontroller is ready to run the loaded program or *firmware* at power up [18].

Figure 2.7 - *Microchip*® Development Kit: MPLAB® IDE development software and MPLAB® ICD2 interface between the PIC MCU and the computer [12].

2.3.1. Universal Asynchronous Receiver/Transmitter – UART.

A UART is usually an individual (or part of an) integrated circuit used for serial communication over a computer or peripheral device serial port.

The UART uses two I/O pins to transmit and receive serial data. Because there is no separate clock signal for asynchronous operation, one pin (TX) is used for transmission while the other pin (RX) is used for reception. Both transmission and reception can occur at the same time and this is known as *full duplex* operation or can be independently enabled – *half duplex* operation. Since there is no separate clock in asynchronous operation, the receiver needs a method of synchronizing with the transmitter. This is achieved by having a fixed baud rate (bits *per* second or bps) and by using START and STOP bits in the communication signal.

The UART outputs and inputs logic level signals on the TX and RX pin of the PIC MCU. The signal is high when no transmission (or reception) is in progress (idle state) and goes low when the transmission starts. The receiving device uses this low-going transition to determine the timing for the bits that follow, *vid. fig. 2.8*.

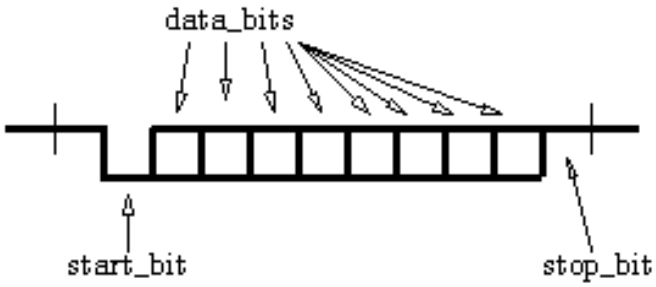

Figure 2.8 – UART communication packet [19].

The signal stays low for the duration of the START bit and is followed by the data bits (typically eight), least significant bit first, so the bit pattern looks backwards in comparison to the way it appears when written as a binary number. The STOP bit follows the last data bit and is always high. After the STOP bit completed, the START bit of the next transmission can occur.

The UART can also be configured to transmit and receive either eight or nine data bits, to implement parity and one or two stop bits in the transmission frame. In this project, all the UART communication frames use one START bit followed by eight data bits and one stop bit.

The scheme for transmitting and receiving data with the PIC MCU is shown in *fig. 2.9*. Every 16-bit microcontroller from *Microchip*® has two built-in UART modules which allow two UART serial communications to be taken at the same time. The modules designated UART1 and UART2 are functionally identical. In this project, it will be only used the UART1 module to communicate with the RF transceivers. So, once data has been written to the U1TXREG register, the eight bits are moved into the Transmit Shift Register (U1TSR). From there they are clocked out onto the TX pin preceded by a START bit and followed by a STOP bit [8].

After the detection of a START bit, eight bits of data are shifted from RX pin into the Receive Shift Register, one bit at a time. After the last bit has been shifted in, the STOP bit is checked and the data is moved into a FIFO buffer. U1RXREG register is the output of a four element FIFO buffer. If the FIFO is full with four characters and a fifth one is received by the U1RXREG, it will occur an overrun error and the first character will be out. To avoid this situation, every character must be read with a precedence of four after been passed to the FIFO [8].

Baud rate refers to the speed at which the serial data is transferred in bits *per* second. In asynchronous mode, the baud rate generator sets the baud rate using the value in the U1BRG register. The BRGH bit from U1MODE register selects between high or low speed options for greater flexibility in setting the baud rate [8, 14]:

$$Baudrate = \frac{Fcy}{16.(U1BRG + 1)} \quad , \qquad BRGH = 0 - low\ speed$$

$$Baudrate = \frac{Fcy}{4.(U1BRG + 1)} \quad , \qquad BRGH = 1 - high\ speed$$

where F_{CY} denotes the instruction cycle frequency (F_{OSC} */2).* The baud rate used in this project will be around 115200 bps with U1BRG = 21 and BRGH = 1.

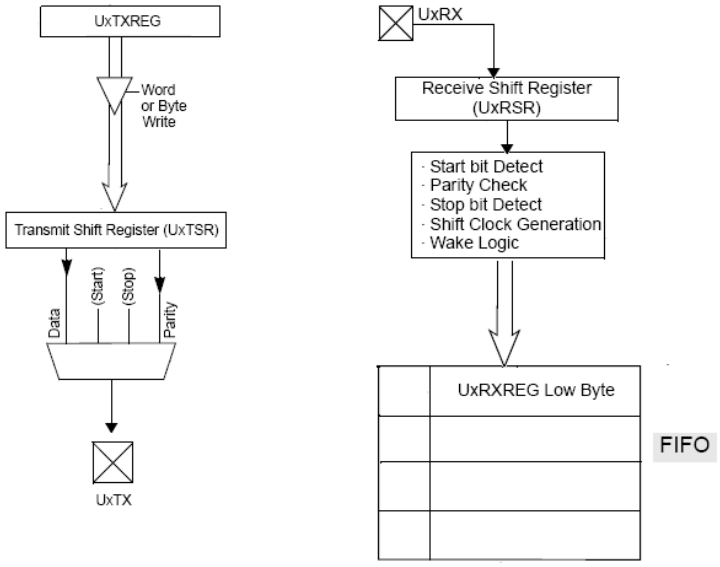

Figure 2.9 – Internal register mappings involved in UART [18].

2.3.2. Serial Peripheral Interface – SPI.

The Serial Peripheral Interface Bus is a synchronous serial data interface that operates in *full duplex* mode. It is useful for communications between a microcontroller and peripheral devices such as serial EEPROMs, display drivers and ADCs. The SPI always involves the use of master and slave devices within the communication, being the master one the responsible for initiating the data frame. The SPI bus specifies four logic signals [8]:

- SCK – Serial Clock (output from the master);
- SDI – Serial Data In;
- SDO – Serial Data Out;
- CS or $\overline{SS}$ – Chip Select or Slave Transmit Enable.

The SPI module can be configured to operate using 2, 3 or 4 pins. In the 3-pin mode, $\overline{SS}$ is not used while in the 2-pin mode, either SDO or SDI and $\overline{SS}$ are not used. Most of the time, the master device is a microcontroller and the SDI/SDO convention requires that the SDO on the master be connected to the SDI on the slave and vice-versa.

The PIC24FJ64GA002 offers two functionally identical SPI modules. These modules are referred together as SPIx or separately as SPI1 or SPI2. The center of the data transmission and reception is the SPIxBUF register, *vid. fig. 2.10*. When the PIC MCU writes data to SPIxBUF, this data is moved into the next transmit buffer location of an 8-level FIFO.

The SDOx pin begins to transfer the data after the first write to SPIxBUF and continues until the transfer has completed. At the same time, the SPIx pin updates the next receive buffer location with the incoming data. When reception is complete, the microcontroller can read it. So, transmission and reception occur simultaneously and data transfer in both directions, one bit at a time, is clocked out by the pulses on the SCKx.

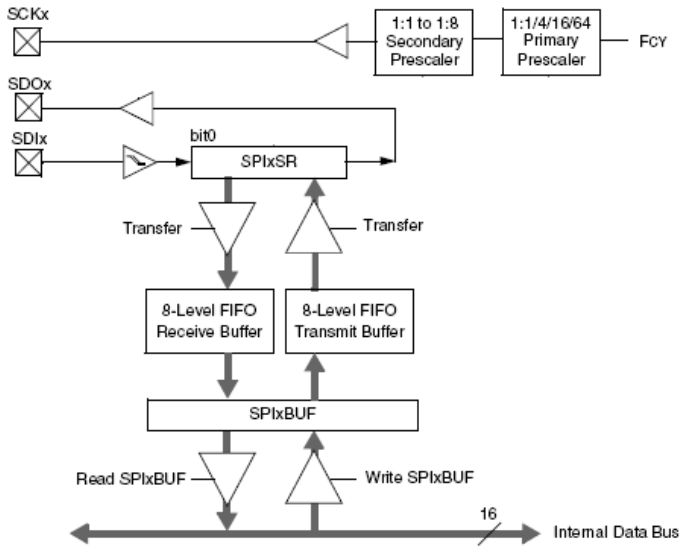

Figure 2.10 – Internal register mappings involved in SPI communications [14].

The PIC24FJ64GA002 can also communicate in either 8-bit or 16-bit mode [18]. The functionally will be the same for each mode, except for the number of bits that are received and transmitted. When transmitting or receiving data, 8 clock pulses at the SCKx pin are required to shift in/out data in 8-bit mode while 16 clock pulses are required in 16-bit mode.

The clock pulses are always provided by the master device and its frequency value can be set up to the instruction cycle frequency of the microcontroller. The shift of data in and out occurs either at the rising or falling edges of the pulses as it can be seen in *fig. 2.11.*

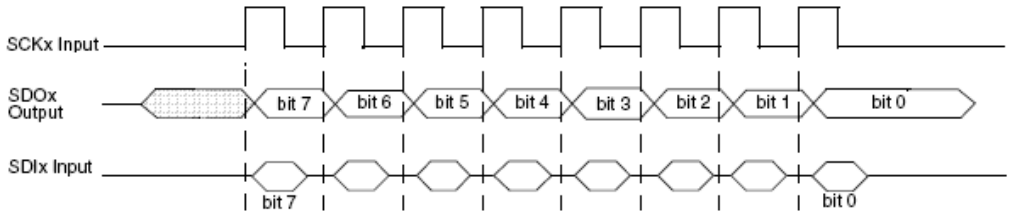

Figure 2.11 – SPI communication frame. Data bit shifting occurs are clocked out by the master clock frame [18].

Chapter 3

ZigBee Wireless Protocol

ZigBee is a wireless network protocol provided by *ZigBee® Alliance* whose first appearance was in December 2004. It is designed for low data rate sensors and control networks, based on the IEEE802.15.4 standard for wireless personal area networks (WPANs) [20]. The technical differences between ZigBee and other network protocols such as Wi-fi and Bluetooth are summarized in *Table I.*

Table I – Comparison amongst the available wireless technologies in the market.

	Physical Layer	Data Transfer	Range	Power Consumption
Wi-fi	IEEE 802.11b/g	54 Mbps	> 100 m	**> 400 mA TX, standby 20 mA**
Bluetooth	IEEE 802.15.1	1 Mps	1 – 10 m	**> 400 mA TX, standby 20 mA**
ZigBee	IEEE 802.15.4	250 kbps	70 - 100 m	**> 30 mA TX, standby 0.2 µA**

There are a number of applications that can benefit from the ZigBee protocol: home security systems, industrial control, embedded sensing, medical data collection, smoke and intruder warning, building automation, etc.

3.1. Technical Details.

The IEEE802.15.4 defines three frequency bands of operation in the ISM radio bands which are license-free: 868 MHz in Europe, 915 MHz in countries such as USA and Australia and 2.4 GHz in most jurisdictions worldwide [20].

Each frequency band offers a fixed number of channels. For instance, the 868 MHz frequency band offers 1 channel (channel 0); 915 MHz offers 10 channels (channels 1 – 10) and 2.4 GHz offers 16 channels (channels 11 – 26). Each ZigBee channel requires 5 MHz of bandwidth around the central frequency and, for the 2.4 GHz frequency band, each channel frequency can be calculated as $F_c = (2350 + (5.ch))$, where $ch = 11, 12, \ldots, 26$.

The bit rate of the protocol depends on the operational frequency as well as the packet overhead and processing delays. The 2.4 GHz provides 250 kbps, 915 MHz provides 40 kbps and 868 MHz provides a 20 kbps data rate.

In terms of modulation, the radios use *O-QPSK* (offset quadrature phase shift keying) in the 2.4 GHz frequency band and *BPSK* (binary phase shift keying) in the 868 MHz and

915 MHz. Transmission range is between 10 and 75 meters although it is heavily dependent on the particular environment.

3.1.1. Device Types.

A ZigBee network can consist of three different device types [21, 22]:

- ZigBee Coordinator (abbreviated to ZC);
- ZigBee Router (abbreviated to ZR);
- ZigBee End Device (abbreviated to ZED);

ZC is the most capable device on the network. Every device that is instructed to start a network becomes a so-called coordinator. There is only one ZC in each network which is responsible to store all the information about the network, including acting as a trust center and repository for security keys. ZR can act as an intermediate router passing data messages between ZigBee devices. A coordinator is effectively a router which has started the network. A ZED contains just enough functionality to talk to the parent node (either a ZR or ZC); it cannot pass data from other device in the network. In most of the time, it can be asleep which, therefore, gives a long battery life. So, a ZED requires the least amount of memory and energy as compared to a ZR or ZC.

3.1.2. Network Configuration.

A ZigBee protocol wireless network may assume many types of configuration. In all network configurations there must be at least one coordinator node and an end device. ZigBee defines three network topologies as [22]:

- Star Topology: it consists of one ZigBee protocol coordinator node and one or more end devices. All these end devices communicate only with the coordinator. So, if an end device needs to transfer data to another one, it sends its data to the coordinator first, that, in turn, forwards the data packet to the intended end device, *vid. fig. 3.1*.

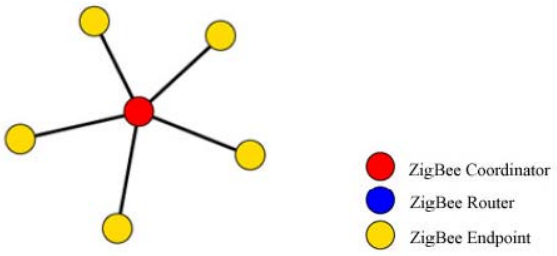

Figure 3.1 – ZigBee Star Topology [23].

➢ Cluster Tree Topology: in this configuration, end devices may join either to the ZigBee protocol coordinator or to the ZigBee protocol router. In this topology ZR serves two functions: one is to increase the number of nodes that can be on a network while the other one is to extend the physical radio range of the network. With the addition of a router, an end device need not be in radio range with the coordinator and all messages are routed along the tree, *vid. fig. 3.2*.

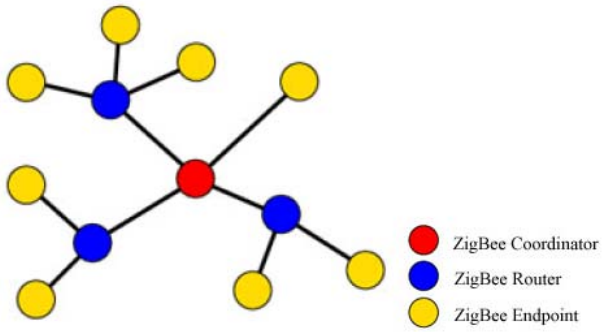

Figure 3.2 – ZigBee Cluster Tree Topology [23].

➢ Mesh Topology: it is similar to a cluster tree configuration, except that all the ZR and ZC nodes can route messages directly to other ZCs and ZRs without following any hierarchical structure. The advantages of this topology are that message latency can be reduced and reliability is increased, *vid. fig. 3.3*.

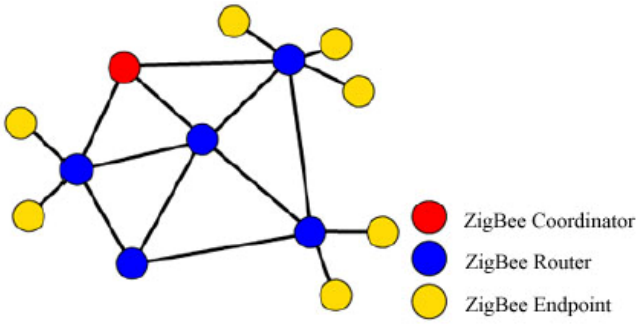

Figure 3.3 – ZigBee Mesh Topology [23].

The cluster tree and mesh topologies are also known as multi-hop networks due to the ability to route packets through multiple devices while the star topology is a single hop network.

There are two types of access to the medium of communication: beacon and non-beacon. In a non-beacon enabled network, all nodes are allowed to transmit at any time as long as the communication channel is available. In a beacon enabled network, nodes are allowed to transmit in predefined time slots which are settled by the coordinator node only.

3.1.3. ZigBee Stack Architecture.

The ZigBee stack architecture is made up of a set of blocks called layers schematically represented in *fig. 3.4*. Each layer performs a specific set of services for the layer it is passed next into. The lowest two layers of the stack are the physical layer, PHY, and the medium access layer, MAC, both defined by the IEEE802.15.4 standard. Above them, there are the network layer, NWK, and the application layer, APL, both defined by the ZigBee protocol. The transmission packets are built from the highest level to the lowest one in a RAM buffer before being passed to the PHY layer for transmission trough the radio [24].

The PHY layer is responsible for the transmission and reception of messages through a physical radio frequency channel. It is also responsible for the RF transceiver activation and deactivation as well as energy channel detection and link quality indication.

The MAC layer has the role of controlling the access to the RF channels, using multiple access/collision avoidance mechanisms to communicate with the inferior layer – PHY. It also specifies the network device types, the structure of the admissible frames like the ACK signalization flags and the synchronization and transmission of beacon frames.

The NWK layer is, hierarchically, the first layer defined by the ZigBee protocol whose responsibility includes: to begin and end a device connection in the network, to scan for new devices in the neighbourhood (and storing this information) and to provide address IDs if the device is a coordinator. It is also responsible for finding new transmission routes through the network.

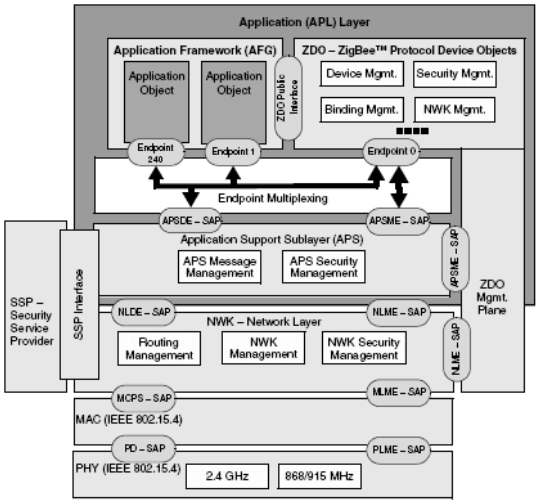

Figure 3.4 – Fundamental Layers that compose the ZigBee Stack Architecture [24].

Finally, the APL layer includes the application support sub-layer, APS, the ZigBee device object, ZDO, and the application framework, AFG. This layer has managing and support functions and, above this layer, the user can develop its application.

3.2. ZigBee Development Kit.

Nowadays, there are many companies in the market dedicated exclusively to the implementation and configuration of *ad-hoc* wireless networks. These companies sell their solutions accompanied with all the technical guidance on how to set up and fully operate their products in a short period of time. Most of the wireless protocol *firmware* needed to set up a network as the ZigBee stack described above is already implemented on integrated circuits, namely on RF transceivers. The user only has to follow the manufacturer instructions in order to program the transceiver's registers correctly and send the appropriate commands to it through a serial interface to quickly build a functional wireless network.

The STRX2DVKP from *Telegesis*® is a development kit of this kind, intended to construct a ZigBee network operating at the 2.4 GHz frequency band. The contents of the kit utilized to implement a wireless network in this project were [18]:

- 1 x STRX2DV USB Development board;
- 1 x STRX2USB Stick;
- 2 x STRX2 Transceiver;
- 1 x USB Cable.

The development board hosts a USB connection to a personal computer as well as a 3.3V regulation circuit which powers the STRX2 transceiver plugged via a 20-pin socket to the development board for programming, *vid. fig. 3.5*. The USB Stick consists of a STRX2 transceiver with a privileged communication with the USB ports of the computer: it can be used as a central coordinator node and, therefore, the PC becomes a wireless server responsible for controlling all the network transactions [25, 26].

The STRX2USB drivers necessary to install the development board and the USB stick can be freely obtained from reference [27] which generates a virtual COM port for each of them, allowing easy access to the serial port of the embedded STRX2 transceiver.

The command line of the STRX2 can be accessed using any terminal software program such as HyperTerminal®. In the beginning, the STRX2 factory default port communication is set to 19200 bps, 8-Data bits, no Parity and no Flow Control. To speed up evaluation, Telegesis provides its own Terminal Application Software program which can be downloaded from reference [27] and is shown in *fig. 3.6.*

Figure 3.5 - *Telegesis*® Development Kit: development board, STRX2 transceivers and USB stick [25].

The STRX2 transceiver will accept commands with the "AT" prefix after it has powered up successfully. All the commands are composed by 8-bit ASCII characters. After executing a command, the module will prompt "OK" or an error code.

In order to communicate with other ZigBee devices, a node must be part of a Personal Area Network or PAN. To find about the status of the module in the network, it is used the "AT+N" command. If the module is not part of the PAN, it can be instructed to join an existing PAN using the "AT+JN" command, or start a new one and, thus, becoming a coordinator node. To find other nodes in the same PAN, it must be send an "AT+SN" command to the module and the coordinator node is responsible for giving a 64-bit IEEE802.15.4 address in hexadecimal to all the nodes present in the network.

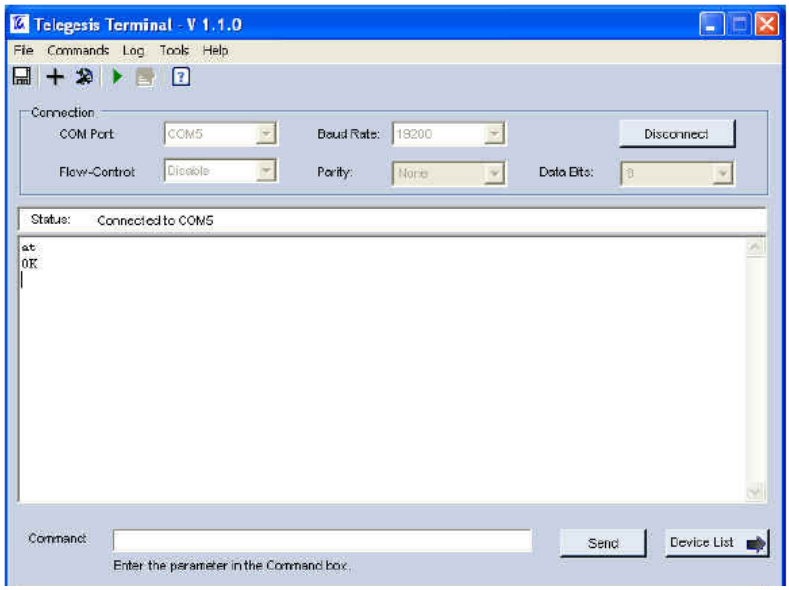

Figure 3.6 - *Telegesis*® Terminal for programming the STRX2 transceivers [26].

3.2.1. Internal Programmable Registers.

The STRX2 transceiver also contains a number of items of configuration data – the S-registers – which can be programmed by the user through the Terminal. The registers define the radio network parameters, I/O status, textual prompts and responses. Most of them are non-volatile, retaining their values when the module is powered down. Commands "ATS" and "ATSREM" read and write the register contents locally as well as remotely.

The write command is *ATS_ _ = XXXX*, where _ _ represents the 8-bit register number in hexadecimal (from 00 to 33) and *XXXX* represents a value between 0000 to FFFF used to program the state of the corresponding 16-bit register.

Some of the most important registers and commands are shown in *fig. 3.7*. For example, the S0B register is where the UART transmission protocol is defined while the S06 register defines the type of ZigBee device (ZC, ZR or ZED).

S-Register Overview	
S00	Channel Mask
S01	Preferred PAN ID
S02	Transmit Power Level
S03	Encryption key[1]
S04	User Definable name
S05	OEM Word[1]
S06	Main Function[1]
S07	Extended Function1
S08	Extended Function2
S09	Password[1]
S0A	Revision Number
S0B	UART Setup

Command Overview	
ATS	**S-Register access**
ATSREM	**Remote S-register access**
AT+ESCAN	**Scan the energy of all channels**
AT+EN	**Establish PAN**
AT+JN	**Join next best network**
AT+PANSCAN	**Scan for active PANs**
AT+JPAN	**Join specific PAN**
AT+DASSL	**Disassociate local device from PAN**
AT+DASSR	**Disassociate remote device from PAN**
AT+BCAST	**Transmit a broadcast**
AT+BCASTB	**Transmit a broadcast of binary data**
AT+UCAST	**Transmit a unicast**
AT+UCASTB	**Transmit a unicast of binary data**
AT+SCAST	**Transmit data to the Sink**
AT+SCASTB	**Transmit binary data to the sink**

Figure 3.7 – Principal Internal Registers of the STRX2 transceivers and AT-Commands [28].

When working at baud rates that exceed 19200 bps, the Telegesis Terminal stops working properly. A solution to communicate with the transceivers at the maximum allowed baud rate of 115200 bps is to use the Realterm Software which can also be freely downloaded from reference [29].

This was the strategy adopted in the present project to program the transceivers to be used in the biomedical sensors' network. All the previous commands are stored in the data memory of the PIC MCU in a 16-bit vector of integers. So, each 8-bit character of the command string will occupy one position in the 16-bit vector whose internal values will range from 0 to 255 only. The communication between the STRX2 transceiver and the PIC MCU is done through the UART interface: the RXD pin of the transceiver will be connected to the U1TX pin of the microcontroller while the TXD pin will be connected to the U1RX pin. To fully operate with the transceiver it necessary to use two more pins: V_{cc} and GND, which are the power pins.

3.2.2. Data Transmission.

The aim of a sensor's network is to send data between nodes. This data is formatted as a string of successive 8-bit ASCII characters with predefined or undefined length. The maximum payload for any message is 65 bytes, which reflects the small and efficient messaging structures of the STRX2 ZigBee transceivers. The time delay for data to be transmitted from one node to another one with one hop of separation cannot last for more than 100 ms and if the sender node expects an "ACK" from the receiver, it will take another 100 ms for the message find its way back.

Data messages can be sent to a particular node – **unicast** - or to all the nodes in the network that are within the radio range of the sender node - **broadcast**. The Telegesis Terminal has two available commands to perform these tasks. For sending a broadcast message, it is necessary to type: "AT+BCAST: *nn*, <data>" and the string <data> will be sent to all the nodes within *nn* hops. To send a message to a specific node and wait for and "ACK" or "NACK", the command is: "AT+UCAST: <EUI64>, <data>", where the string <EUI64> is the 64-bit IEEE802.15.4 address ID of the target node [28].

In a network constituted by sensor nodes which constantly need to send data to a remote recording system, there is a more efficient way of passing the data messages through the network: the solution is to configure the remote recording system as a sink node. A sink is a node intended to be a central receiver of data. A coordinator and a sink node are quite the same device with the exception that the former is allowed to leave the network after starting it and thus a separate node must be selected to operate as a data sink. To send data messages to a sink node, a sensor device has to type: "AT+SCAST: <data>". Because there is no need to type the address ID for the sink in the message, it should only exist a single data sink in the network. The pins of the transceiver used for UART communication are shown in *fig. 3.8*.

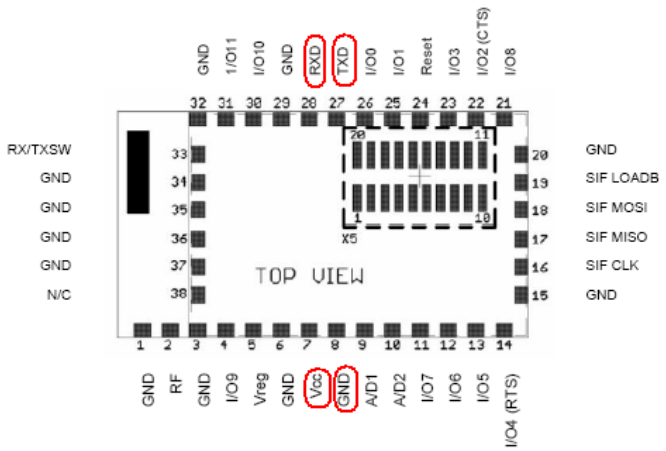

Figure 3.8 – Pin diagram of the STRX2 transceivers [25].

Chapter 4

Developed Devices

4.1. PROTOTYPE I: Wireless EASI – ECG System.

An electrocardiogram is a graphical representation of the electrical activity of the heart used for applications such as screening and diagnosing cardiovascular diseases. As the body is a volume conductor, fluctuations in electrical potential that represents the algebraic sum of the action potentials of myocardial fibers during the cardiac cycle can be recorded extracellularly [30].

The ECG may be recorded by using an active or exploring electrode connected to an indifferent electrode at zero potential – **unipolar recording** - or by using two active electrodes – **bipolar recording**.

The quality of an ECG analysis depends on the placement of the electrode lead wires. In addition, such placement is important because clinicians are trained to interpret ECG signals based on expected patterns. The electrodes are placed at the same anatomical locations on all patients; however, there is an acceptable margin of error for each placement.

Bipolar leads were used before unipolar ones were developed. The standard limb leads - leads *I, II,* and *III* -, each record the differences in electrical potential between two limbs, *vid. fig. 4.1*. Lead *I* is measured from the right arm to the left one; lead *II* is measured from the right arm to the left leg, and lead *III* is measured from the left arm to the left leg.

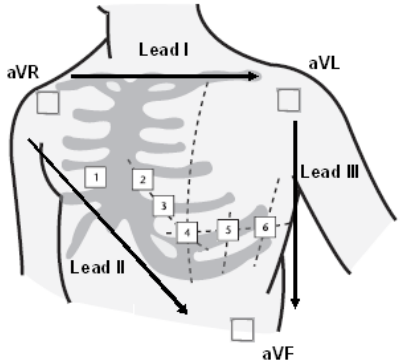

Figure 4.1 – Unipolar and Bipolar Leads. Translated from [30] with modifications.

An additional nine unipolar leads record the electrical potential difference between an exploring electrode and an indifferent electrode located centrally in the chest and computed

from the average of the limb recordings. There are six unipolar chest leads (**precordial**) designated, V_1 – V_6, and three unipolar limb leads or **Augmented** limb leads – *aVR* (right arm), *aVL* (left arm) and *aVF* (left foot) – which record the difference between one limb and the other two limbs.

The inferior leads (leads *II*, *III* and *aVF*) provide electrical activity reflective of the inferior wall of the heart, which is the apex of the left ventricle. The lateral leads (*I*, *aVL*, V_5 and V_6) provide electrical activity reflective of the lateral wall of the heart, which is the lateral wall of the left ventricle. The anterior leads (V_2 through V_4) represent the anterior wall of the heart or the frontal wall of the left ventricle.

4.1.1. Normal ECG Recordings.

Figure 4.2 represents a typical ECG recording and its characteristic waves. By convention, an upward deflection is recorded when the active electrode becomes positive relative to the indifferent one, and a downward deflection is recorded when the active electrode becomes negative.

The **P wave** is produced by atrial depolarization, the **QRS complex** by ventricular depolarization and the **ST segment** and **T wave** by ventricular repolarization. The manifestations of atrial repolarization are not normally seen because they are obscured by the QRS complex.

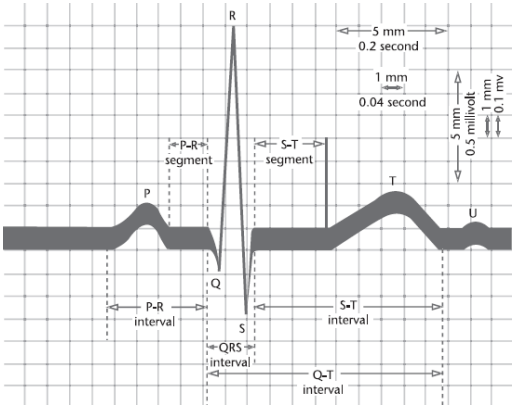

Figure 4.2 – Typical ECG recording and its characteristic waves [30].

The introduction of the standard twelve ECG leads over half a century ago (and described above) still remains the most important diagnostic tool to access the electrical activity of the heart. Several other systems have been developed and tried ever since in order to produce the conventional twelve leads using the minimum leads as possible [31]. Within this approach, regression or other techniques are used to generate a model that predicts ECG lead signals by a linear combination of the other leads.

The **EASI lead system** uses only four electrodes placed at anatomic points on the torso plus a ground reference. This system has been evaluated in adults and has been reported to be less sensitive to noise and artifacts than the conventional twelve ECG leads. Derived ECG recordings using EASI lead positions have been considered sufficiently similar to the conventional lead system to allow them to be used in clinical routine.

The three bipolar leads of the EASI system are generated by pairwise subtraction of the potentials recorded at the *E*, *A*, *S* and *I* electrodes (*vid. fig. 4.3*), yielding three ECG leads:

- Lead *AI*, which records the electrical activity of the heart in a left-to-right direction;
- Lead *ES*, which records the electrical activity of the heart in a caudal-cranial direction;
- Lead *AS*, which record the electrical activity of the heart in an anterior-posterior direction.

Using the voltages from the bipolar leads of the EASI lead system as reference voltages, the voltage V_i of any arbitrary lead *i* is a linear combination of the voltages in leads *ES*, *AS* and *AI*, as expressed in equation (1).

$$V_i = \alpha_i V_{ES} + \beta_i V_{AS} + \gamma_i V_{AI} \quad (1)$$

This linear equation can be represented in terms of the constant dimensionless coefficient triplet (α_i, β_i, γ_i). The unknown values of the three coefficients can be determined by fitting them to the measured sets of voltages V_i, V_{ES}, V_{AS} and V_{AI}. This statistical approach is based under the assumption of the **dipole hypothesis** – the electrical activity of the heart can be represented by a single dipole or heart vector – and the linearity of the body's volume conductor.

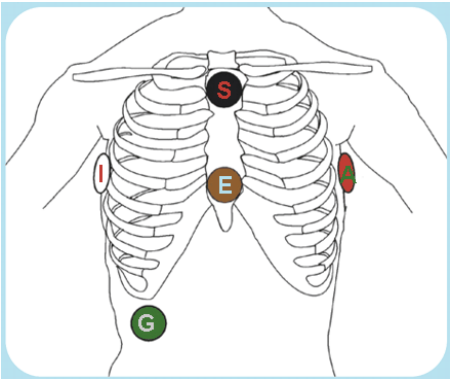

Figure 4.3 – Position of the electrodes in an EASI – ECG recording. Translated from [31] with modifications.

4.1.2. Electronic Device.

A block diagram of the prototype developed to perform the ECG recordings based on the EASI lead system is shown in *fig. 4.4*.

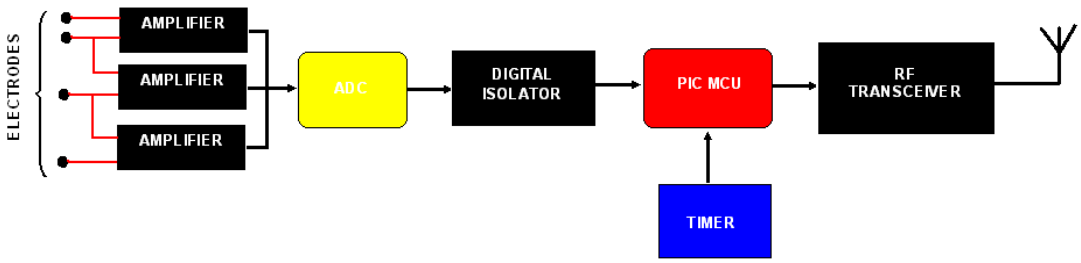

Figure 4.4 – Block diagram of the EASI - ECG device.

To perform a biopotential recording, electrodes are attached to the patient and then connected to a high gain differential amplifier with good common mode rejection. As biopotential recording necessitates that a low impedance connection is made to the patient, his safety has to be assured [32]. Because the device developed is expected to transmit the measured potentials *via* wireless to the recording equipment, it is not necessary a physical power line to feed the device and only a low voltage battery is used. This practically assures the safety of the patient since he is no longer at risk of electric shock in the event of a fault from an equipment fed by power lines.

Another important issue is precisely the environment that surrounds a patient. We are surrounded by power lines, operating at levels of hundreds of *volts*. A patient standing in a room is capacitively coupled to the power lines. As the ECG signal is of order of 1 mV, this capacitive interference may completely mask the biopotential signal. The strategy adopted to prevent such interference is to give some sort of shielding to the exploring electrodes. Since the developed device uses four electrodes, each of them is surrounded, on its entire extension, by a dielectric material and, just above, by a conductor material connected to the device's ground, *vid. fig. 4.5*. This creates an electrical field that shields, to some extent, the electrode from capacitive coupling of external power lines. If this shielding method is not sufficient, it can always be implemented in software a notch filter to remove the main frequency component of the power lines, typically at 50 Hz, from the acquired signal.

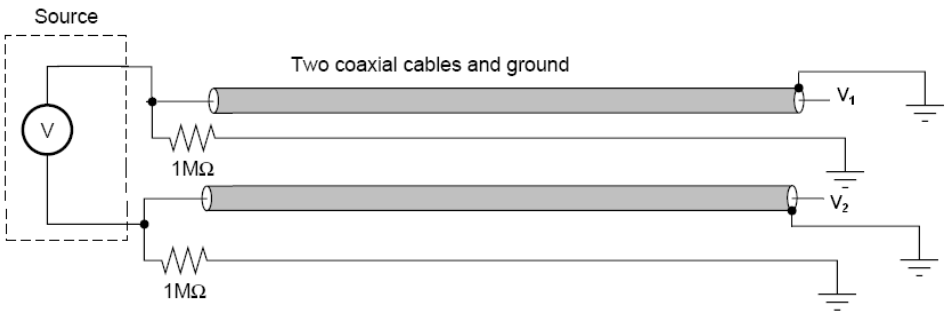

Figure 4.5 – Structure of the electrodes to capture the biopotentials. Translated from [33] with modifications.

The electrode lead wires form a loop which potentially generates a current in the presence of a varying magnetic field. To reduce this effect the leads are twisted and screened.

In addition, the patient's skin resistance can vary between 100 Ω and 2 MΩ, depending on its condition [32]. Skin resistance is highly affected by moisture and presence of mineral salts. To maintain a standardised low impedance interface with the patient, electrodes with a metal salt solution are used. This ensures that the skin is moist and the resistance stable and low.

4.1.2.1. RFI Filtering.

After being captured by the electrodes, the biopotential signal passes through a RFI filter before it enters the amplification stage. The purpose of using a filter of this kind is to define the bandwidth for both common-mode and differential signals that appear at the input terminals of the instrumentation amplifier. The attenuation of the common-mode by the amplifier is less efficient when the common-mode is present at high frequencies. This situation can lead to the decrease of the common-mode rejection ratio of the instrumentation amplifier which, by its turn, increases the captation of noise by the equipment that contributes for masking even more the captured differential signal. To eliminate high frequency noise we can think of a solution involving a lowpass filter placed in the input terminals of the amplifier. This was the approach adopted in this project and a 1st-order lowpass filter was made using a passive RC circuit, as shown in *fig. 4.6*.

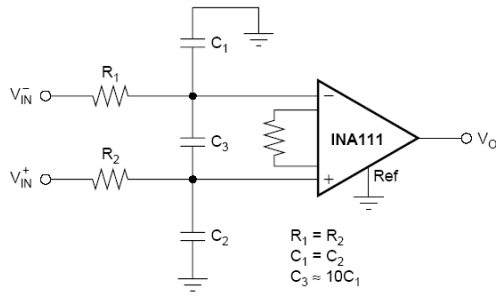

Figure 4.6 – RFI filter placed at the input terminals of the instrumentation amplifier [34].

The line impedance in both terminals must be strictly kept at the same value to preserve the equilibrium in what concerns the noise capturing in each input terminal. Because of that, the components used must be the same in each terminal: $R_1 = R_2$ and $C_1 = C_2$. In practise, a complete match between the values of the components is not achieved and, again, this mismatch can cause small perturbation in the required equilibrium which causes the amplifier to decrease its CMRR value. To invert the situation, an additional capacitor with higher value of capacitance is incorporated between the input terminals of the instrumentation amplifier and thus, the RFI filter is now complete.

As mentioned before, the RFI filter has two bandwidths. The differential one reflects the behaviour of the RFI filter when dealing with differential input signals. The formula for calculating it is expressed in equation (2).

$$LB_{dif} = \frac{1}{2\Pi R_1(C_1 + 2C_3)} \tag{2}$$

The values used for R_1, C_1 and C_3 were 10 kΩ, 1 nF and 10 nF, respectively, and this gives a 760 Hz differential bandwidth. The formula for calculating the common-mode bandwidth is similar to the last one and is given by equation (3).

$$LB_{cm} = \frac{1}{2\Pi R_1 C_3} \tag{3}$$

In these conditions, the common-mode bandwidth is around $15900\ \mathrm{Hz}$. By limiting the frequency range for common-mode signals, the CMRR of the amplifier will be assured to remain at high values even when it is necessary to use a high gain in the amplification stage.

4.1.2.2. Amplification Stage.

Following the filtering stage, the biopotential signal enters the amplification stage. The instrumentation amplifier used in the device was the INA111 from *Burr Brown*®, whose internal structure is shown in *fig. 4.7*. This amplifier has high input impedance as well as high common mode rejection ratio and an adjustable gain. The purpose of an instrumentation amplifier is to amplify the difference between the signals at the two electrodes.

The ECG signal measured at one electrode is out of phase with respect to the potential measured at the other electrode and, therefore, the difference signal is amplified and the noise and power supply coupling, both common to the two electrodes, are attenuated. The ratio of the amplification of the required differential signal to the amplification of common mode signal is the so-called CMRR and it is gain dependent.

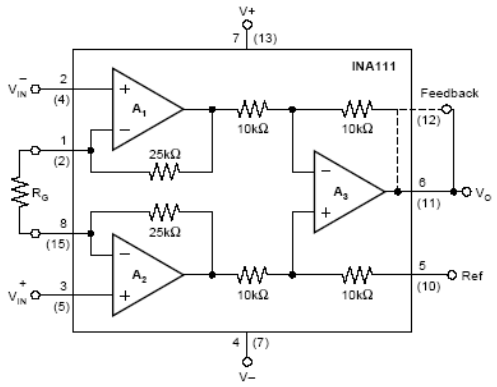

Figure 4.7 – Internal structure of the INA111 [34].

The common mode rejection ratio for ECG recordings is normally between 80 and 120 dB [32]. Having this in mind and other technical parameters of the INA111, such as the curve of the CMRR *versus* frequency (*vid. fig. 4.8*), gain and bandwidth of the input signals, the choice for the amplification level was 500 V/V. This value prevents also the amplifier to reach the saturation levels because the maximum amplitude found in a typical ECG recording do not exceed a few microvolts which, in turn, produces an amplified difference signal whose amplitude is within the battery supply range of – 5 to 5 V.

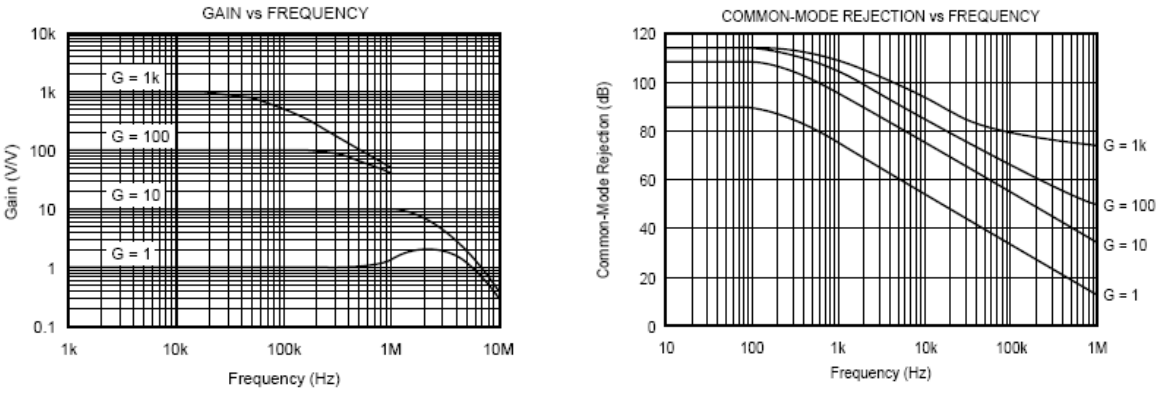

Figure 4.8 – Graphics showing the dependence of the amplifier's gain and CMRR with frequency [34].

The gain of the INA111 amplifier is established with a single external resistor, according to equation (4). The value for R_G is, therefore, 100 Ω.

$$G = 1 + \frac{50k\Omega}{R_G} \tag{4}$$

In ideal sense, the very act of measurement should not alter the value of the measured signal [32]. The INA111 input impedance controls the energy that is drawn from the biopotential source to the measurement device. To minimize power loss, the input impedance is very large ($\approx 10^{12}$ Ω). Also, this large value of impedance means that the biopotential is developed across the input terminals of the amplifier and not across the patient electrode interface.

The input bias current – current that flows out of the input terminals – of the INA111 is very small (≈ 20 pA), but a path consisting of a resistor of 1 MΩ connected to the ground was provided (and shown in *fig. 4.5*) for proper operation of the amplifier. Without a bias current path, the inputs would float to a potential that exceeds the common mode range and the amplifier would saturate.

Finally, to reduce the noise generated by the integrated circuit it was used a decoupling capacitor of 0.1 µF between the power supplies and ground.

After the amplification stage, the output signal is now single-ended and passes through a low-pass filter with a cut-off frequency, f_c, around 500 Hz to prevent anti-aliasing effects in the frequency spectrum of the reconstructed signal after the digitalization process. The low-pass

filter is a simple RC circuit of 1st order connected at the output terminal of the amplifier. The values for R and C are 3.2 kΩ and 0.1 µF.

4.1.2.3. Analog-to-Digital Conversion.

The analog-to-digital converter used in this project was the AD974 integrated circuit from *Analog Devices*®. The AD974 is a four channel data acquisition system with a serial interface. It contains an input multiplexer and a high-speed 16-bit sampling ADC with a maximum throughput of 200 kSPS, operating from a single + 5 V power supply.

The AD974 is specified to operate with three full-scale analog input ranges but, in this project, it will only accommodate ± 10 V analog input ranges. Such bipolar range configuration will produce a LSB value of 305.2 µV, according to equation (5).

$$LSB = \frac{V_{IN\max}^{+} - V_{IN\min}^{-}}{2^{16} - 1} \tag{5}$$

Figure 4.9 shows the interface diagram between the AD974 and the SPI equipped microcontroller. The SPI interface is a 2-wire connection between the master device – PIC MCU – and the slave device – AD974. The clock pulses are, therefore, generated from the microcontroller and are outputted on the *SCK* pin towards the *DATACLK* pin of the ADC. The convert pulses are initiated in response to an external timer interrupt produced by an integrated circuit – 555 timer – which, therefore, controls the sampling frequency. The reading of the output data (binary code), one bit at a time, is performed through the *SDI* input pin.

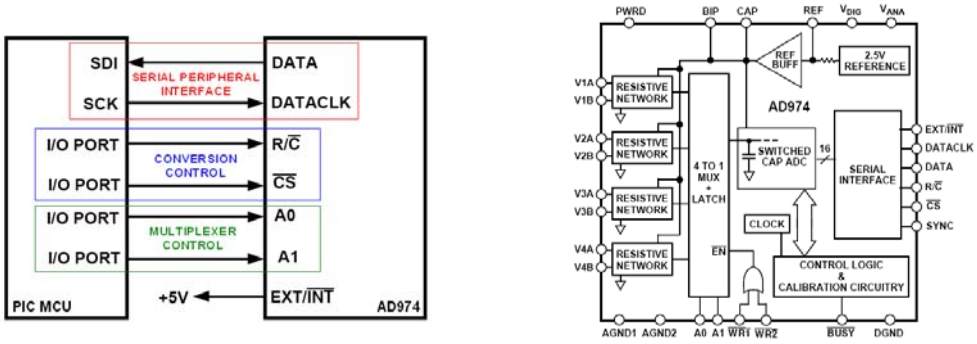

Figure 4.9 – Interface diagram between the PIC MCU and the ADC (left) and internal block diagram of the ADC (right) [35].

Four additional I/O port pins of the PIC MCU are used to control the conversion process and the internal multiplexer of the ADC. To choose between one of the four input channels available to sample it's only necessary to control the levels (high or low) of the *A0* and *A1* input pins, according to *Table II*. In the beginning of each conversion the ADC "sees" the levels of the multiplexer pins and starts to acquire and sample the channel coded by *A0* and *A1*.

Table II – Combination of the Multiplexer control input pins [35].

A1	A0	Data Available from Channel
0	0	AIN 1
0	1	AIN 2
1	0	AIN 3
1	1	AIN 4

The AD974 is controlled by two input signals: $R/\overline{C}$ and $\overline{CS}$, provided by the microcontroller, *vid. fig. 4.10*. The first signal to be taken low is $R/\overline{C}$ followed by $\overline{CS}$ with a minimal time delay. When both $R/\overline{C}$ and $\overline{CS}$ are low for a minimum of 50 ns, the analog input signal will be held on the internal capacitor array of the ADC and a conversion will begin.

After the start of the conversion, $\overline{CS}$ is brought high first, followed by $R/\overline{C}$. The conversion will last for about 4 to 5 µs and the result of that conversion – binary code, consisting of 16 bits – can be read when $\overline{CS}$ is brought low again.

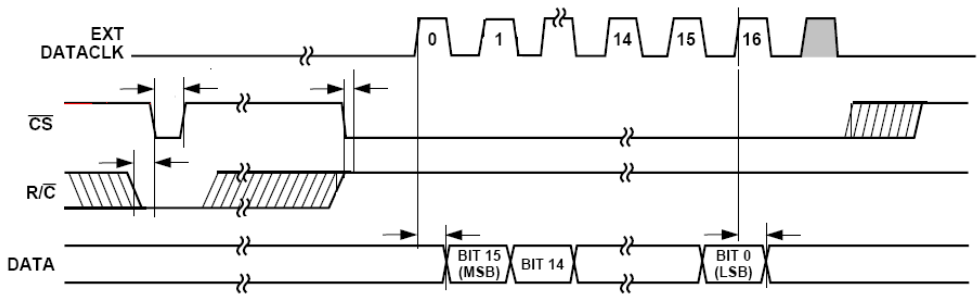

Figure 4.10 – Timing diagram that controls the sampling and bit-reading processes. Translated from [35] with modifications.

For the reading process, it is necessary to provide the *DATACLK* pin of the ADC with an external discontinuous clock. The highest frequency of the clock pulses permitted for *DATACLK* is 15.15 MHz; since we are measuring low-speed signals it is enough to use a clock frequency of 1.25 MHz derived from the internal oscillation frequency of the microcontroller which is 20 MHz.

The MSB will be the first bit to be released and it will be valid on the first falling edge of *DATACLK*. Thus, a minimum of 16 clock pulses are required to complete transfer the binary sequence from the ADC.

This binary sequence will be held in a vector of binary data samples inside the data memory of the PIC MCU before being transmitted *via* wireless.

The binary signals that come from the ADC follow the 5 V TTL logic. Since the PIC24FJ64GA002 works with a 3.3 V power supply, it only accepts logic signals within its supply range on the input terminals. To convert between the two different logics it was intercalated a digital isolator between the ADC and the PIC MCU. It was used the ADuM140x

family of devices from *Analog Devices*®. These unidirectional 4-channel digital isolators operate with the supply voltage on either side ranging from 2.5 V to 5.5 V, providing compatibility with lower voltage systems as well as enabling voltage translation functionality across the isolation barrier, as in *fig. 4.11*.

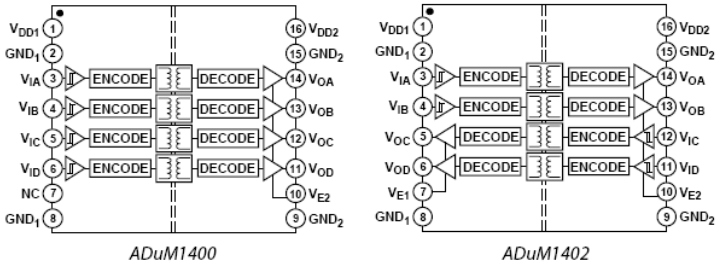

Figure 4.11 – Internal configuration of the ADuM140x integrated circuit family: unidirectional (left) and bidirectional flow transfer (right) [36].

4.1.2.4. Timing Circuit.

In the developed device, the accuracy of the timing is of paramount importance because it controls the sampling period, T_s, of the ADC or, inversely, the sampling frequency, F_s.

The timing circuit was built with the well-known 555 timer IC. The purpose of the timing circuit is to provide a stable rectangular time signal with a duty-cycle well above the 50% to work as an external trigger, which can cause the PIC MCU to enter a special interruption subroutine whenever it "sees" a transition from high to low (a falling edge) of the rectangular signal, as shown in *fig. 4.12*.

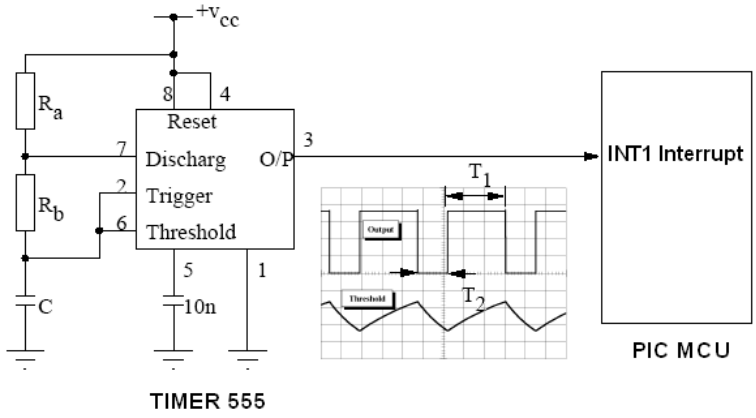

Figure 4.12 – Interface between the 555 timer and the PIC MCU for external triggering of the latter.

After entering the interruption subroutine, the PIC MCU starts to acquire and sample the data available in each channel of the ADC sequentially, e.g, channel 1 first, followed by channel 2 and finally channel 3. Thus, by manipulating the external timing circuit (*hardware*) we can easily change the sampling period of our acquisition system without the need to use timer

delays (*software*) inside the PIC MCU; internal timer delays which can be time affected by the other high priority interruption subroutines working at the same time inside the microcontroller such as the interruptions caused by the wireless protocol.

To build an efficient external timing circuit it was necessary to study the 555 timer and its behaviour when operating on astable mode.

In the astable mode [37], it is necessary two external resistors, R_a and R_b, and one capacitor, C. The trigger pin is tied to the threshold one. At power-up, the capacitor is discharged, holding the trigger low. This triggers the timer, which establishes the capacitor path through R_a and R_b. When the capacitor reaches the threshold level of *2/3* V_{cc}, the output drop low and the internal discharge transistor turns on. The timing capacitor now discharges only trough R_b and, when the voltage reaches *1/3* V_{cc} the trigger comparator trips, automatically retriggering the timer (output high) and the cycle repeats itself. In resume, the timer output is high for the time T_1 that $V_{threshold}$ takes to rise from *1/3* V_{cc} to *2/3* V_{cc} and it is low for the time T_2 that $V_{threshold}$ takes to drop from *2/3* V_{cc} to *1/3* V_{cc}.

Depending on the modality and returning path, the charging and discharging times are given by equations (6) and (7).

$$T_1 = 0.7(R_a + R_b)C \tag{6}$$

$$T_2 = 0.7R_bC \tag{7}$$

For the developed device, C = 22 nF, R_a = 56 kΩ and R_b = 3.4 kΩ, which give $T_1 \approx$ 950 µs and $T_2 \approx$ 50 µs. In these conditions, the period of the rectangular signal is 1 ms which corresponds to a sampling frequency of 1000 SPS for each channel of the ADC.

Since the established bandwidth of the input signals do not exceed 250 Hz, a sampling frequency of 1000 SPS seems to be overkill, but this high frequency will provide greater detail level since there will be more data samples available to reconstruct the signal by interpolation.

4.1.2.5. Wireless Transmission.

To send data via wireless, we need at least two network nodes, each of them with a RF transceiver. One node will be responsible for collecting the data – sensor node – while the other one will record or store it for visualization and processing purposes. For the node of the remote recording system it was used the STRX2USB Stick programmed to function as a sink node while the sensor node was programmed to be a ZigBee end device. Both of them use the same UART velocity (115200 bps) and the same PAN ID; network which was first established by the sink node. With the purpose of setting up a communication, one channel, amongst the 16 available ones, must be open first by the sink node to exclusively exchange data with a particular sensor. Every transmission packet sent from the remote sensor has to start with the command string “AT+RDATAB:” and follow the structure shown in *fig. 4.13*. This structure allows the fastest rate for messages’ exchange provided by the STRX2 RF transceivers.

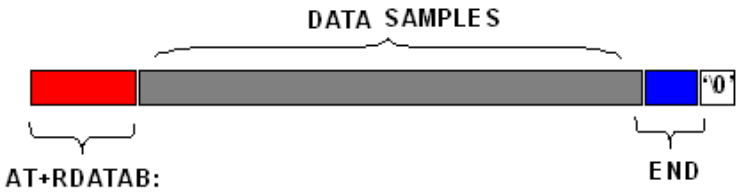

Figure 4.13 – Data transmission packet used by the sensor node.

The data section of the packet was defined to have a fixed length of 60 bytes, that is, it was reserved 60 locations on the transmission packet to the biopotential acquired samples and 3 locations to code an “END” of the packet, followed by a location for the terminator character. This structure provides equal transmission packets in terms of dimensions and format that helps the remote recording system to recognize quickly the positions for the beginning and end of the samples’ frame and extract it easily whenever a complete transmission packet has successfully arrived.

Each acquired sample consists of a 16-bit data word and the UART interface transfers only a data byte or character (8-bits) in every communication frame. So, in order to transmit a 16-bit data word, each sample must be broken into 2 x 8-bit codes that will occupy two locations on the data packet. This is achieved by sending the 8 MSBs of the sample to a location and the remaining 8 LSBs to the following one through binary operations of bit manipulation that take place inside the PIC MCU. In the end, the remote recording system has to put together every two consecutive characters of the transmission packet to obtain the true coded analog voltage.

Inside the program memory of the PIC MCU, it was implemented a function that writes one character at a time to the U1TXREG register to be transmitted via UART interface to the RF transceiver. This function has a C pointer that initially points to the beginning of the vector that contains the transmission packet and when the communication takes place, it runs through the entire vector and passes the contents of every memory position to the UART transmission register. When it reaches the terminator character, the function stops sending characters to the transceiver and the pointer comes back to its original position and waits till the transmission vector is filled again for a new transmission.

The UART interface takes about 0.625 ms to send the entire transmission packet to the RF transceiver when working at a baud rate of 115200 bps. The packet received by the sink node will have the same format as the one transmitted by the end device. The structure of the transmission packet received by the recording node is shown in *fig. 4.14*.

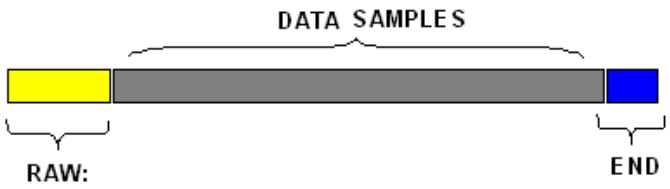

Figure 4.14 – Data reception packet used by the sink node.

Finally, the reception of the data packets has revealed some limitations due to the fact that the bandwidth involved in data exchange between remote nodes was lower than it was expected initially. An experimental procedure has shown that the real bandwidth was only 4 kbps *per* channel instead of 16 kbps. This means that only one quarter of the packets sent by the sensor node successfully arrive at the recording node. A bandwidth of 4 kbps means that only 250 data words can be received in every second. So, the maximum frequency component of the input signal recorded in these conditions is 125 Hz, 25 Hz below the maximum spectral component of an ECG signal. It might be sufficient to obtain an ECG recording with its features perfectly discernible but, for higher rate sensors like reography, other communication solution must be found.

4.1.2.6. Microcontroller C Program: Overview.

Once the microcontroller is powered up, the program stored inside its memory starts to run in a cyclic-way, triggering the coded sequence of events that lead to the final transmission of the data packets. In the very beginning, the program starts to configuration the I/O ports as digital ones, the SPI1 protocol is defined as the communication interface between the PIC MCU and the ADC while, by its turn, the UART1 protocol is defined as the communication interface between the microcontroller and the RF transceivers, *vid. fig. 4.15*. The initialization phase ends with the configuration of all the interruption routines that will work in parallel with the main cycle of the program. There are two interruption events: the INT1 interruption that controls the external trigger signal that starts every acquisition phase and the RX1 interruption that results from the wireless protocol.

The single instruction that the PIC MCU has to execute when it enters the main cycle is to check if the data packet for wireless transmission is complete to trigger the instruction necessary to send it via UART1 to the RF transceiver. The program only leaves its main cycle if it reports an interruption. An interruption is a way that microcontrollers have to optimize their temporal tasks. When a module inside the microcontroller needs its attention, it emits a warning or interruption flag that stops the program's main cycle. The PIC MCU by its turn saves the machine states at that time and loads the interruption vector. If the interruption flag detected corresponds to the INT1 interruption routine, the microcontroller gives orders to start three consecutive acquisition processes through the SPI1 protocol and store the binary words inside

the data transmission packet before it clears the IF and returns to its main cycle. If the interruption flag corresponds to the RX1 interruption routine, the microcontroller updates itself with the new commands received before returning to the main cycle.

Whenever the collected data samples from the ADC fill the 60 available positions inside the data transmission packet, the PIC MCU starts to transmit it, disabling all the interruption routines to avoid time delays when transmission is in progress. The cycle then keeps repeating itself with all interrupts enabled again as shown in the flowchart behind.

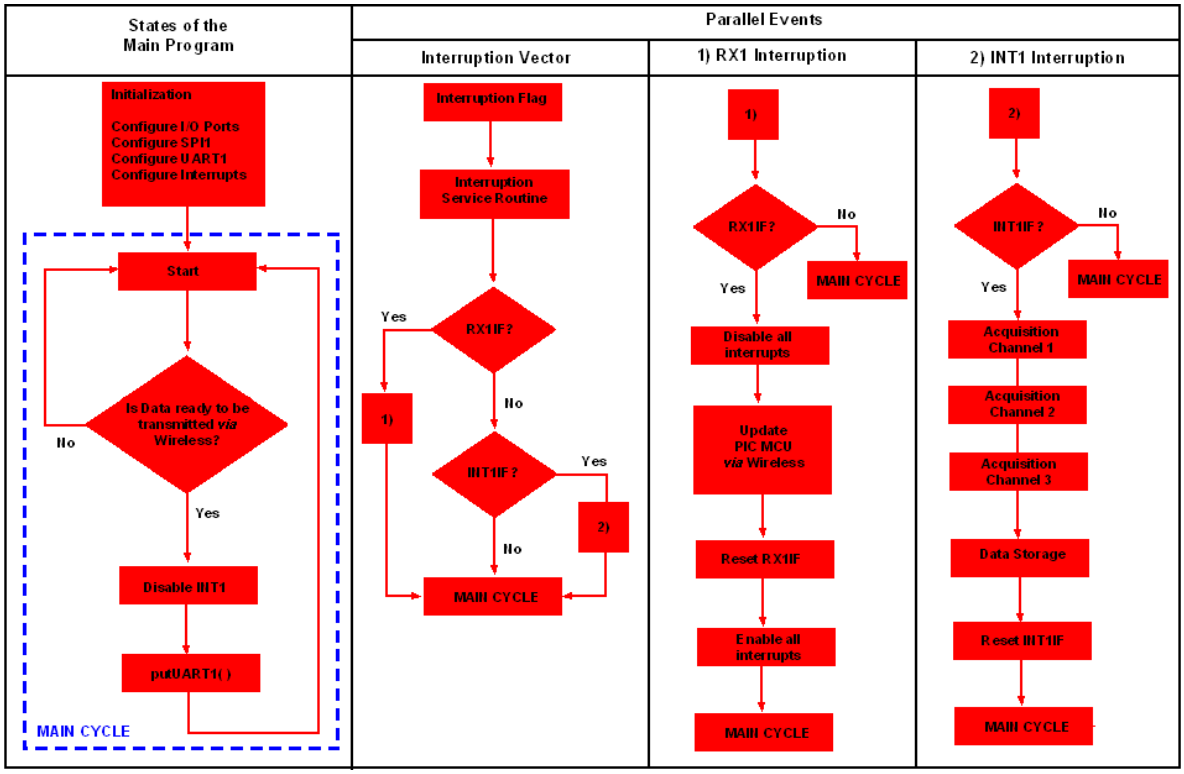

Figure 4.15 – Flowchart of the instruction events that run inside the program memory of the microcontroller.

4.1.3. Signal Processing Techniques.

The need for conditioning low-level AC signals in the presence of environmental electric interference has lead to the development of signal noise reduction techniques implemented not only in hardware but also in software. It is always desirable to eliminate the interference before it enters the amplification stage, for example, by proper shielding of the subject, leads and electronic instrument and by grounding the subject and instrument. Interference induced on the body common to the biopotential sensing electrodes is the so-called common mode interference.

When this interference is not completely attenuated by analog electronic devices it is usual to implement digital filtering algorithms stored inside the program memory of the recording system whose central processing unit will be responsible for applying these algorithms to the collected data. A digital filter is a time-discrete system *h(n)* in which the input signal *x(n)* is reshaped into a beneficial output signal *y(n)* as shown in *fig. 4.16*. Filters can be divided into FIR and IIR filters. FIR filters have the advantages of being always stable and having linear phase shifts. These filters are also referred to as non-recursive systems because only the input signal is used in the filter algorithm to compute the output response and the convolution in time domain uses a moving set of multiplier weights known as filter coefficients [1].

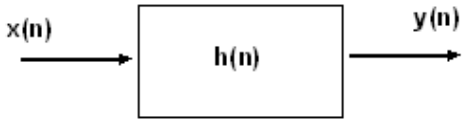

Figure 4.16 – Time-discrete filter operation.

According to the *h(n)* function a FIR filter can be classified as highpass, lowpass, bandpass or bandstop filter. Each name derives from the corresponding frequency spectrum and the range of frequencies that is not attenuated in the spectrum. The FIR filter coefficients can be obtained by applying an inverse Fourier Transform to these rectangular spectral structures with the appropriate associated shapes [1].

The developed project implements a notch filter with bandstop frequency ranging from 45 to 55 Hz to illustrate the attenuation of the electrical interference that comes from the capacitive coupling of power lines which shows up in the base line of the acquired biopotential, *vid. fig. 4.17*.

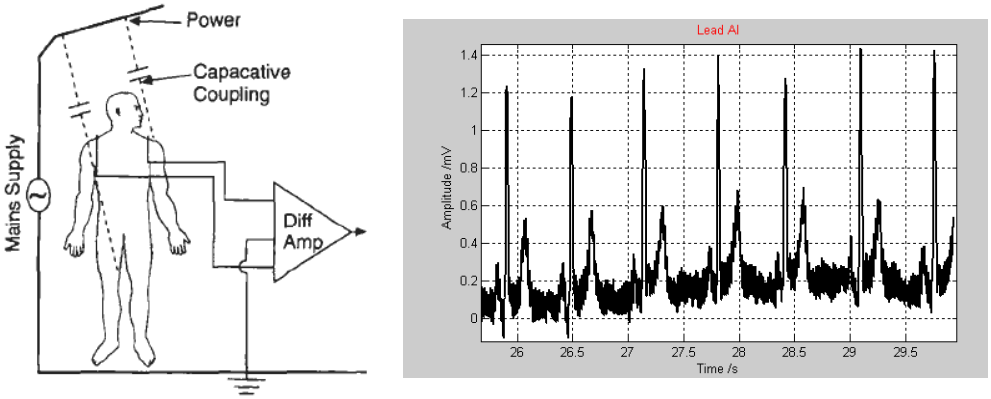

Figure 4.17 – Capacitive coupling effects from power lines (left) [32] and its repercussions on the measured ECG signal (right).

The removal of the 50 Hz frequency component of the power lines from the biopotential signal is shown in *fig. 4.18*.The frequency spectrum of an ECG signal features its main spectral components around the DC level, *vid. fig. 4.19*. The maximum spectral component recorded corresponds to the heartbeat rate. This must be within the physiological range of 54 to 180 bpm (beats *per* minute) or within the frequency range of 0.9 to 3 Hz.

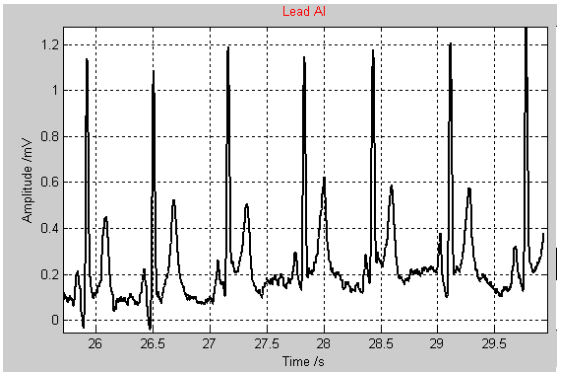

Figure 4.18 – Filtered ECG signal.

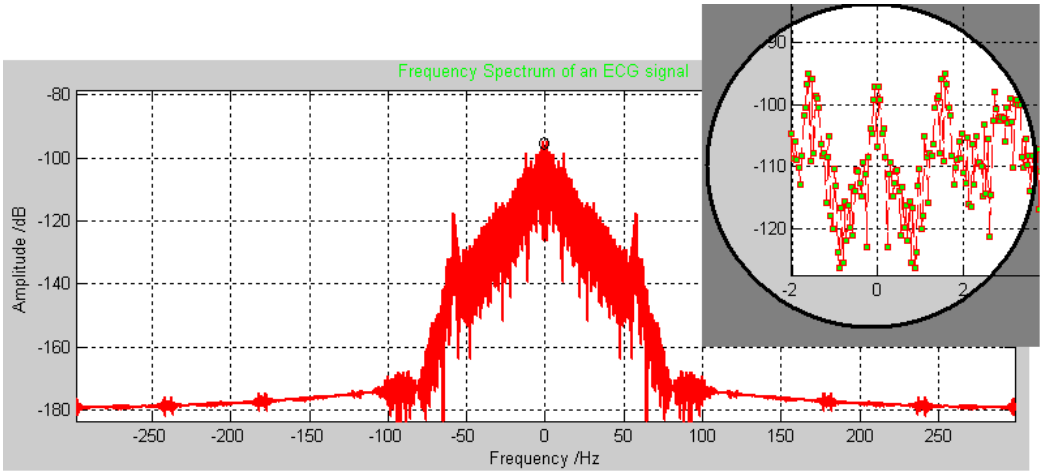

Figure 4.19 – Frequency spectrum of the ECG signal.

4.2. PROTOTYPE II: Wireless Pulse Oximeter.

The red, oxygen-carrying pigment in the red blood cells is called haemoglobin or hemoglobin. Hemoglobin (abbreviated to Hb) is a globular molecule made up of four subunits. Each subunit consists of an iron-containing porphyrin derivative moiety called heme conjugated to a polypeptide, referred collectively as the globin portion of the hemoglobin molecule, *vid. fig. 4.20*.

Hemoglobin binds O_2 to form **oxyhemoglobin** - HbO_2 - with oxygen attached to the Fe^{2+} in the heme. Thus, each Hb molecule within the red blood cell is able to reversibly carry up to four oxygen molecules.

The affinity of hemoglobin for O_2 is affected by pH, temperature and the concentration in the red cells of 2,3-diphosphoglycerate (abbreviated to 2,3-DPG). This molecule and H^+ compete with O_2 for binding to deoxygenated hemoglobin, decreasing the affinity of hemoglobin for oxygen by shifting the positions of the four peptide chains (quaternary structure).

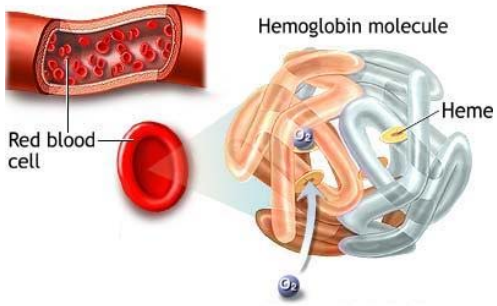

Figure 4.20 – Quaternary structure of hemoglobin [32].

When blood is exposed to various drugs and other oxidizing agents, the ferrous iron, Fe^{2+}, is converted to ferric iron, Fe^{3+}, forming **methemoglobin**, a dark-colored hemoglobin. When it is present in large quantities in the circulation, it causes a dusky discoloration of the skin resembling cyanosis. Some oxidation of hemoglobin to methemoglobin occurs normally, but an enzyme system in the red blood cells, the NADH-hemoglobin reductase system converts methemoglobin back to hemoglobin.

Carbon monoxide (abbreviated to CO) also reacts with hemoglobin to form carbon monoxyhemoglobin or **carboxyhemoglobin**. The affinity of Hb for O_2 is much lower than its affinity for CO which, consequently, displaces O_2 on hemoglobin, reducing the oxygen carrying capacity of blood.

Normal arterial blood with a hematocrit around 45% by volume is able to carry about 20 mL of O_2 *per* 100 mL of blood. This is two orders of magnitude more O_2 than it is possible to carry in water or in blood plasma.

Combined spectrophotometric and electrochemical measurements have been made in whole blood samples to characterize the chemical and spectral properties of the human oxyhemoglobin equilibrium curve, as shown in *fig. 4.21*.

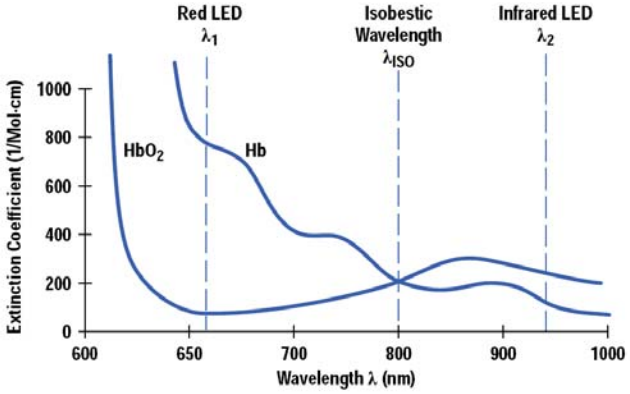

Figure 4.21 – Absorption spectrum of hemoglobin (Hb) and oxyhemoglobin (HbO_2). Translated from [3] with modifications.

4.2.1. Theory of Pulse Oximetry.

Oxygen saturation which is often referred to as SaO_2 or SpO_2, is defined as the ratio of oxyhemoglobin (HbO_2) to the total concentration of hemoglobin present in the blood, i.e., oxyhemoglobin plus reduced hemoglobin, as shown in equation (8).

$$SaO_2 = \frac{[HbO_2]}{[HbO_2] + [Hb]} \tag{8}$$

Arterial SaO_2 is a parameter measured with oximetry and it is normally expressed as a percentage. Under normal physiological conditions arterial blood is 95% saturated, whilst venous blood is 75% saturated. The common anatomical locations to place the oximeter are the finger and earlobe and the obtained recordings are considered the fifth vital signal.

It is possible to use the differences in absorption spectra of HbO_2 and Hb for the measurement of arterial oxygen saturation *in vivo* because the wavelength range between 600 nm and 1000 nm is also the range for which there is least attenuation of light by body tissues. Tissue and pigmentation absorb blue, green and yellow light whereas water absorbs the longer infrared wavelength.

Oxyhemoglobin does not absorb much red light, but as the hemoglobin oxygen saturation drops, more and more red light is absorbed and the blood becomes darker. At the near infrared range of light however oxyhemoglobin absorbs more light than reduced hemoglobin. Thus, pulse oximetry is based upon two physical principles that combine the two technologies of spectrophotometry, which measures hemoglobin oxygen saturation, and optical plethysmography, which measures pulsatile changes in arterial blood volume [38].

Modern pulse oximetry was born with the recognition that pulsatile changes in light transmission through living tissues are due to alteration of the arterial blood volume in the tissue. Measurement of the pulsatile component of blood will rule out the variable absorption of

light by bone, tissue, skin, pigment, etc., from analysis. So, the only pulsatile absorbance between the light source and the photo detectors is that of arterial blood.

The two optimum wavelengths for pulse oximetry are in the red (λ_1 = 660 nm) and near infrared (λ_2 = 940 nm) regions. At 660 nm, reduced hemoglobin absorbs about ten times as much light as oxyhemoglobin while, at 940 nm, the absorption coefficient of oxyhemoglobin is greater than that of reduced hemoglobin. The pulse oximeter directly senses the absorption of red and infrared light and the ratio of pulsatile to non-pulsatile light at the red and infrared are translated through complex signal processing techniques to a function of the arterial oxygen saturation [38].

4.2.1.1. Pulse Oximetry: *Beer-Lambert* law.

Light propagation in a uniform medium is described by the *Beer-Lambert* law [39]. According to it, the intensity I of the light in the medium is proportional to the transmitted intensity I_0 and decreases exponentially with the extinction coefficient of the absorbing medium ε, the concentration of the absorbing medium β and the path length L as expressed in equation (9).

$$I = I_0 \exp\left[-\varepsilon(\lambda)\beta L\right] \tag{9}$$

The unscattered absorbance, $A(\lambda)$, is given by taking the logarithm of the transmitted intensity over the receiving intensity, that is,

$$A(\lambda) = Ln\left(\frac{I}{I_0}\right) = -\varepsilon(\lambda)\beta L \quad , \tag{10}$$

and, for all the substances present in the medium, last expression becomes equation (11).

$$A_{total}(\lambda) = \sum_i \varepsilon(\lambda i)\beta i L \tag{11}$$

Both Hb and HbO_2 have different extinction coefficients at each wavelength. However, light is scattered in many directions as it enters the skin. Therefore, light received by the photodetectors rarely travels in a straight path and it is heavily attenuated, *vid. fig. 4.22*.

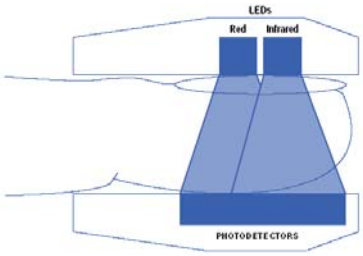

Figure 4.22 – Placement of the oximeter spring around the finger [3].

The total absorbance at the two wavelengths in study is given by expressions (12) and (13).

$$A_{total}(\lambda 1) = (\varepsilon HbO2(\lambda 1)[HbO_2] + \varepsilon Hb(\lambda 1)[Hb])L \quad (12)$$

$$A_{total}(\lambda 2) = (\varepsilon HbO2(\lambda 2)[HbO_2] + \varepsilon Hb(\lambda 2)[Hb])L \quad (13)$$

In determining SaO_2 it is necessary to isolate the arterial component. By taking the time derivative of the absorption in equations (12) and (13) and assuming that only the blood path length – distance between the arterial vessel and the photodetector (*vid. fig. 4.23*) – changes, the ratio of the time derivatives is expressed by the *R* value in equation (14).

$$R = \frac{dA(\lambda 1)/dt}{dA(\lambda 2)/dt} = \frac{\varepsilon HbO2(\lambda 1)[HbO_2]dL_{HbO2}/dt + \varepsilon Hb(\lambda 1)[Hb]dL_{Hb}/dt}{\varepsilon HbO2(\lambda 2)[HbO_2]dL_{HbO2}/dt + \varepsilon Hb(\lambda 2)[Hb]dL_{Hb}/dt} \quad (14)$$

Now, making a new assumption that vasodilatation (and vasoconstriction) of the arterial vessels are the same over the time, so $dLHbO_2 / dt = dLHb / dt$, last expression becomes equation (15).

$$R = \frac{\varepsilon HbO2(\lambda 1)[HbO_2] + \varepsilon Hb(\lambda 1)[Hb]}{\varepsilon HbO2(\lambda 2)[HbO_2] + \varepsilon Hb(\lambda 2)[Hb]} \quad (15)$$

The relationship between *R* and SaO_2 can then be expressed as equation (16).

$$SaO_2 = \frac{[HbO_2]}{[HbO_2] + [Hb]} = \frac{\varepsilon HbO2(\lambda 1) - R\varepsilon Hb(\lambda 2)}{(\varepsilon Hb(\lambda 1) - \varepsilon HbO2(\lambda 1)) - R(\varepsilon Hb(\lambda 2) - \varepsilon HbO2(\lambda 2))} \quad (16)$$

This last equation deviates slightly from theory. This happens because scattering effects have been ruled out from calculations; the sources' spectrums that produce the two wavelengths are not a narrowed band and the assumption about the changes in path length is not absolutely true.

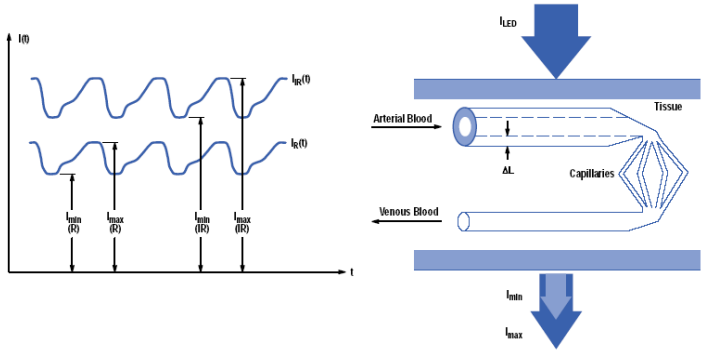

Figure 4.23 – Typical pulse oximetry curves (left) and interaction of the light with the dynamics of blood vessels (right).

An empirical relationship between R and SaO_2 must be determined for each particular sensor design by plotting the R value against known-values of SaO_2. Within this approach, the R value is calculated by taking the normalized ratio of the red absorbances to the infrared ones. This normalized value is obtained by dividing the AC component of the absorbance at that frequency by the DC component which is the same to take the time derivative of absorbances as expressed in equation (17).

$$R = \frac{AC_{red} / DC_{red}}{AC_{ir} / DC_{ir}} \tag{17}$$

4.2.2. Electronic Device.

Figure 4.24 shows the developed device for pulse oximetry. The pulses that pass through the finger are produced by two light emitting diodes or LEDs, which one with a characteristic wavelength. It is of paramount importance to fix the two LEDs and respective photodetectors to the finger by some kind of spring to prevent the appearance of motion artifacts on the recordings.

The infrared LED used was the SFH4209 from *OSRAM*® which has a characteristic wavelength around 950 nm. Its spectrum is not a narrowed peak but has a small bandwidth around the central wavelength which covers the stipulated infrared wavelength of 940 nm.

The red LED used was the L-934SRC-G from *Kingbright*® and has a similar emitting spectrum of the infrared one but centred at 660 nm.

Another important electrical parameter to receive a special attention was the maximum value of the forward current permitted to flow through the LEDs without damaging them. When working close to the maximum value of this current, the LEDs will have its maximum irradiance (intensity) of light.

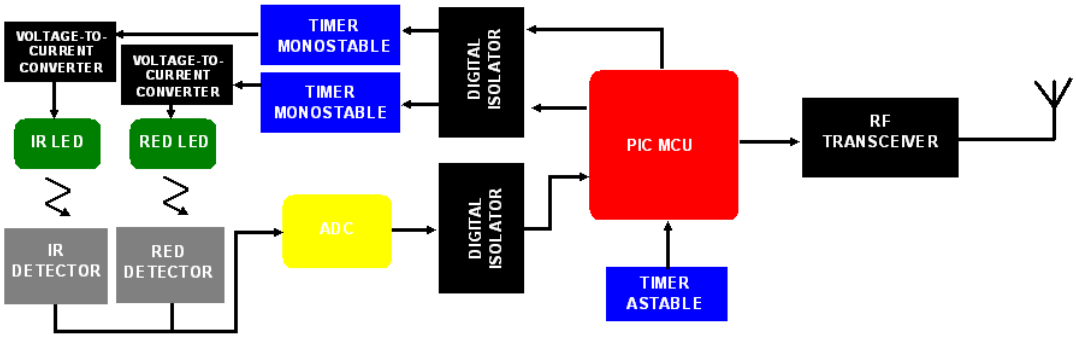

Figure 4.24 – Block diagram of the pulse oximetry device.

The infrared LED permits a forward current that do not exceeds 100 mA while the red one permits a current of 30 mA. This current is provided by a voltage-to-current converter built around the operational amplifier OPA2604 from *Burr Brown*®, as shown in *fig. 4.25.*

The OPA2604 is a dual, FET-input op amp designed for enhanced AC performance. Very low distortion (0.0003% at 1 kHz), low noise (10 nV/√Hz) and wide bandwidth (20 MHz) provide enough performance to work as a voltage-to-source converter that fully fits the project specifications.

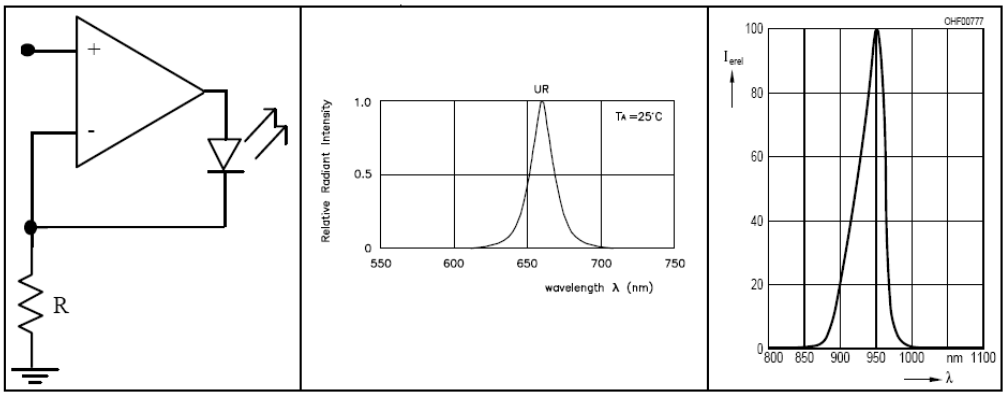

Figure 4.25 – Voltage-to-current converter (left). Spectral emission of the RED (center) [40] and IR (right) [41] light emitting diodes.

Working as a current source implies that the op amp will have a configuration which is different from its typical operation as an amplifier. The input voltage pulses will be applied to the positive input terminal, V_{IN}^{+}, instead of the negative one, V_{IN}^{-}, and, in the usual negative feedback loop will be placed the LED with the cathode connected to the voltage output terminal, V_{OUT}. In such configuration and having in mind that there is no current flowing in the input terminals of the op amp, all the current will flow from V_{OUT} to ground through the resistor *R*.

Applying the *Ohm's law* to this path and the fact that $V_{IN}^{+} = V_{IN}^{-}$, the flowing current *I* will be given by equation (18).

$$I = \frac{V_{IN}^{-}}{R} \tag{18}$$

That is, the voltage applied in the input will be converted in current by *R*, hence the name voltage-to-current converter or current source controlled by voltage. This flowing current is the forward current mentioned above and needs to be kept within certain ranges. The pulses will have an amplitude of 5 V (TTL logic) which implies a minimum value of 50 Ω for the IR resistor to give a maximum value of 100 mA for the forward current and a value of 160 Ω for the RED resistor. In practise and because the pulse signal has a duty-cycle less than 10%, the value for *I* can be exceeded without damaging the LEDs.

4.2.2.1. Generation of the Excitation Pulses.

The excitation pulses or the rectangular signals that will excite the two LEDs are produced by the PIC MCU. As mentioned, each rectangular signal will be a TTL signal with a

frequency of 500 Hz and a duty-cycle of 5%, which means that, each signal will stay on for no more than 100 µs in a period of 2 ms.

The reasons for choosing such parameters are the following ones:

- The need for signals to be taken on alternatively, that is, in each time interval of 1 ms, only one LED – the red or infrared – alternatively stays on for 100 µs. This prevents the photodetectors to respond to the excitation pulses others than the corresponding LED pulses, given that the spectral responsivity of each photodetector is not a narrowed band centred in the characteristic wavelength and, consequently, it will appear some distortion in the detected signal if the pulses were to be taken on simultaneously.
- The signal on will last for about 100 µs to allow the ADC to acquire at least five data samples of the corresponding photodetector response when there is light passing through the finger. If this time was expanded there would be the risk of the pulses do not pass through the finger and reach the detector.

To produce the excitation pulses, two digital I/O port pins of the PIC MCU were used. The voltage levels at these pins are, at most of the time, 3.3 V with a drop to 0 V only when it is time to trigger the excitation circuit. Once again, to convert the levels outputted by the microcontroller to the 5 V TTL logic it was used the available digital isolator - ADuM1400 – and, to invert the trigger signals, it was used the 555 timer, now working in monostable mode, *vid. fig. 4.27*.

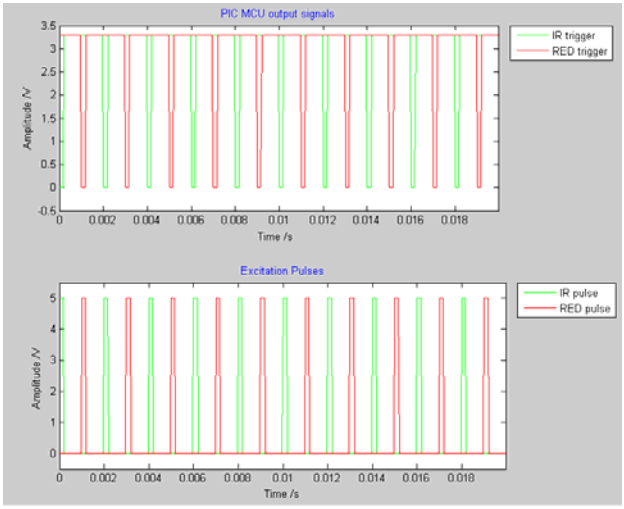

Figure 4.26 – Trigger signals produced by the microcontroller (top) and corresponding excitation pulses (bottom).

In contrast with the astable mode, the operating mode of the timer in the monostable configuration requires only an external resistor *R* and a capacitor *C* [37]. The threshold and discharge pins are now tied together while the trigger pin works as an input pin that waits for the negative-going pulse provided by the PIC MCU, *vid. fig. 4.27*. The sequence of events starts when a voltage below *1/3* V_{cc} is sensed by the trigger comparator. On the falling edge of the input pulse, the device triggers, the output goes high and the discharge transistor turns off. *C*

starts charging through the timing resistor *R*. The voltage on the capacitor increases exponentially with a time constant $T = RC$, and it will reach $2/3\ V_{cc}$ level in 1.1 time constants.

This voltage level trips the threshold comparator which in turn drives the output low and turns on the discharge transistor. The capacitor discharges very rapidly and the timer completes its cycle. It will now wait for another trigger pulse from the PIC MCU.

To give a signal on that lasts for 100 µs, *R* has a value of 10 kΩ and *C* a value of 10 nF.

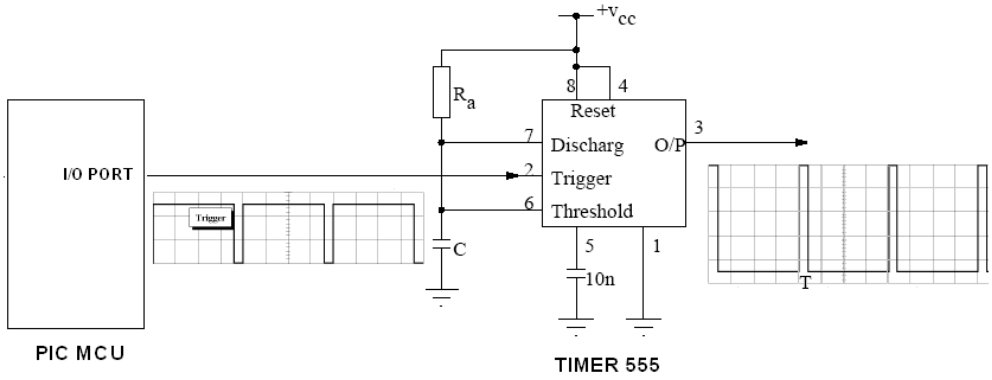

Figure 4.27 – Conversion from trigger inputs to excitation pulses by the 555 timer.

4.2.2.2. Detection Stage.

Having described the excitation circuit for the two light sources, now it is time to look at the detection circuit. It is made by two photodetectors with a spectral responsivity that resembles a Gaussian curve centred at the characteristic wavelength and a *FWHM* that permits the detectors to respond to a large set of wavelengths around the characteristic one. For instance, in this project and with the available electronic components, the red photodetector is able to respond perfectly to the IR pulses. For this reason, it was necessary to take the pulses on alternatively to avoid this kind of responses, as explained earlier.

The photodetector responsible to respond to the red pulses that was used in this project was the TSL257 while for the infrared one was the TSL260R, both from the same family of light-to-voltage converters from *TAOS*®. The spectral responsivity of each one is shown in *fig. 4.28*, as well as the internal functional block diagram and the external aspect which resembles a bipolar transistor.

The optoelectronic converters used combine a photodiode with a transimpedance amplifier on a single monolithic CMOS integrated circuit. The output voltage is directly proportional to light intensity (irradiance) on the photodiode and it is within the supply ranges of 0 – 5V. The basic principle involved is that of the **photoelectric effect**: when the photodiode is stricken by the photons from the excitation pulse, its internal material releases electrons in proportion to the intensity of the incident beam, forming a current of free electrons which is converted to a proportional voltage by the RC circuit present in the negative feedback loop of the transimpedance amplifier.

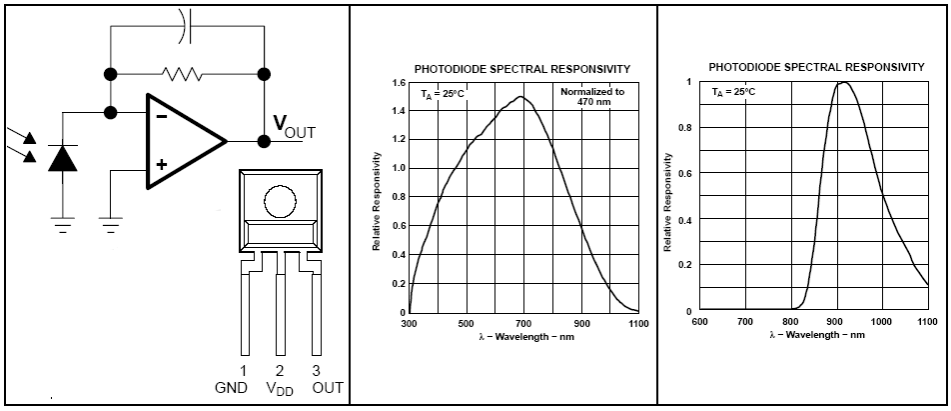

Figure 4.28 – Transimpedance amplifier (left) [42]. Spectral responsivity of the RED (center) [42] and IR (right) [43] photodetectors.

4.2.2.3. Sampling Process and Control.

To sample the voltage output from the two detectors it was used the same ADC as in the ECG wireless device – the AD974 – so, all the conversion control and data reading processes are the same as the ones explained before. The only difference is that, now, only two channels are required, each one with a higher sampling frequency, i.e., 12.5 kSPS *per* channel. That is, within every time interval of 1 ms, the ADC must acquire and convert 25 data samples altering from one channel to the other.

Again, the event that triggers the sequential acquisition of 25 data samples for a period of 1 ms is a negative-going pulse seen by the PIC MCU and provided by the 555 timer, operating in astable mode.

Such higher sampling frequency is needed to acquire at least 5 data samples when an excitation - which lasts for only 100 µs – is on and 20 data samples when the excitation pulse is off for background noise reduction. These samples are then used in a clustering process implemented inside the program memory of the PIC MCU. After the processing, the result of the clustering will be held in a vector of calculated median values inside the data memory of the microcontroller before being transmitted in a packet *via* wireless, quite in a similar way as in the ECG wireless device.

4.2.2.4. Microcontroller C Program: Overview.

At power-up, the microcontroller starts to configure the I/O ports as well as the SPI1 and UART1 interfaces and the interruption routines. When the program reaches the main cycle of events, the microcontroller starts to acquire five consecutive data samples from a particular photodetector, *vid. fig. 4.29*. Then, it computes the median value from the acquired samples using a *bubble sort* routine, storing the value in a temporary cluster vector inside the data

memory. If this vector is already filled with five median values, the PIC MCU subtracts the first median point acquired when an excitation pulse was on by the mean of the last four median points, taken when the pulse was off. This operation is performed for background noise reduction. The value thus obtained is stored inside the data transmission packet. If the cluster vector is not filled with all the five median points, the program goes back to the beginning of the main cycle and starts to perform more five acquisitions.

The interruption routines working in parallel to the main cycle are the same as the ECG interruption routines: RX1 and INT1. This last interruption is responsible for changing the excitation circuit between the RED and IR signals hence, making that, at each time interval of 1 ms, the data samples are acquired alternatively from each photodetector.

Again, whenever the computed values resulting from noise subtraction fill the 60 available positions in the data transmission packet, the PIC MCU starts to transmit it.

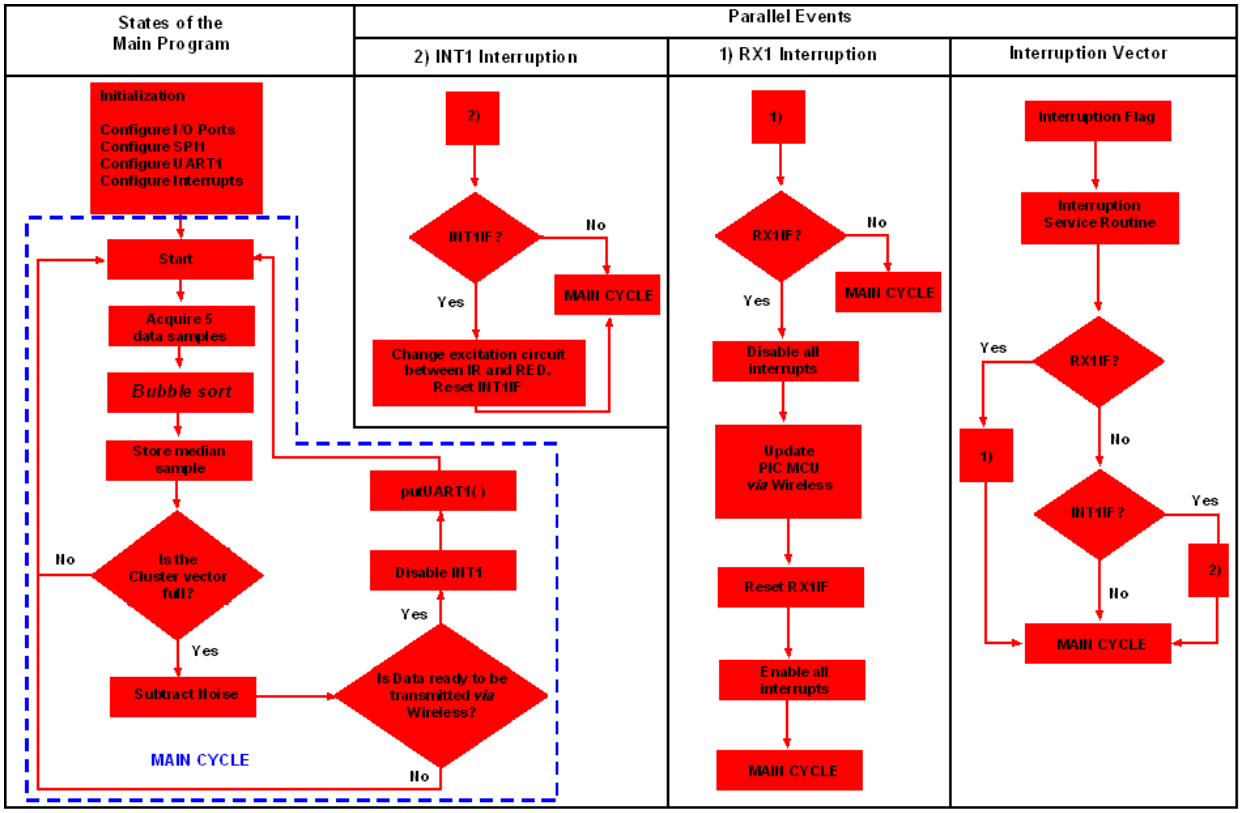

Figure 4.29 – Flowchart of the instruction events that take place inside the program memory of the microcontroller.

4.2.3. Signal Processing Techniques.

Signal processing algorithms in pulse oximetry waveforms are typically applied in the time domain utilizing clustering and moving average (filtering) techniques.

In a clinical environment, a photodetector picks up ambient light and electromagnetic noise from various sources. The major source for ambient light is room illumination, typically fluorescent ceiling lamps. Electrical noise also comes from the power lines that shows up as harmonics of the line frequency. In addition, patient motion and respiratory variation also show up in the captured waveforms which lead to an inaccuracy in computing the oxygen saturation level. To optimize the signal-to-noise ratio it is usual to use analog filtering and weighted moving average processes.

The first algorithm used in this project to optimize this ratio was the clustering method, implemented inside the program memory of the PIC MCU.

A typical signal that comes from the photodetectors is shown in *fig. 4.30*. As it can be seen, for the case of the infrared detection, the signal is corrupted with bands of data points that deviate up and down from the pulse oximetry curve. This noise can be eliminated using a clustering algorithm applied to the data that results from the analog-to-digital conversion and is temporarily available inside the data memory of the PIC MCU.

The clustering algorithm developed for pulse oximetry consists of taking every five consecutive data samples from the ADC and to determine the respective median value. The reason to take the median value instead of the mean value is that the latter is more sensitive in the presence of extreme data values than the former one. So, by applying this algorithm it is the same as doing a decimation process in the data sequence because from five data samples taken when a pulse signal is on, we ended up with only one data value and, from twenty data samples taken when a pulse is off, we get four data values. The overall sampling frequency is reduced from 25 kSPS to 5 kSPS.

Since the PIC MCU has a limited instruction set it was developed the simplest clustering algorithm possible to run inside the program memory without causing the microcontroller to stop executing instructions due to the complexity of the clustering code. So, the strategy adopted was to store every five consecutive binary samples inside a vector as soon as they were available and to perform a *bubble* sort to the vector. Finally, in the end of the processing, the median value can be read from the index position number three of the vector.

With the median data points available, one last operation was performed by the microcontroller: the median data point that corresponds to the pulse taking on was subtracted by the mean value of the four median data points that correspond to the pulse taking off in each time interval of 1 ms. Again, the overall sampling frequency is reduced to 1000 SPS and the difference signal can be seen in the bottom of *fig. 4.30*. It is the result of this subtraction that is stored in the transmission packet and subjected, after being received in the remote recording system, to the second signal processing algorithm – the moving average method.

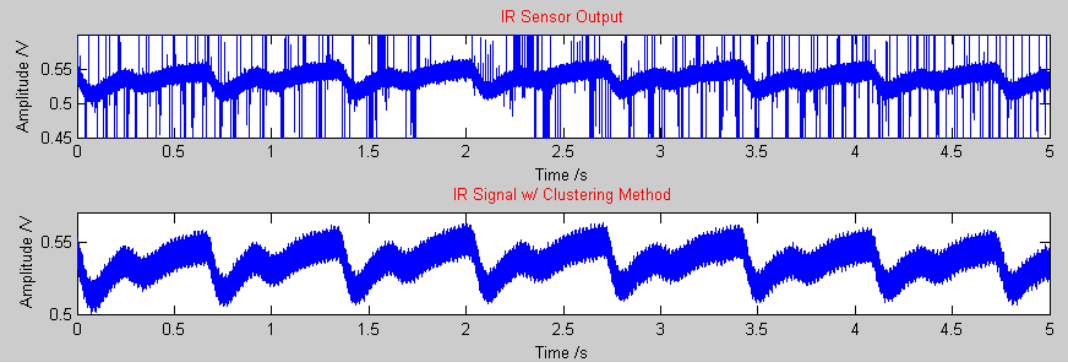

Figure 4.30 – Output signal that comes from the IR detector (top) and corresponding signal after the application of the clustering method (bottom).

The moving average algorithm is a time-discrete system defined mathematically as a transformation that maps an input sequence with values *x[n]* into an output sequence with values *y[n]* [1] and denoted according to equation (19).

$$y[n] = T\{x[n]\} \tag{19}$$

The value of the output sequence at each value of index *n* can depend on *x[n]* for some values of *n*. The general moving average system used in this project is defined by equation (20).

$$y[n] = \frac{1}{M_1 + M_2 + 1} \sum_{k=-M1}^{M2} x[n-k] \tag{20}$$

The system computes the *nth* sample of the output sequence as the average of $(M_1 + M_2 + 1)$ samples of the input sequence around the *nth* sample. The tested values for the algorithm that better fit to the typical pulse oximetry waveforms are $M_1 = 10$ and $M_2 = 10$. This process is also referred to as FIR filtering.

The moving average algorithm just described is applied to the data received *via* wireless by the recording equipment because, as it can be seen, by applying this algorithm, the length of the output data sequence is not abruptly reduced as in the case of the clustering process. So it was worthless to order the PIC MCU to internally compute the moving average algorithm in a situation in which the transmission packet size wouldn't be reduced and it would certainly exist a remote processor in the recording equipment with a better performance. In addition, the values for M_1 and M_2 can easily be changed in software, as the case of MATLAB®, running on the recording equipment. The result of the moving average algorithm is shown in top of *fig. 4.31*. It is this signal that is used for the computation of the oxygen saturation level.

After signal processing and for visualization purposes only, the pulse waveform was subtracted by its mean value, followed by an inversion along the time axis for the signal resemble the typical pulse oximetry curve seen in clinical monitors.

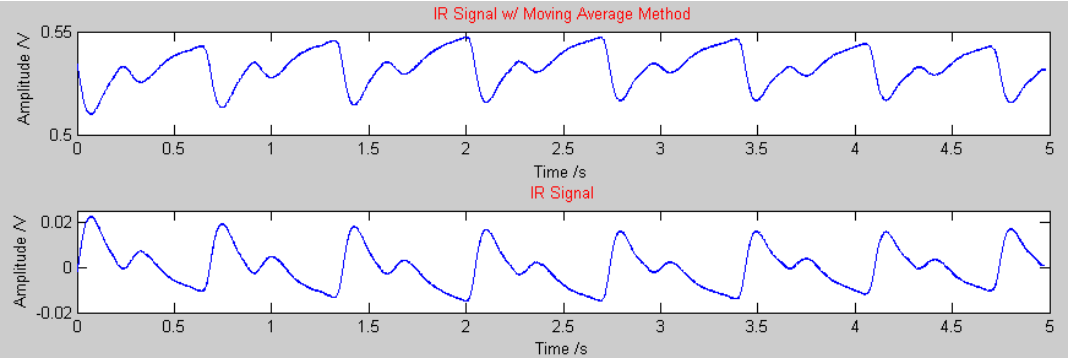

Figure 4.31 – IR signal after the application of the moving-average method (top) and typical pulse oximetry curve (bottom).

4.2.3.1. Computation of the Saturation Level.

Fast Fourier transformation of time series oximetry waveforms has produced some important spectral components, as shown is *fig. 4.32* for the pulse signal with DC level and *fig. 4.33* for a more detailed signal around the DC level. These components are: a DC offset component at 0 Hz; a respiratory component at 0.2 Hz and an AC component at 1.5 Hz and its harmonics.

In computing the *R* value only the magnitudes of the DC and AC components detected in both red and infrared frequency spectrum are used, in accordance with equation (17). To do that, an algorithm implemented in the recording equipment quickly calculates the mean value (DC) of both red and infrared signals and also searches for the maximum magnitude peak present within the cardiac physiologic spectrum of both signals, from 0.5 Hz to 2.5 Hz, which corresponds to the pulsatile component of blood.

To obtain the real SaO_2 it was used the approximate formula: $SaO_2 = 110 - 25R$, from commercial pulse oximeters [13]. Of course, to reach a more accurate value for the SaO_2 it would be necessary to run a calibration procedure with volunteers whose pulse saturation levels were known by an available commercial pulse oximeter and to adjust those values to the *R* ratio obtained with the developed device at the same time.

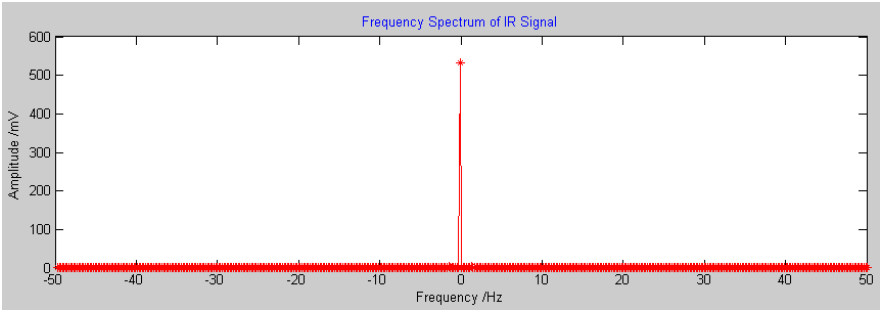

Figure 4.32 – Frequency spectrum of an oximetry waveform: the DC offset is quite evident.

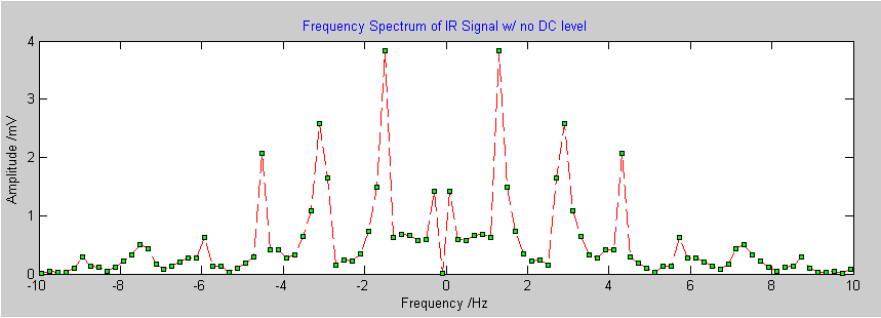

Figure 4.33 – A more detailed frequency content of the oximetry curve without the DC component.

A more rigorous method to obtain an absolute accurate value for oxygen level saturation would consist in an intra-arterial catheter oximetry performed to volunteers.

4.3. PROTOTYPE III: Bioimpedance Reography.

When we apply electricity from an external source outside the living organism under study, we are measuring bioimpedance. This **exogenic current** emerges in opposition with the electric currents associated with life processes and their biopotentials, the so-called **endogenic currents** that are internally generated in the tissue [44].

Tissue can be characterized as a dielectric or an electrolytic biomaterial that can be examined with sine, step or other waveform signals. Bioimpedance measurements give information about electrochemical processes in the tissue and can hence be used for characterising the tissue or monitoring physiological changes.

Bioimpedance and its frequency dependence differs greatly between different cell suspensions and tissues and significant changes in the electrical properties are also found when cells or tissues go from one physiological state to another.

Some of the physiological quantities estimated from electrical impedance measurements include respiration, blood flow and volume changes, autonomic nervous system activity, muscle contraction, eye movement and the activity of brain cells.

A typical bioimpedance measuring system is comprised of a sine-wave oscillator followed by a voltage to current converter [45]. This converter outputs sinusoidal current of constant amplitude which can be passed through the tissue segment with a pair of injector electrodes. Voltage signal developed along the current path is then sensed with another pair of electrodes and the signal is used to calculate the tissue bioimpedance under study as a function of time.

4.3.1 *DC* Current Effects.

DC which stands for direct current is a current flowing in the same direction all the time in contrast with the alternate current or AC. A galvanic current is the same as DC current and the term is used in particular for therapeutic applications. A galvanic (electrolytic) cell produces or passes DC. If it does not, it is a dielectric cell and only displacement AC passes. The effects produced in a tissue by a DC current in comparison with an AC current are therefore quite different [44].

DC implies tissue polarization caused by a transport of matter to an extent not found in AC due to the unidirectional flow of current. Living tissue is electrically and macroscopically predominantly an electrolytic conductor. An electrolyte is a substance with ionic DC conductivity. In pure electrolytes the charge carriers are ions and there is no separate flow of electrons: they are all bound to their respective atoms. Tissue DC currents are, therefore, ionic currents in contrast to the electronic current found in metals. Ion current implies a transport of substance, so, an externally applied DC current can not flow forever without changing its conductor and must be blocked when performing living tissues studies, allowing only AC displacements within certain frequency ranges (far enough from DC) to pass.

The electric current appears whenever there are free charges and a field acting over them. In a conductor and for weak electric fields it is valid the *Ohm's Law* given by equation (21).

$$J = \sigma E \quad , \tag{21}$$

where J is the current density (A m^{-2}), σ is the conductivity (Ω^{-1} m^{-1}) of the conductor and E is the applied electric field (V m^{-1}). In metals, for instance, it is this electric field that gives an extra oriented velocity to electrons, originating an electric current. It is worth to note that, according to *Ohm's Law*, the charges are not accelerated: the field equilibrates the friction shocks and velocity keeps constant.

If J is constant through the entire extension of a cylindrical conductor with length L and cross sectional area A, as shown in *fig. 4.34*, the electric current I that flows between its extremities is expressed in equation (22).

$$I = AJ = A\sigma E \tag{22}$$

The potential difference V developed between the bases of the cylinder is related to the applied electric field as expressed by equation (23).

$$V = V_1 - V_2 = EL = RI \tag{23}$$

Equation (23) is the most known version of the *Ohm's Law* which associates the potential difference developed between two points of a conductor material with the current that flows between them and the resistance of the material. In the cylindrical model, resistance R is a property of the material and its geometry and it can be given by

$$R = \frac{L}{\sigma A} = L\rho A \quad , \tag{24}$$

where ρ is the resistivity of the material with units of Ω.m which are the inverse of the conductivity σ.

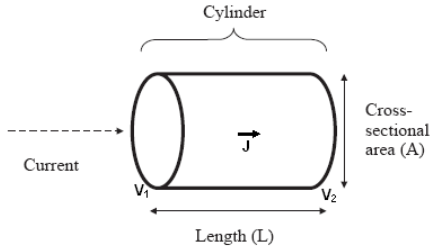

Figure 4.34 – Cylindrical geometry used for bioimpedance calculations. Translated from [44] with modifications.

4.3.2. Biological Tissue Resistivity.

Biological tissues show some variations in the values of their electrical resistivity. For instance, the electrical resistivity values for plasma, cerebrospinal fluid, blood, cardiac muscle, fat and bone are 63, 65, 150, 750, 2500 and 16600 Ω cm respectively [45]. Though these values are higher when compared to a good conductor of electricity like cooper, the wide variation in the resistivity values from one biological tissue to another makes the measurement of electrical resistance useful in understanding the functioning and viability of internal organs of the body.

Impedance is a more generic term used in electronics and it is defined as the opposition that a device offers to the passage of an electric current through it, at some frequency value. The general formula for impedance is given by equation (25).

$$Z = \frac{V}{I} = \frac{|V| \exp(j\alpha_v)}{|I| \exp(j\alpha_i)} \tag{25}$$

That is, it depends on the voltage and current signal modules as well as their phases. So, impedance can be represented by a complex quantity as the sum of a real part – resistance *R* – with an imaginary one – reactance *X* – for each frequency value as expressed in equation (26).

$$Z = R + jX = |Z| \exp(j\theta), \quad |Z| = \sqrt{(R^2 + X^2)} \tag{26}$$

The vectorial representation of impedance is shown in *fig. 4.35*. Sometimes, for practical reasons, it is more convenient to use its inverse, *1/Z*, which is called admittance, represented by *G*.

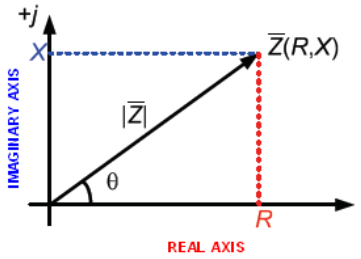

Figure 4.35 – Complex representation of impedance.

When current is applied to a body tissue instead of an electronic component it is sometimes called bioimpedance or biological impedance.

In this project, the target of study is the electrical impedance changes in blood stream within the ventricular chamber during the cardiac cycle. Since blood is a good conductor of electricity, the amount of blood in a given body segment is reflected inversely in the electrical impedance of the body segment. Pulsatile blood volume increases in the body segment caused

by systemic blood circulation and, therefore, causes proportional decrease in the electrical impedance. This variation gives adequate information about the blood circulation. Thus, the impedance value of blood volume with resistivity ρ based on the cylindrical geometry described above is given by

$$|Z| = \rho \frac{L}{A} \quad , \tag{27}$$

where, L is the length of the homogenous cylinder and A is its cross sectional area. For practical reasons, $|Z|$ will be represented simply by Z in the next equations because they dismiss phase information. The relationship between changes in blood volume v and the blood volume impedance is found by solving equation (27) for the blood volume and differentiating as shown in equation (28).

$$dv = d(LA) = -\frac{\rho L^2 dZ}{Z^2} \tag{28}$$

Finally, the dependence of the change in blood volume on the changes of blood impedance is expressed by equation (29).

$$\frac{dv}{dZ} = -\frac{\rho L^2}{Z^2} \tag{29}$$

4.3.3. Intra-cardiac Impedance Reography

Biological tissues offer two types of resistance to an electric current: capacitive and resistive. The capacitive component arises from cell membranes and it is particularly important when electrodes are placed at the body surface. Skin is the main responsible for this capacitive resistance due to its keratinized layer that blocks DC current and low frequency alternate displacements. The conduction of high frequency AC current is made by capacitive effect that occurs between surface electrodes and the inner layers of the skin which have high conductivity. So, the keratinized layer of the skin acts like a capacitor in-between the electrodes and the layers beneath [7].

The resistive component arises from extra and intracellular fluid. Several electrical circuits or networks have been used ever since to describe the behaviour of biological tissues *in vivo*. A commonly used network is shown in the left of *fig. 4.36*. It consists of a capacitor that mimics the skin capacitance in series with a circuit with two parallel electrical arms: one arm is composed by a single resistor that represents the overall resistance offered by the liquid which is directly crossed by the current; the other one consists of a resistor that represents the total electrostatic resistance along the current path which is in series with a network made by another capacitor in parallel with a resistor, representing both the capacitance and resistance of cell membranes.

The bioimpedance value decreases when the frequency goes higher which is reflected by the decrease of the value of reactance from cell membranes. At frequencies in the range of 20 kHz, membranes act as conductors of reactance even though skin still offers a considerable reactive component – this can be totally eliminated with frequencies above 100 kHz. Because of the weak capacitance of the biological tissues when working at 20 kHz, it is admissible to consider that, at that frequency, the current distributes itself through the tissue as it was a pure resistive element and it would look like the network shown in right of *fig. 4.36*.

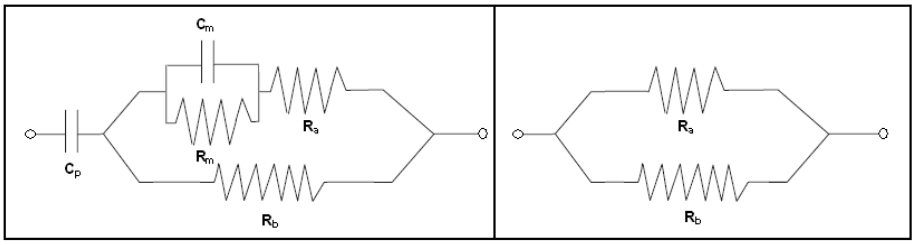

Figure 4.36 – Network simulating the total impedance from skin surface to inner cells (left). Corresponding impedance network when working at 20 kHz (right).

In the reography of the cardiac chambers, it is necessary to avoid that the electrodes move out of the cavity when it reaches the minimum volume. Thus, in most of the cardiac cycle the electrodes wouldn't occupy the poles of the cavity [7].

The blood volume within a cavity is proportional to its cross-section, thus, it is proportional to admittance as seen before. So, in measuring blood volume changes is more advantageous to record admittance changes than impedance ones as performed in classical reography. If the electrodes occupy the cavity axis, the value of admittance will be higher than with the electrodes placed in the walls due to the fact than the line forces of the electrical field close to the cavity's walls are obliged to longer trajectories. If the electrodes oscillate inside the cavity there would exist changes in the admittance recordings that are not related to blood volume changes. Hence the correct placement of the electrodes in an unchanging position must be established [7].

4.3.4. Electronic Device.

For bioimpedance measurements, the developed prototype was split in two parts: one circuit is responsible for producing the 20 kHz sine wave and to inject the current in the tissue while the other one is responsible for sensing the voltage developed and to perform all the calculations required to obtain the bioimpedance value.

A block diagram for the first circuit is shown in *fig. 4.37.* It is composed by a microcontroller whose task is to provide the binary codes for the DAC to perform the digital-to-analog conversion, generating the analog voltage sine wave. After some stages of filtering, the signal is driven to a voltage-to-current converter to produce the injection current.

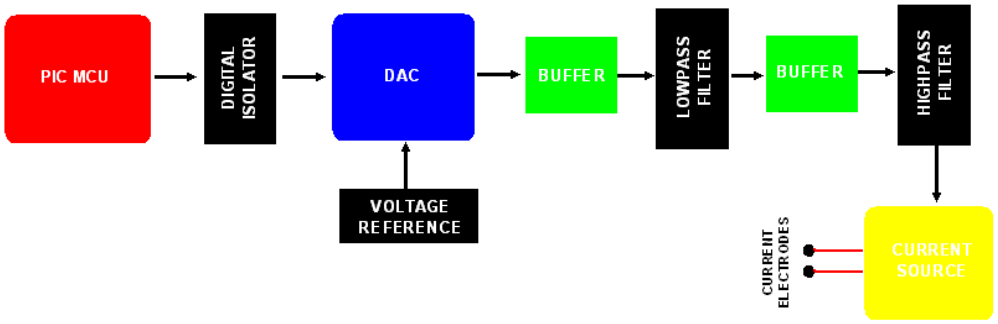

Figure 4.37 – Block diagram of the 20 kHz sine-wave generator circuit.

4.3.4.1. Digital-to-Analog Conversion.

The digital-to-analog converter used in this project was the AD5542 integrated circuit from *Analog Devices*®. The AD5542 is a single, 16-bit, serial input, voltage output DAC that operates from a single 5 V supply. Data is written in a 16-bit word format via a 4-wire SPI interface with the PIC MCU. The microcontroller uses two I/O port pins to control the serial interface, one output pin to transfer the binary words and another one to provide the clock to the DAC, as shown in *fig. 4.38*.

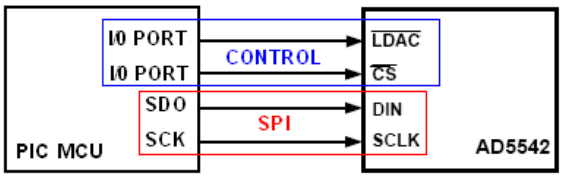

Figure 4.38 – Interface between the microcontroller and the DAC.

The only task executed by the microcontroller in the first circuit is precisely to provide the binary words via SPI to the DAC. So, in order to produce the 20 kHz sine wave, it was necessary to store in the microcontroller's data memory the binary codes needed to reproduce two periods of the sine wave in an accurately time of 100 µs. That is, in a program cycle which lasts for only 100 µs, the PIC MCU has to control and supply the DAC with 20 binary words that code the wave oscillations before the cycle repeats itself again.

The DAC architecture is segmented in two parts: the 4 MSBs of the 16-bit data word are decoded to drive 15 switches which of them connected through a resistor to either the analog ground or reference voltage. The remaining 12 bits of the data word drive the switches of a 12-bit voltage mode R-2R ladder network (*vid. fig. 4.39*).

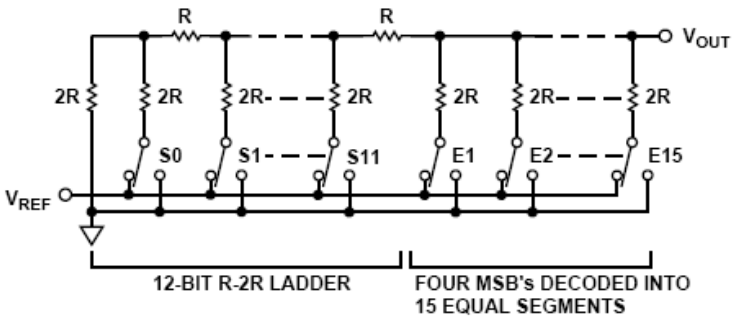

Figure 4.39 – Internal ladder network of the DAC [46].

The analog output voltage V_{out} depends on the reference voltage V_{ref} as well as the decimal data word D_w and the resolution of the DAC. The complete equation is given in equation (30).

$$V_{out} = \frac{V_{ref} D_w}{2^{16}} \tag{30}$$

The voltage level used for the reference was 2.5 V, supplied by the ADR430 IC also from *Analog Devices*®. A Kelvin connection was made for the force and sense reference voltages included in the DAC, according to the diagram shown in *fig 4.40*. This connection offers a convenient method of eliminating the effects of voltage drops in circuit wires.

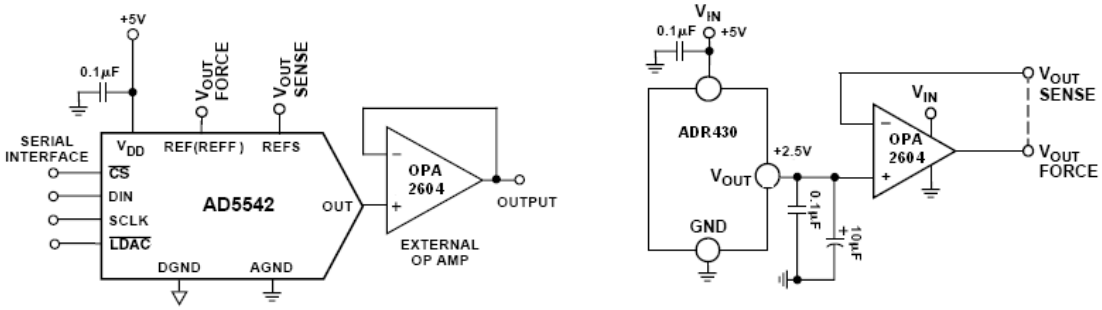

Figure 4.40 – Pin diagram of the DAC (left) and Kelvin connection for force and sense reference voltage input pins (right). Figure on the left was translated from [46] with modifications and figure on the right was translated from [47] with modifications.

The AD5542 is controlled by a 4-wire SPI interface which can operate at clock rates up to 25 MHz. The timing diagram for the digital-to-analog conversion process appears in *fig. 4.41*. A high-to-low transition on $\overline{CS}$ starts the transfer of data words from the *SDO* pin of the microcontroller towards the *SDI* pin of the AD5542.

The data is loaded MSB first to the input register on every rising edge of the serial clock $SCLK$, also provided by the PIC MCU. After 16 data bits have been loaded into the input register, a low-to-high transition on $\overline{CS}$ transfers the contents of the shift register to the DAC. Finally, a high-to-low transition on the $\overline{LDAC}$ pin allows the DAC to be updated with the voltage level coded by the data word.

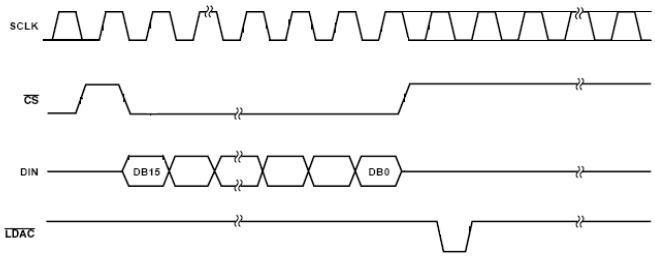

Figure 4.41 – Timing diagram that controls the process of updating the DAC with new binary words. Translated from [46] with modifications.

4.3.4.2. Buffering and Filtering Stages. Voltage-to-Current Conversion.

The analog voltages outputted by the DAC pass through an op amp mounted in a buffer configuration. The selected op amp was again the OPA2604 which has a very low-offset voltage as well as very low input bias current and high input impedance needed to minimize gain errors and not to impede the settling time of the DAC. This buffer configuration is frequently used in electronic circuits because it takes advantage of the high input impedance (and low output impedance) of the op amp, isolating two independent blocks of any circuit.

The next stages on the diagram block of the circuit are the filtering ones, shown in *fig. 4.42*. In order to obtain a 20 kHz sine wave with low harmonic distortion, the upper harmonics of its frequency spectrum were attenuated first by a lowpass filter of 1st order with a cutoff frequency around 32 kHz. To do so, it was used the typical RC circuit dimensioned with a resistor of 5 kΩ and a capacitor of 1 nF.

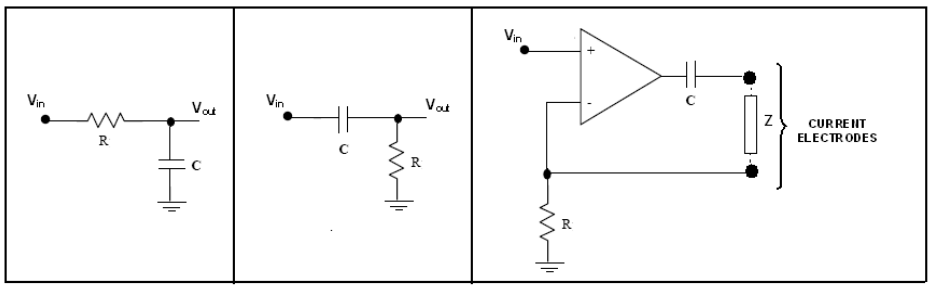

Figure 4.42 – 1st order lowpass (left) and highpass (center) filters. Current source with ejecting electrodes (right).

The following filtering stage consists of a 1st order highpass filter projected to attenuate the low frequencies of the spectrum attempting to block the DC component. The cutoff frequency chosen for this filter was 5.3 kHz derived from a RC circuit with R = 3 kΩ and C = 10 nF.

The last stage of the circuit is a current source controlled by voltage. The positive input terminal of the OPA2604 is fed with the 20 kHz sine wave whose amplitude is 2.5 V_{pp}.

As mentioned before, the current that flows in the negative feedback loop and will be injected in the tissue is given by V_{in}/R so, to have a safety maximum current of 1 µA it was used a resistor of 3 MΩ. The capacitor placed in the feedback loop is used to block the DC component that can arise from the operation of the op amp for the current signal not to have mean value. The frequency spectrum of the sine wave that enters the source current is shown in *fig. 4.43*.

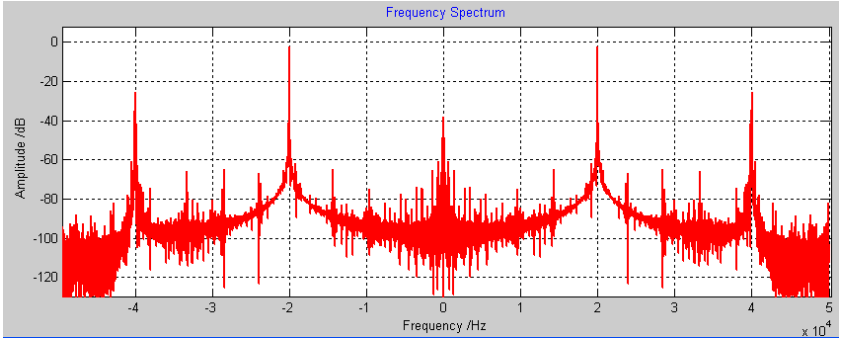

Figure 4.43 – Frequency spectrum of the 20 kHz sine-wave.

4.3.4.3. Acquisition and Processing Circuit.

The second circuit involved in the bioimpedance measurement system is shown in *fig. 4.44*. Briefly, it consists of an amplification stage followed by a processing one performed by the PIC MCU and the obtained result can be outputted in two ways: via USB or digital-to-analog conversion through a wire connection.

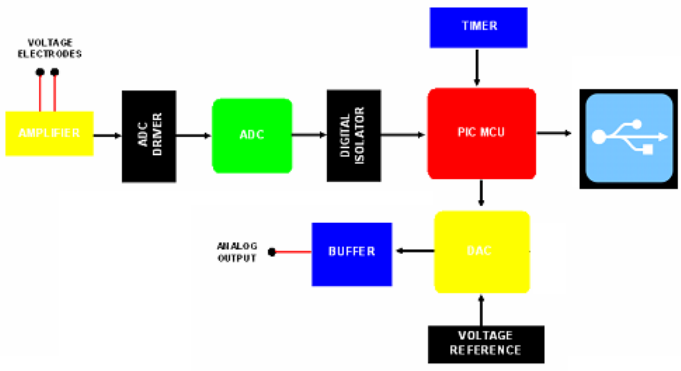

Figure 4.44 – Block diagram of the acquisition circuit.

Two voltage electrodes are responsible for sensing the voltage difference developed across the tissue current path. This voltage difference is then amplified by the INA116 integrated circuit from *Burr Brown*® with a gain settled to 500 V/V.

The INA116 is a complete monolithic FET-input instrumentation amplifier with extremely low input bias current (≈ 3 fA) and high input impedance (≈ 10^{15} Ω). It has guard pins adjacent to both input terminals that are used to drive circuit board and input cable guards to maintain extremely low input bias current, *vid. fig. 4.45*. The rest of the diagram block of the amplifier is similar to the INA111 used before in the ECG biopotential measurements.

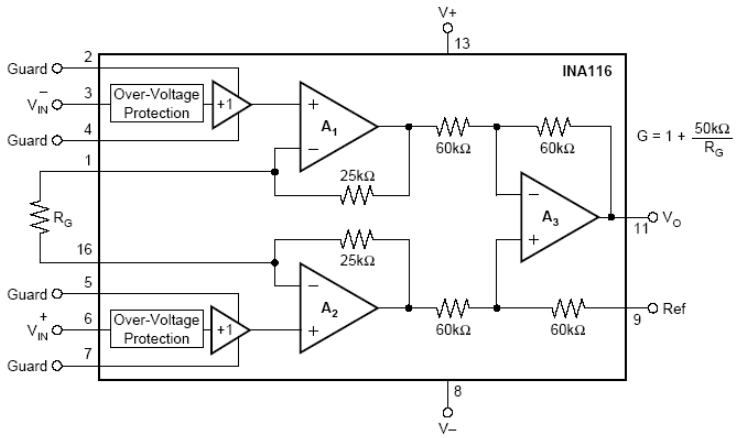

Figure 4.45 – Internal structure of INA116 [33].

The use of guard pins connected to the electrode cable guards has made the use of any kind of filter circuit between the electrodes and the input terminals of the INA116 to become useless and unpractical.

The analog-to-digital conversion is performed by the AD7982 integrated circuit from *Analog Devices*®. The AD7982 is an 18-bit, single channel, successive approximation ADC that operates from a single power supply of 5 V. It also has a 3-wire SPI interface with a sampling frequency up to 1 MSPS which is enough to acquire and sample 20 data points of the input signal in a time interval of 100 µs as desired for the bioimpedance calculations. Because this ADC is a differential converter that samples the difference voltage between its two input terminals, it was necessary to transform the single-ended analog signal that comes from the amplifier into a differential input to the ADC.

To do that, it was used the AD8139 IC from *Analog Devices*®. This low noise and wide bandwidth single-ended-to-differential driver is ideal for driving ADCs with resolutions up to 18 bits. It provides two closely balanced differential outputs using simple external feedback networks consisting of a total of 5 resistors and 2 capacitors placed at the input terminals of the ADC as shown in *fig. 4.46*. Because the differential ADC has an 18-bit resolution and uses a reference voltage of 5V, the LSB value will be 38.15 µV, according to equation (5).

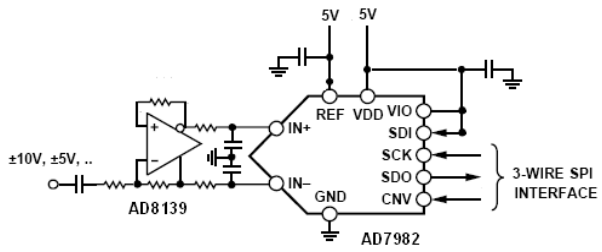

Figure 4.46 – ADC and single-ended to differential driver connections. Translated from [49] with modifications.

The timing diagram for this ADC is quite simple. A low-to-high transition on *CNV* starts every conversion. The conversion proceeds very fast and the binary code is outputted MSB first on every falling edge of the clock. After two consecutive series of 16 clock pulses, the 18-bit data code is stored in two data memory positions of the PIC MCU for further processing.

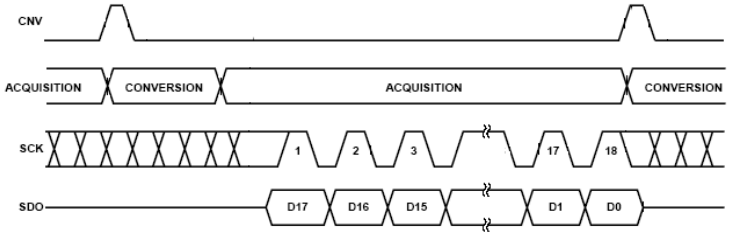

Figure 4.47 – Timing diagram that controls the sampling and bit-reading processes [49].

Once again, the programmed cycle of events inside the microcontroller is controlled by an external timer which establishes a time execution period of 1 ms. In this period the PIC MCU has to give instructions to acquire 20 consecutive data samples within a time interval of 100 µs while, in the remaining 900 µs, it has to perform all the calculations required to obtain the impedance value from the acquired samples.

After the computation, the result is converted from an 18-bit to a 16-bit data word through a cast procedure before being converter to an analog voltage value through the DAC and the digital code will be stored in a vector inside the data memory of the microcontroller before being transmitted, now, in a packet *via* USB to the computer. The limitation found on the data transfer bandwidth of the STRX2 RF transceivers used in the last two sensors has lead to the substitution of the wireless block of the circuit by a microcontroller with incorporated USB module that can communicate at rates up to 2 Mbps.

4.3.5. Bioimpedance Value Computation.

The developed device solely permits to calculate the impedance module given that it only uses one acquisition channel that measures the voltages produced across the impedance

segment. Besides, all the available information from the injected current comes from the theory, that is, it has 1 μA of amplitude and a frequency of 20 kHz. So, there is no way of estimating the value for the impedance phase. This does not constitute a big issue because in calculating blood volume changes with respect to impedance changes, it is only necessary to know the impedance module, in accordance with equations (27) to (29). To compute the impedance module it was used equation (31).

$$| Z |= \frac{V_{r.m.s.}}{I_{r.m.s.}} \tag{31}$$

The *r.m.s* value of a sine-wave signal is frequency and phase-independent and it is given by the ratio of the signal amplitude by the square root of 2. So, in what concerns the determination of the current signal's *r.m.s* value it was quite simple. For voltage it was used the mathematical formula for *r.m.s.*, given by

$$V_{r.m.s.} = \frac{\sqrt{\sum_i V_i^2}}{\sqrt{N}} \quad , \tag{32}$$

where V_i constitutes the individual N voltage samples taken by the ADC; twenty samples in total.

Due to the fact that the PIC MCU only has 900 μs of available time to make all calculations and the fact that binary operations of square power and square root are very time and memory consuming processes, it was established that the microcontroller only has to compute equation (32). The resulting voltage is then send to a personal computer where the impedance module is finally calculated and corrected from parasite impedances developed throughout the sensing device.

4.3.5.1. Microcontroller C Program: Overview.

The program developed for the microcontroller involved in the 20 kHz sine-wave generator circuit consists of sending the binary codes at precise time intervals to the DAC for the coded voltage pattern look like a sine-wave. So, in order to achieve this, the program starts by initializing all the I/O ports involved and the SPI1 interface with the DAC. No interruption routines were used. When the program reaches its main cycle, it sends sequentially 20 binary words in a 100 μs time interval before the cycle repeats itself.

The program developed for the PIC MCU integrated in the acquisition circuit is shown schematically in *fig. 4.48*. It also starts by initializing all I/O ports as well as the SPI1, SPI2 and USB *on-to-go* interfaces and INT1 interruption routine. The main cycle of the program consists, again, in waiting till the transmission packet is filled with the values that result from computing the r.m.s. of the acquired data samples. The routine responsible for collecting 20 data samples is the INT1 interruption that, after the acquisition process, computes the r.m.s. value and sends

it via SPI2 to be available in the analog interface of the circuit and also to the data transmission packet for storage.

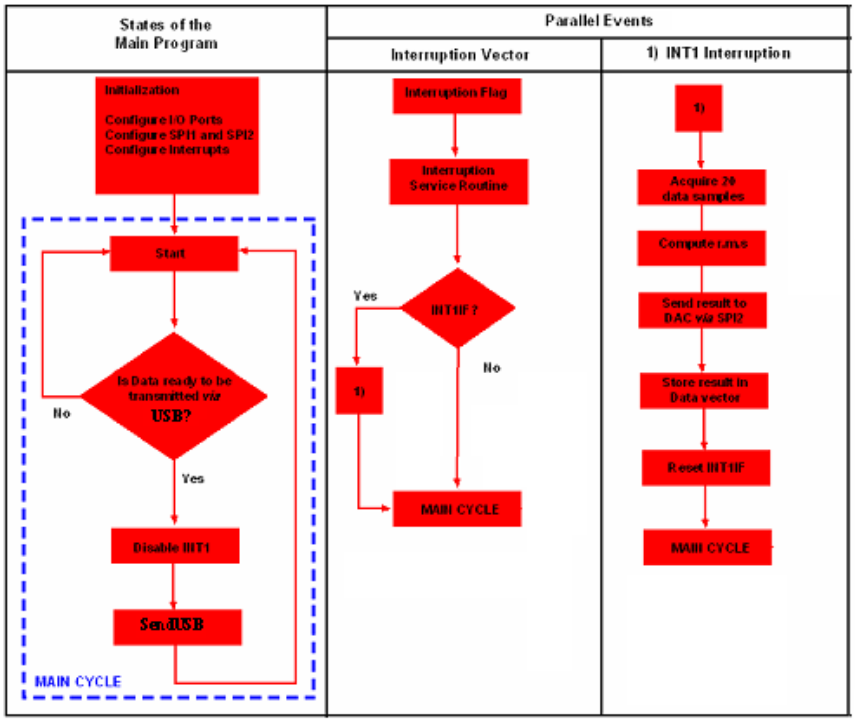

Figure 4.48 – Flowchart of the instruction events that take place inside the program memory of the microcontroller.

4.3.5.2. Calibration Stages.

The final stage consists in calibrating the acquisition circuit with external resistors whose impedance value is known in advance and some NaCl solutions with different conductivity. As external resistors have a constant value of impedance (with an associated tolerance) it is expected that the acquisition device will output a corresponding constant value for the r.m.s. voltage. Seeing that the r.m.s. value of a sinusoidal wave does not change within a period of the signal, the very fact of the injected current to pass through a resistor will result in a sinusoidal voltage signal with constant r.m.s. voltage whose value is proportional to the resistor's impedance.

In order to obtain the proportional relationship between r.m.s. voltage and impedance, it was settled an experimental procedure consisting in recording different voltage levels outputted by the acquisition system and to match them to the resistors been tested. Figure 4.49 shows a recording performed this way. It can be seen four different steps corresponding to four different resistors as well as high step variations that occur anytime a resistor is taken from the feedback loop of the voltage-to-current source and current path is therefore open.

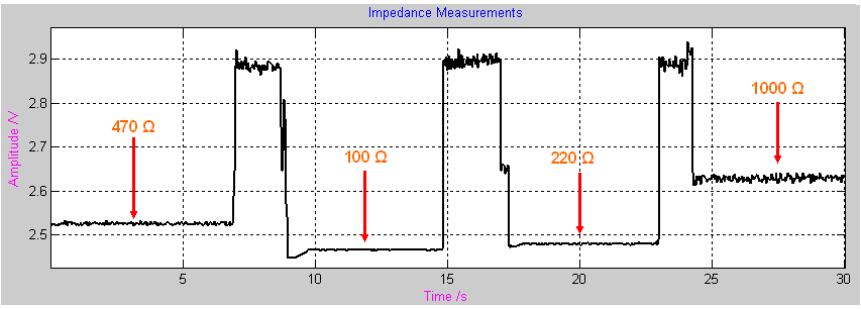

Figure 4.49 – Some impedance measurements performed with external resistors to calibrate the acquisition device.

The voltage changes are very subtle since we are dealing with current amplitudes that do not exceed 1μA and impedance values expected not to reach more than 2 kΩ. The calibration curve obtained is in *fig. 4.50*. It has an R-squared value that approaches the unity.

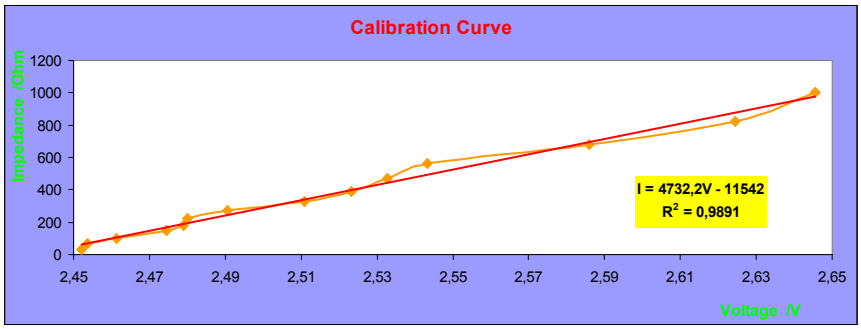

Figure 4.50 – Graphic showing the obtained fit between the computed r.m.s voltage given by the PIC MCU and the impedance values tested.

In order to obtain flat steps in the recordings, it is also implemented inside the microcontroller an algorithm that calculates the mean value of every eight consecutive calculated r.m.s. values. This way, the temporal resolution passes from 1 ms to 8 ms with no relevant consequences for the physiological variable been recorded.

For NaCl solutions, it was necessary to use a goblet with a pair of copper wires placed at each side of the goblet's diameter. In this configuration, the parasite impedances that arise from using extensive wires must be subtracted from measurements. This system is distant from been ideal because, for rigorous measurements, it must be used one pair of electrodes to inject the current while the other is used to sense the voltage developed across the impedance. Even though, it was performed a temporal impedance recording with several solutions whose impedance values were fitted by the parameters of the previous calibration and considering that the current path was the diameter of the goblet. The tested solutions had conductivity values comprised from 1413 to 12880 μS cm^{-1} or, inversely, impedance values ranging from 78 Ω to 708 Ω in a 1 cm path length.

Chapter 5

Results

5.1. Graphical Interface.

The graphical interface developed for visualization of the acquired signals is shown in *fig. 5.1*. The interface was made using the Graphical User Interface menu of MATLAB® and it displays all the physiological variables acquired in this project: EASI – ECG biopotentials, pulse oximetry and reography as well as some physiological parameters resulting from the application of digital processing algorithms such as the computation of blood oxygen saturation level and cardiac frequency.

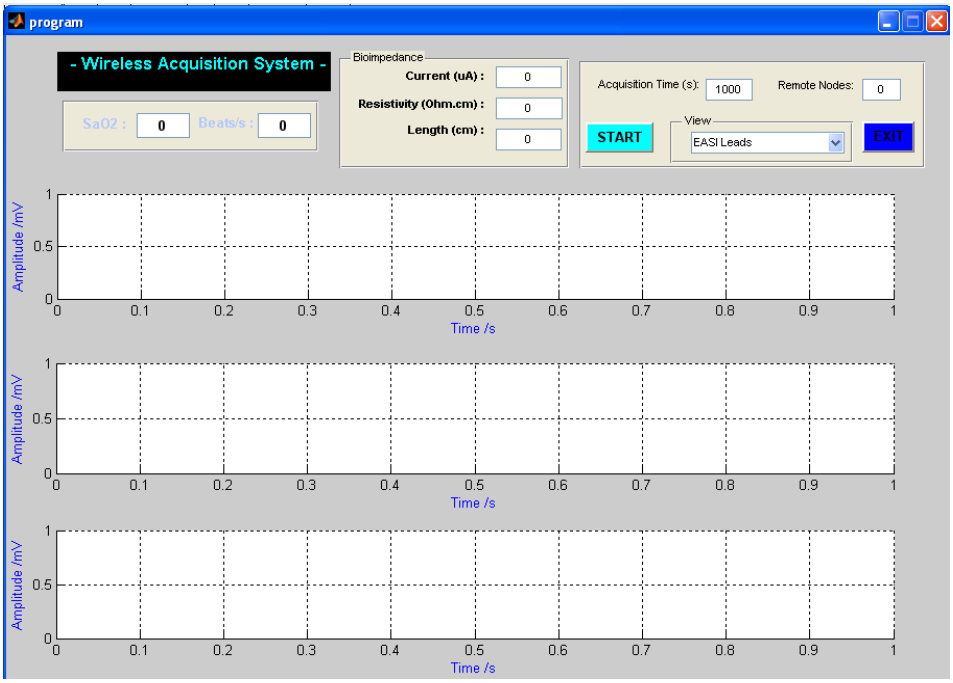

Figure 5.1 – Graphical interface developed for the acquisition system.

5.2. ECG Recordings.

For ECG recordings, temporal samples were taken from every EASI system lead. Because each lead records the potential differences between two points, the deflections in each lead at any instant indicate the magnitude and direction of the cardiac vector. Figures 5.2 to 5.4 show temporal ECG recordings obtained with the developed device.

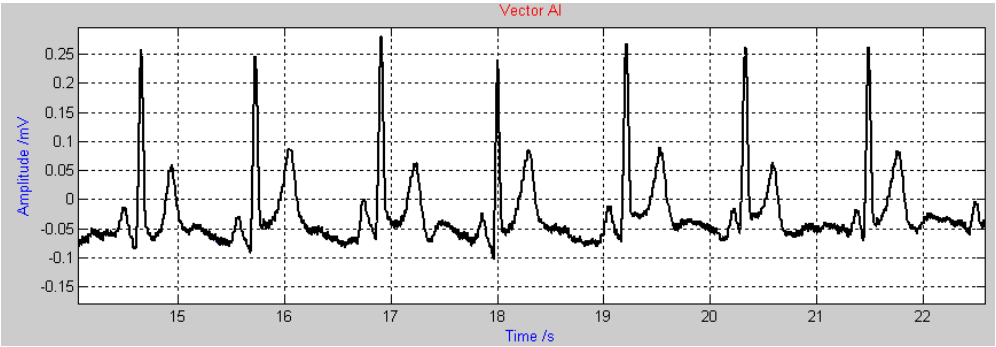

Figure 5.2 – ECG recording corresponding to the AI lead.

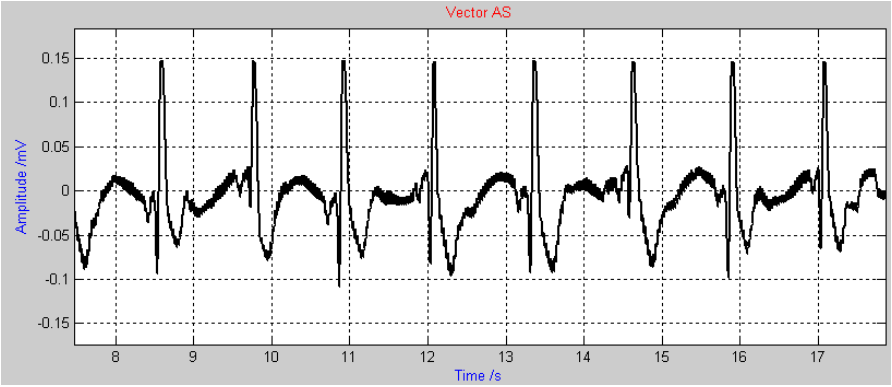

Figure 5.3 – ECG recording corresponding to the AS lead.

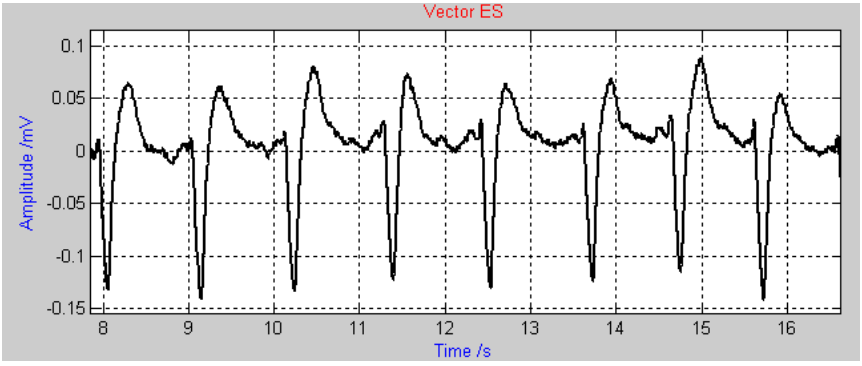

Figure 5.4 – ECG recording corresponding to the ES lead.

The device amplifies the difference between the electrode placed at the positive input terminal of the instrumentation amplifier and the electrode placed at the negative one. The

voltage convention adopted in the system was that of the electric circuits, that is, $V_{AI} = V_A - V_I$, $V_{AS} = V_A - V_S$ and $V_{ES} = V_E - V_S$. So, when a depolarization wavefront moves toward a positive electrode, it creates an upward deflection on the ECG in the corresponding lead whereas a downward deflection is created when a depolarization wavefront moves away from the positive electrode.

From the ECG curves, it can also be seen that there are seven QRS complexes reported in a time interval of 6 s which, extrapolating, gives a heart beat of 70 bpm.

5.3. Oximetry Recordings.

For pulse oximetry measurements, several tests were performed to volunteers during normal breathing and forced breath-holding to see the repercussions on the pulse waveforms and, most importantly, on the oxygen saturation levels. Before that, *figs. 5.5* and *5.6* show some of the first oximetry curves ever obtained with the developed prototype with one channel and with both channels working at the same time.

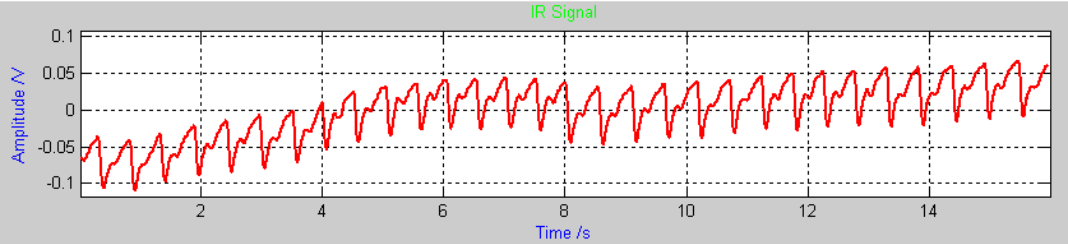

Figure 5.5 – One of the first pulse oximetry curves obtained with the developed device.

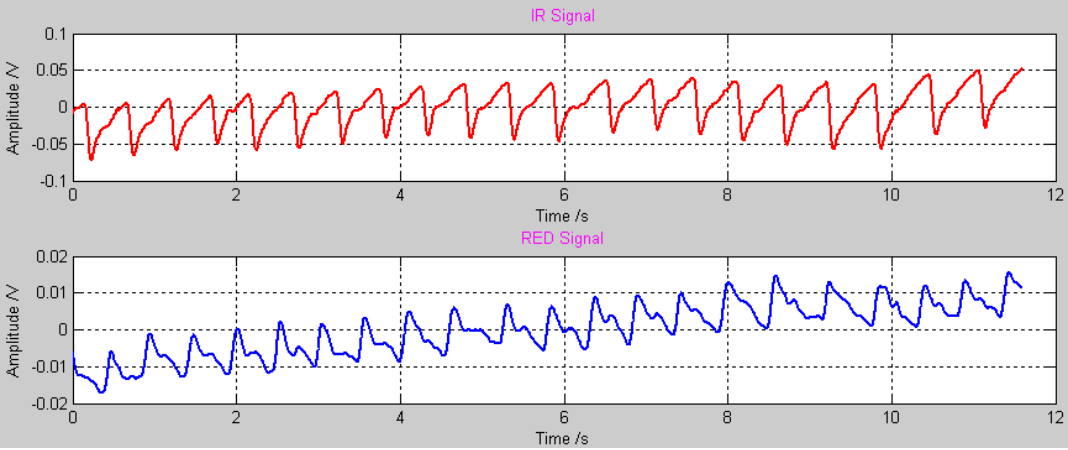

Figure 5.6 – Pulse oximetry curves corresponding to the IR (top) and RED (bottom) signals, both recorded at the same time.

As it can be seen, the IR and RED curves show a symmetric pattern. This happens so, because, at each wavelength, light is more prone to be absorbed by one substance – Hb or HbO_2 - than by the other one.

The first recording taken when the volunteer is breathing normally is exposed in *fig. 5.7* and the corresponding SaO_2 rate is shown in *fig. 5.8*.

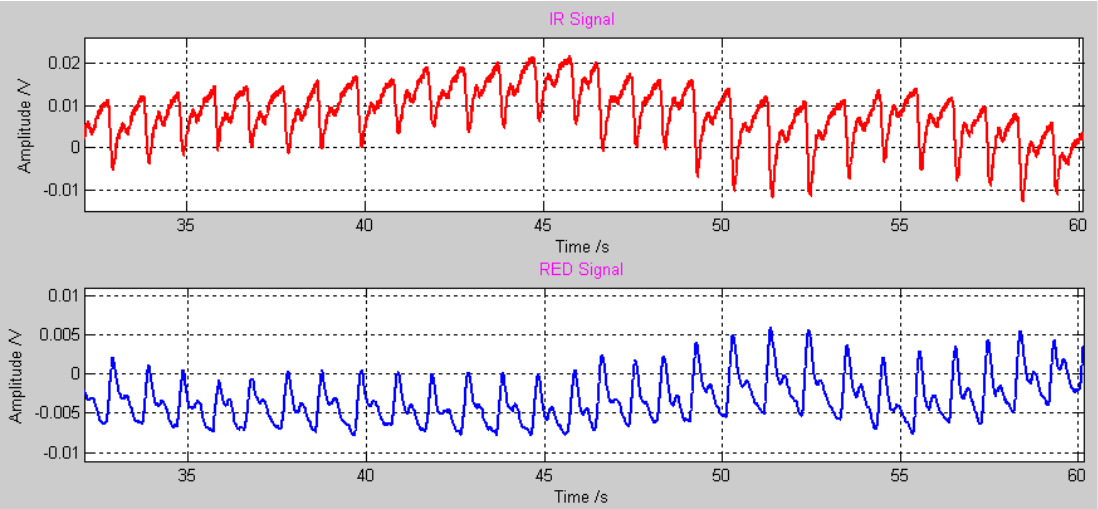

Figure 5.7 – Pulse oximetry curves obtained during normal breathing.

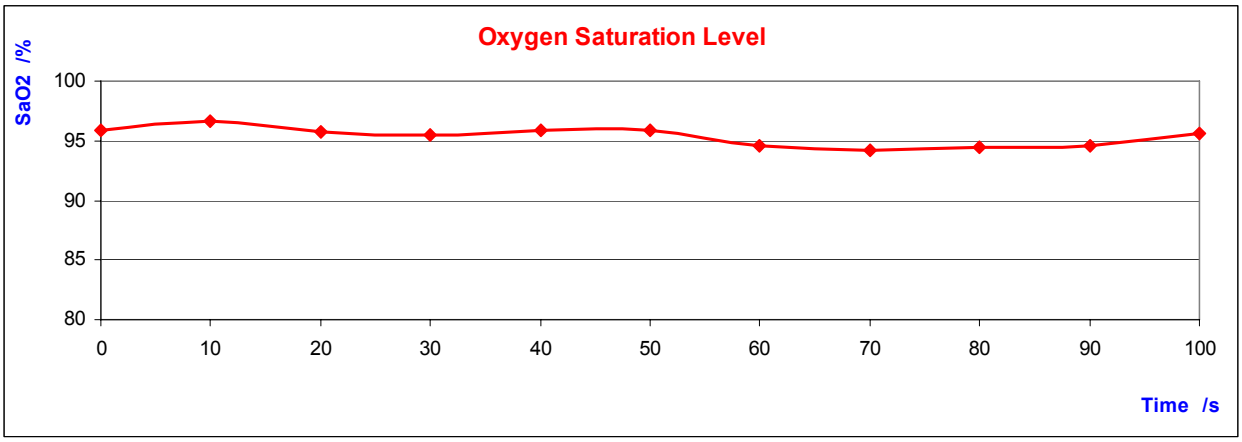

Figure 5.8 – Graphic showing the variation of the oxygen saturation level during normal breathing.

In these conditions, the blood is highly saturated (SaO_2 > 95%) and oximetry curves are perfectly shaped. During a forced breath-holding, the situation gets a little different as documented in *figs. 5.9* and *5.10*.

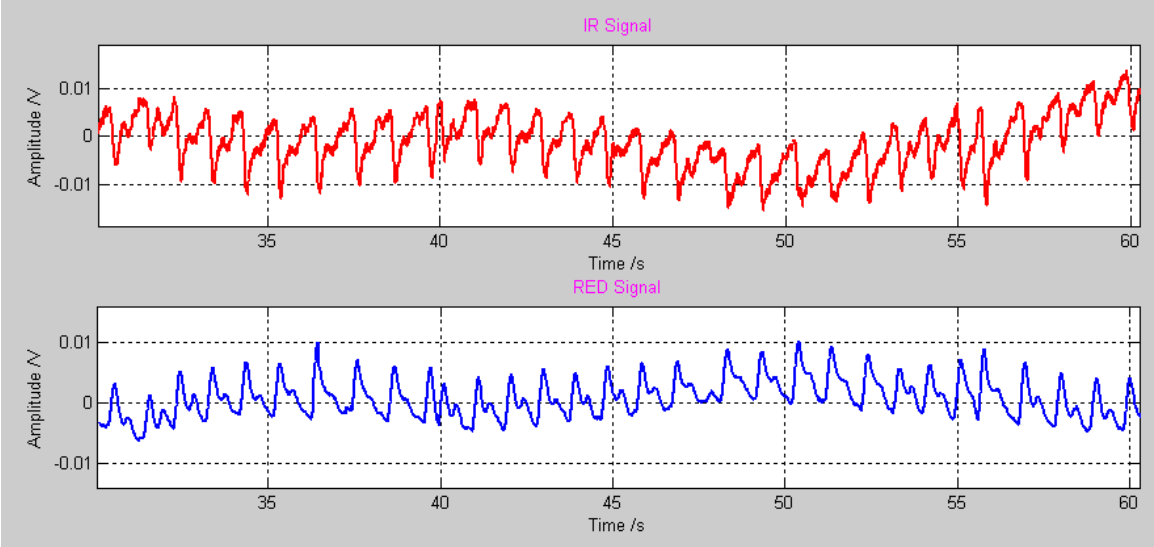

Figure 5.9 – Pulse oximetry curves obtained during forced breath-holding.

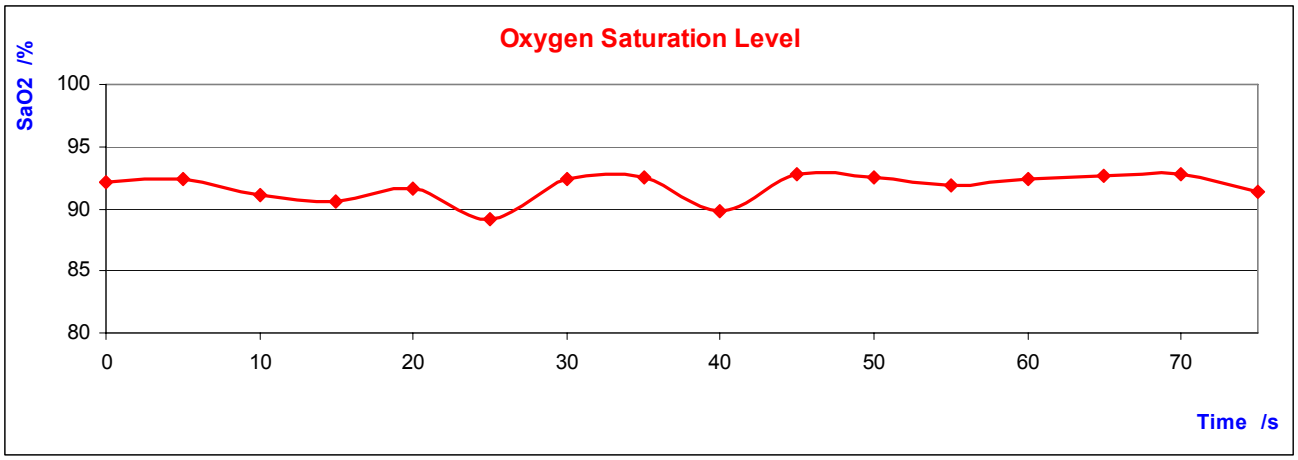

Figure 5.10 – Graphic showing the variation of the oxygen saturation level during normal forced breath-holding.

The oxygen saturation level dropped below 90% while pulse oximetry curves show an evident distortion in their usual contours. The reduction in the concentration levels of oxyhemoglobin results in a much higher absorbance of red light by the reduced hemoglobin causing the blood to get darker. An increase in red light absorbance means that less amounts of red light will reach the corresponding photodetector. A critical drop in the DC component of the red signal will increase the *R* value which, by its turn, lowers the SaO_2 percentage.

5.4. Bioimpedance Recordings.

In this section, it is presented the results obtained with the reography prototype. First of all, the impedance curve shown in *fig. 5.11* represents a recording using external resistors whose value ranges from 33 Ω to 1000 Ω. As explained before, the peaks result from replacing every resistor from the circuit so, the feedback loop of the current source stays open for a few instants; the valleys represent the value of the corresponding resistor.

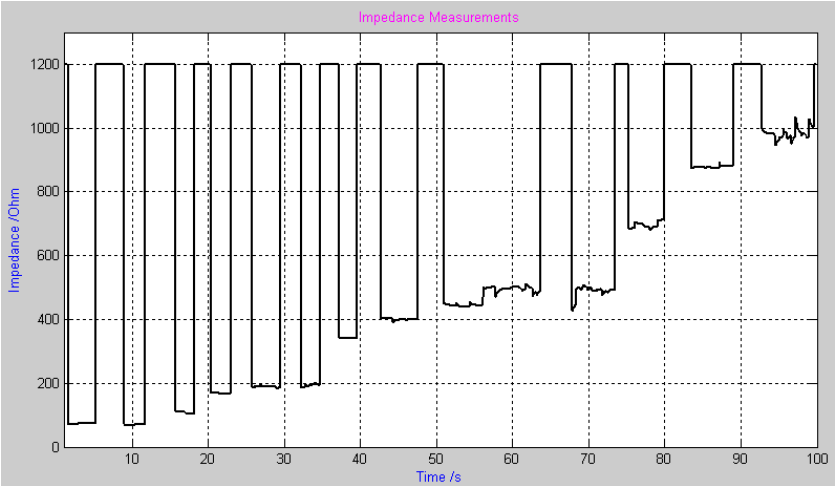

Figure 5.11 – Impedance measurements using external resistors in an up-going fashion way.

Figures 5.12 to 5.16 show the impedance curves obtained for the different NaCl solutions that vary in conductivity. Since the path length between the electrodes is 1 cm and the units for the conductivity are presented in μS cm^{-1}, the corresponding impedance value is straightforwardly identified by the inverse of the solution's conductivity.

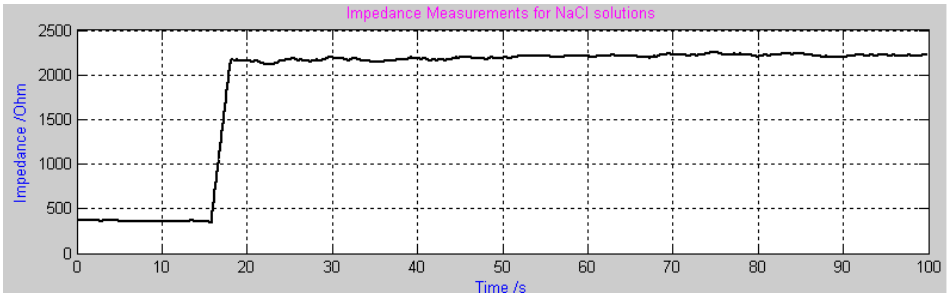

Figure 5.12 – Impedance measurements obtained when feedback loop of the current source is open.

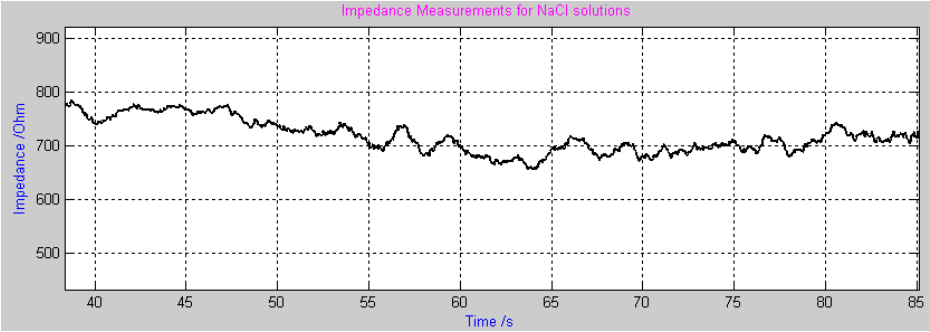

Figure 5.13 – Impedance measurements obtained for a NaCl solution with 1413 μS cm^{-1} of conductivity.

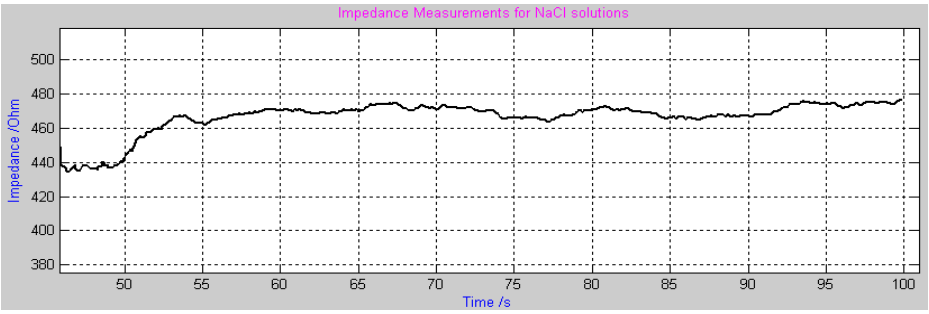

Figure 5.14 – Impedance measurements obtained for a NaCl solution with 2070 μS cm^{-1} of conductivity.

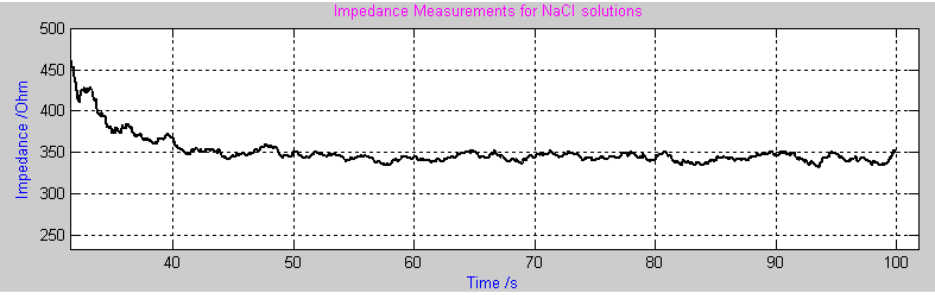

Figure 5.15 – Impedance measurements obtained for a NaCl solution with 2764 μS cm^{-1} of conductivity.

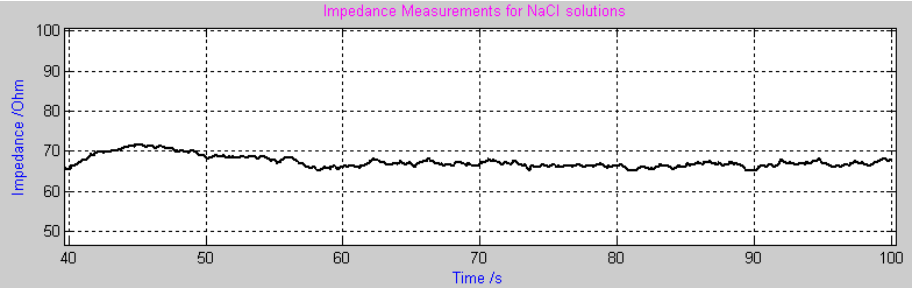

Figure 5.16 – Impedance measurements obtained for a NaCl solution with 12880 μS cm^{-1} of conductivity.

The curves shown so far are close enough to the impedance values that were expected to obtain by theory. These values were: 708 Ω for the NaCl solution whose conductivity is 1413 μS cm^{-1}, 483 Ω for the solution with conductivity 2070 μS cm^{-1}, 362 Ω for conductivity 2764 μS cm^{-1} and 78 Ω for conductivity 12880 μS cm^{-1}. The curves obtained show some variation around the central line but, more importantly, they are quite discernible and blood conductivity is in the middle range of them (6800 μS cm^{-1}).

The deviation from theory occurred only for solutions with conductivity 80 mS cm^{-1} and 447 μS cm^{-1}; values which establish the lower and upper limit for impedance measurements supported by the developed device. The respective impedance curves are shown in *figs. 5.17* and *5.18*.

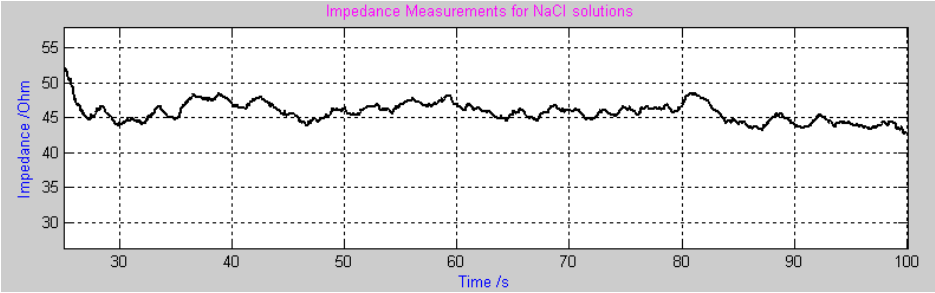

Figure 5.17 – Impedance measurements obtained for a NaCl solution with 80 mS cm^{-1} of conductivity.

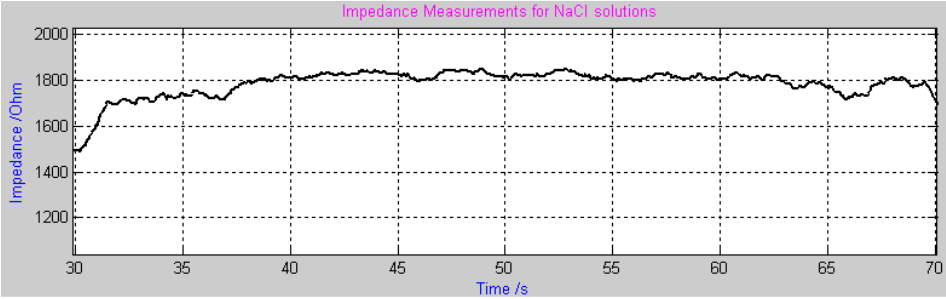

Figure 5.18 – Impedance measurements obtained for a NaCl solution with 447 μS cm^{-1} of conductivity.

Chapter 6

Conclusion

6.1. Discussion of the developed work.

With respect to the initial objectives, the developed work corresponded to their requirements. The electronic prototype on pulse oximetry recordings is completely finished as well as all the algorithms involved in their acquisition and processing stages at the remote node and in the central recording system. For ECG, the substitution of the RF transceivers by other ones with higher bandwidth even inside the ZigBee Protocol is crucial to cover the entire frequency spectrum of the signal, in particular the fast transitions seen in the QRS complex.

All the electronic components used in designing such prototypes were the available and easily-accessible ones found at the market in the moment of conception. Of course, as time passes, more similar components will be produced including those with superior performances.

By its turn and besides obtaining already some satisfactory results, the prototype developed for reography still needs more experimental tests to assess its performance at full operation in medical environment. The prototype has already proved that it can measure the impedance values of external resistors as well as NaCl solutions with different conductivities. However, due to the lack of information about intra-cardiac reographic curves that are expected to obtain during a cardiac cycle, it is difficult to establish an upper limit (if there is any) to the impedance value that can be recorded by a reographic device: in fact, the prototype is not able to accommodate all the voltage levels that can be developed across the impedance segment and if some of them exceeds the projected ranges, the amplifiers will certainly saturate, damaging the recordings. Another technical aspect to be taken in count is to replace the USB communication by RF transceivers with higher bandwidth for data exchange than those used in this project. Because of time constrictions, this solution was not possible to be answered and it will remain a topic for future work.

Finally, the wireless network was developed using a simple star topology and no further steps in exploring other topologies were made because one sink network node was well enough to respond all the requirements inside the limitations of the selected wireless development equipment.

.

6.2. Guidelines for future projects.

Every electronic project is subjected to continuous updating. The network protocol can remain the same while new remote notes can be progressively built and then fully integrated in the wireless system. So, the network can be increased in what concerns the number of member nodes and radio range if router nodes are available. Hospital healthcare units equipped with a system like this can record all the physiological variables of interest from the patient and send them with no physical connection to a central recording system or a PDA of a clinician. One area of particular interest is that one that is concerned in building home-monitoring equipments so the patient can rest and recover at home while his physiological parameters are been sensed. Then, a remote recording system would send them through the internet to hospitals or particular clinics.

Now referring to the particular sensor nodes developed in this project, biopotential recordings like ECG can be improved using a new acquisition paradigm based on the utilization of capacitive electrodes instead of the conventional ones. Within this approach, the body surface will act as a plate of a capacitor while the other one will be the terminal input of an instrumentation amplifier with high impedance. The dielectric created this way will eliminate the direct contact of the electronic device with the patient. Therefore, on every potential point in the human body surface, a sensor of this type can be placed with extensive capability to perform *in situ* both analog-to-digital conversion and wireless transmission processes.

For pulse oximetry, one of the aspects that can constitute a target for innovation is to use more than two photoemitters to cover the maximum extension of the absorption spectrum of hemoglobin as possible, with minimum changes to the excitation circuit already developed. With more information about light absorption and transmission at different wavelengths, the oxygen saturation level can be obtained more accurately. The replacement of the two LEDs by LASER technology would also constitute an innovation because instead of having light sources that irradiate light in all directions, the laser system would produce a direct beam of light, reducing the scattering effects that result from penetrating the finger. The pulse oximetry waveforms would show up with better shape in the recordings without the risk of occurring photoablation if the beam intensity is controlled. The utilization of this technology will inevitably lead to the redesign of the detection spring since light beam will only be captured if the laser and the detector are both in line of sight, situation that did not occur when using LEDs due to their cone of light irradiance and to the fact that photodetectors were able to respond to light beams even with some optical angular displacement.

Finally, the fundamental developments to perform over reography are the following ones: to build an intra-cardiac probe insensitive to external variations that measures the absolute volume of the cardiac cavities by performing impedance measurements; to establish an electromagnetic model of the walls of the cardiac cavities; and to eliminate the need for surgical catheterization by performing measurements using Magnetic Induction Tomography when the intra-cardiac impedance map is intended to be known.

Chapter 7

References

[1] **Semmlow, J. L., *Biosignal and Biomedical Image Processing. MATLAB – Based Applications*. Marcel Dekker Inc., New York, 2004.**

[2] **Zywietz, C., *A Brief History of Electrocardiography – Progress through Technology.* Biosignal Institute for Biosignal Processing and Systems Research, Hannover.**

[3] **Bell, C., *Understanding Contemporary Pulse Oximetry*. GE Healthcare – Clinical Paper, 2005.**

[4] **Kästle, S. *et al., A New Family of Sensors for Pulse Oximetry.* Hewlett-Packard Journal, Article 7, February 1997.**

[5] **Kyle, G. U. *et al., Bioelectrical Impedance Analysis – part I: review of principles and methods.* Elsevier, No. 23, pp. 1226 – 1243, 2004.**

[6] **Jindal, G. D. *et al., 25 Years of Impedance Plethysmography.* Barc Newsletter, No. 236, September 2003.**

[7] **Amado, L. O. D., *Reografia Intracardíaca. Fundamentos teóricos e experimentais e algumas das suas contribuições hemodinâmicas.* Dissertação de Doutoramento apresentada à Faculdade de Medicina de Lisboa, Lisboa, 1980.**

[8] **http://butler.cc.tut.fi/~malmivuo/bem/bembook/25/25.htm**

[9] **http://o.mneina.googlepages.com/microcontroller_architectur.gif**

[10] **Matic, N., *PIC microcontrollers. E - Books.* MiKroElektronika, 2003.**

[11] **http://w3.ualg.pt/~rmarcel/am.html**

[12] ***PIC24F Family Reference Manual.* Microchip Technology Inc., 2008.**

[13] ***16-bit Language Tools Libraries.* Microchip Technology Inc., 2008.**

[14] ***16-bit Language Tools Libraries – Getting Started.* Microchip Technology Inc., 2008.**

[15] ***MPLAB® Assembler, Linker and Utilities for PIC24 MCUs and dsPIC® DSCs User's Guide.* Microchip Technology Inc., 2008.**

[16] ***MPLAB® C Compiler for PIC24 MCUs and dsPIC® DSCs User's Guide.* Microchip Technology Inc., 2008.**

[17] ***MPLAB® C30 C Compiler User's Guide.* Microchip Technology Inc., 2008.**

[18] ***PIC24FJ64GA004 Family Data Sheet.* Microchip Technology Inc., 2008.**

[19] **www.doulos.com/knowhow/verilog_designers_guide/models/universal_asynchro nous_receiver_uart/uart.gif**

[20] ***IEEE Std 802.15.4 – 2006.* IEEE Computer Society, 2006.**

[21] ***ETRXn Wireless Mesh Networking Modules User's Guide.* Telegesis (UK) Limited, 2008.**

[22] ***STRX2DVKA & STR2DVKP – Telegesis Development Kit for ZigBee® Technology – Technical Manual.*** **Telegesis (UK) Limited, 2008.**

[23] www.meshnetics.com/netcat_files/11_148.png

[24] ***AN965 – Microchip Stack for the ZigBee™ Protocol*****. Microchip Technology Inc., 2007.**

[25] ***STRX2 ZigBee® Module – Product Manual.*** **Telegesis (UK) Limited, 2008.**

[26] ***STRX2USB USB Stick – Product Manual.*** **Telegesis (UK) Limited, 2008.**

[27] www.telegesis.com

[28] ***STRX2 Wireless Mesh Networking Modules – AT-Command Dictionary.*** **Telegesis (UK) Limited, 2008.**

[29] http://realterm.sourceforge.net

[30] Klein, M. D., Key-Brothers, I., Feldman, C. L., ***Can the Vectorcardiographically Derived EASI ECG be a Suitable Surrogate for the Standard ECG in Selected Circumstances.*** **IEEE Computers in Cardiology, Vol. 24, 1997.**

[31] Jahrsdoerfer, M., Giuliano, K., Stephens, D., ***Clinical Usefulness of the EASI 12-lead Continuous Electrocardiographic Monitoring System.*** **Critical Care Nurses, No. 25, pp. 28 – 37, October 2005.**

[32] Jennings, D. ***et al.*****,** ***Introduction to Medical Electronics Applictions*****. Edward Arnold, London, 1995.**

[33] ***INA116 Datasheet: Ultra Low Input Bias Current INSTRUMENTATION AMPLIFIER*****. Burr Brown, 2008.**

[34] ***INA111 Datasheet: High Speed FET-Input INSTRUMENTATION AMPLIFIER*****. Burr Brown, 2008.**

[35] ***AD974 Datasheet: 4-Channel, 16-Bit, 200 kSPS Data Acquisition System.*** **Analog Devices, 2008.**

[36] ***ADuM1400/ADuM1401/ADuM1402 Datasheet: Quad-Channel Digital Isolators*****. Analog Devices, 2008.**

[37] ***AN170 – NE555 and NE556 Application Note.*** **Philips Semiconductors, 1988.**

[38] Kamat, V., ***Pulse Oximetry.*** **Indian Journal of Anaesthesia, No. 46, pp. 261 – 268, 2002.**

[39] Zonios, G., Shankar, U., Iyer, V. K., ***Pulse Oximetry Theory and Calibration for Low Saturation.*** **IEEE Transaction on Biomedical Engineering, Vol. 51, No. 5, May 2004.**

[40] ***L-934SRC-G Datasheet: Super Bright Red.*** **Kingbright, 2006.**

[41] ***SFH 4209 Datasheet: High Power Infrared Emitter*****. OSRAM Opto Semiconductors, 2005.**

[42] ***TSL257 Datasheet: High Sensitivity Light-To-Voltage Converter.*** **TAOS, 2006.**

[43] ***TSL260R/TSL261R/TSL262R Datasheet: Infrared Light-to-Voltage Optical Sensors.*** **TAOS, 2006.**

[44] Grimnes, S., Martinsen, O. G., ***Bioimpedance & Bioelectricity – Basics.*** **Academic Press, London, 2000.**

[45] **Babu, J. P.** ***et al., Impedance Plethysmography: Basic Principles.*** **Journal of Postgraduate Medicine, No. 36, pp. 57 – 63, 1990.**

[46] ***AD5541/AD5542 Datasheet: 5 V, Serial-Input Voltage-Output, 16-Bit DACs.*** **Analog Devices, 2008.**

[47] ***ADR430/ADR431/ADR433/ADR434/ADR435/ADR439 Datasheet: Ultralow Noise XFET Voltage References with Current Sink and Source Capability.*** **Analog Devices, 2008.**

[48] ***OPA2604 Datasheet: Dual FET Input, Low Distortion OPERATIONAL AMPLIFIER. Burr Brown, 2008.***

[49] ***AD9782 Datasheet: 18-Bit, 1 MSPS PulSAR 7.0 mW ADC in MSOP/QFN.*** **Analog Devices, 2008.**

[50] ***AD8139 Datasheet: Low Noise Rail-to-Rail Differential ADC Driver.*** **Analog Devices, 2008.**

Chapter 8

Appendix

8.1. Schematic of the EASI-ECG Lead System Prototype.

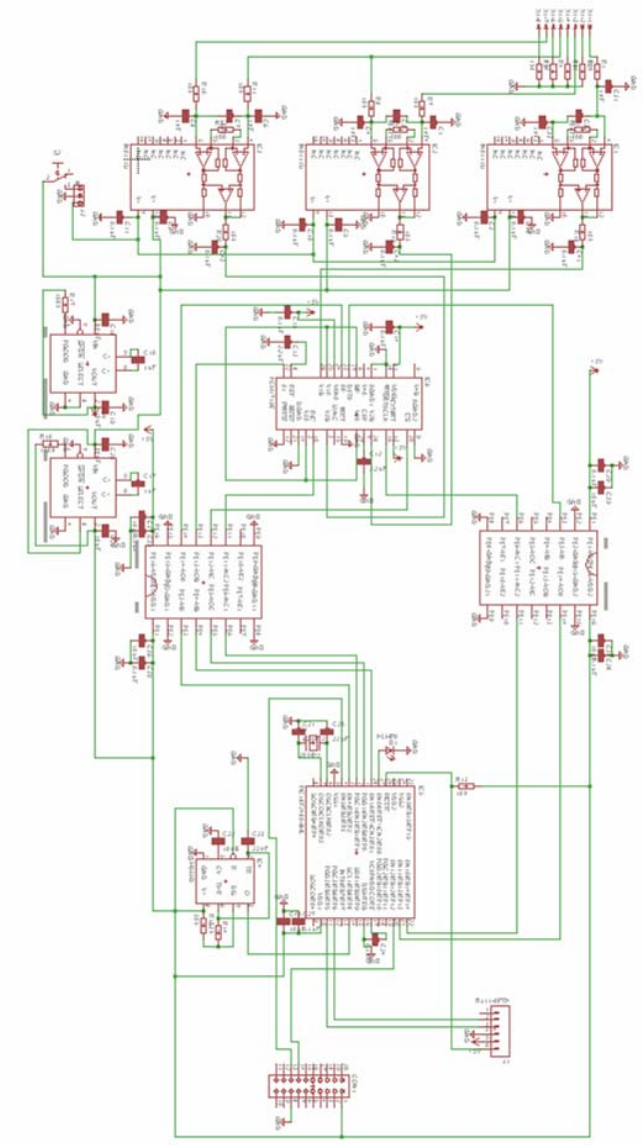

8.2. PCB Layout for the EASI-ECG Lead System Prototype.

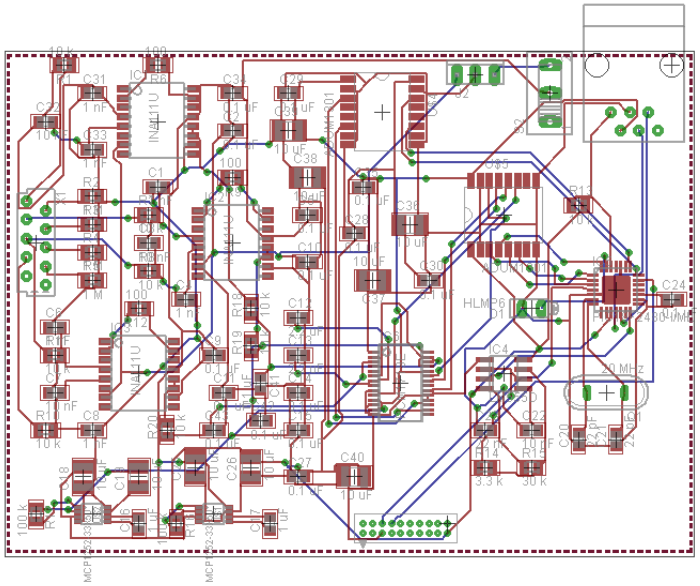

Dimensions: 9,5 cm x 7 cm

8.3. Schematic of the Pulse Oximetry Prototype.

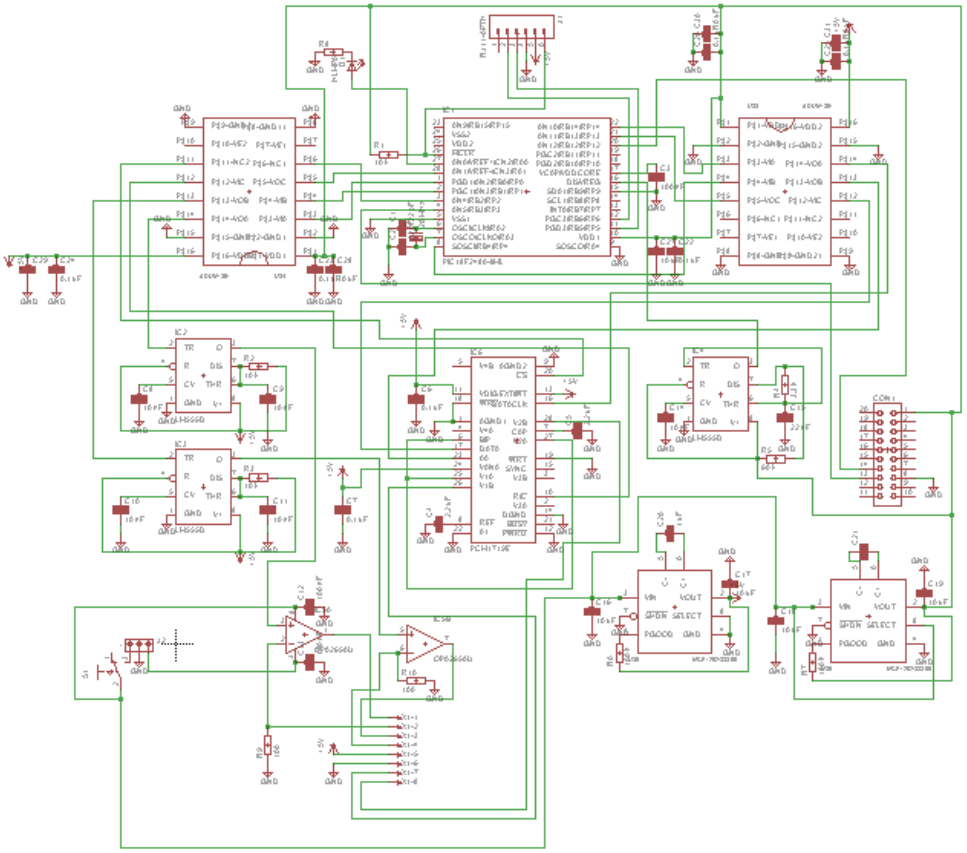

8.4. PCB Layout for the Pulse Oximetry Prototype.

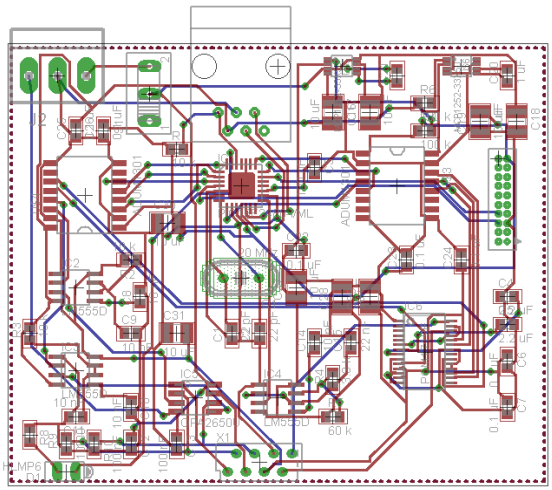

Dimensions: 9,2 cm x 7,5 cm

8.5. Schematic of the 20 kHz Sine-Wave Generator Prototype.

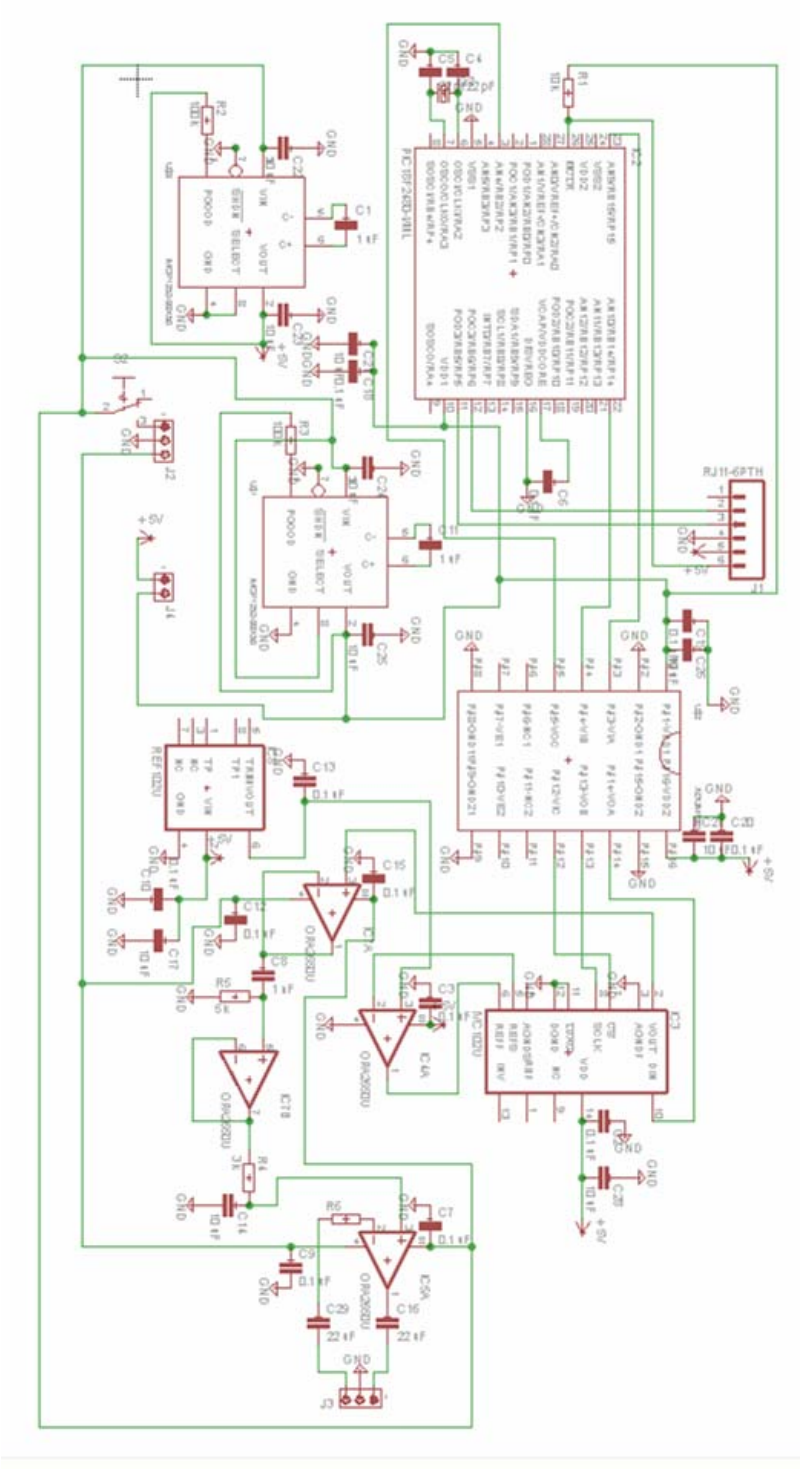

8.6. PCB Layout for the 20 kHz Sine-Wave Generator Prototype.

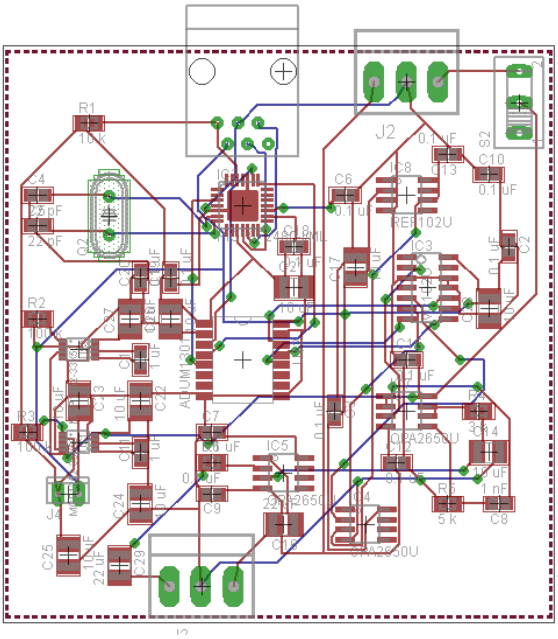

Dimensions: 7,2 cm x 7 cm

8.7. Schematic of the Acquisition Prototype for Reography.

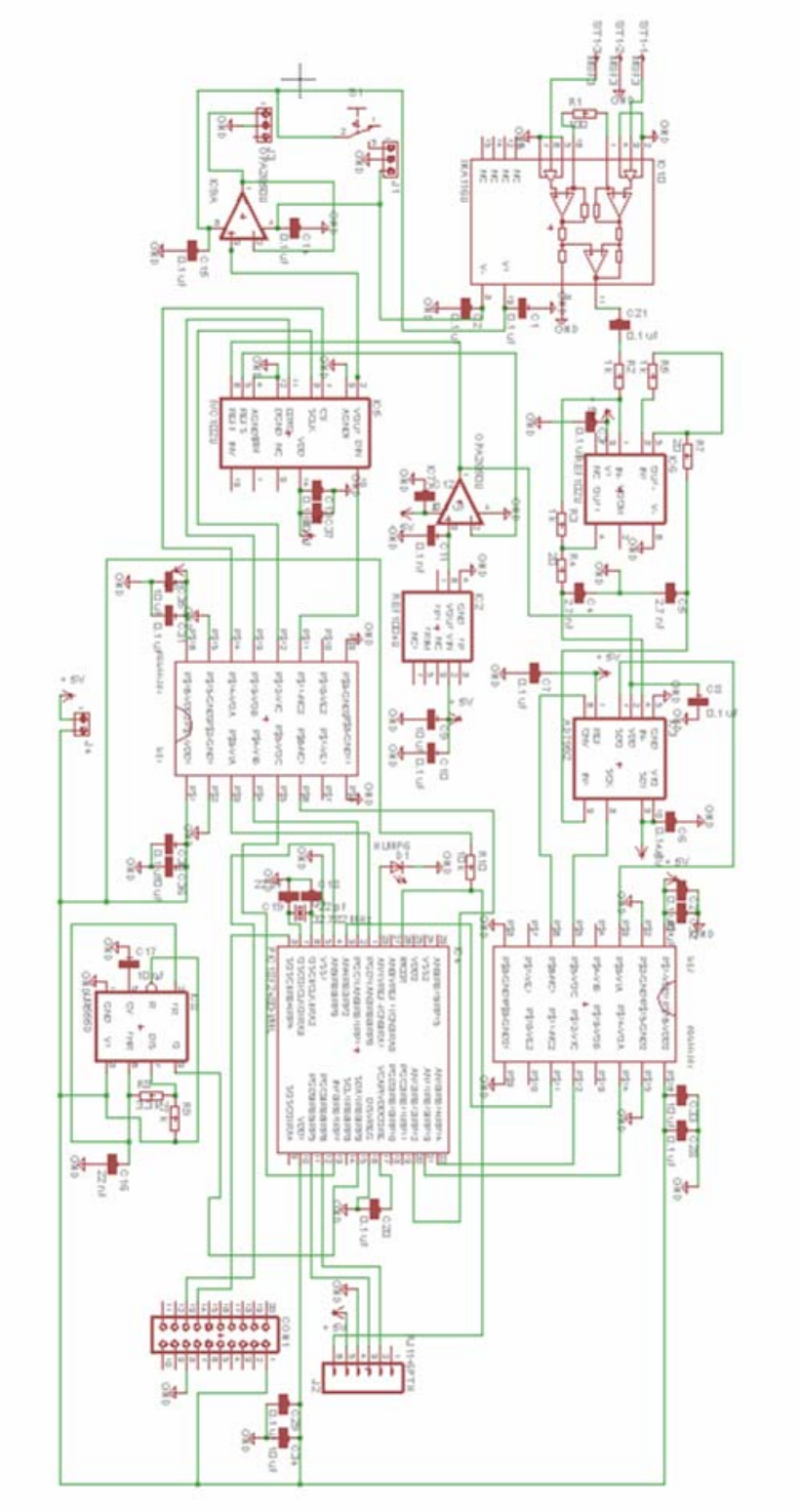

8.8. PCB Layout of the Acquisition Prototype for Reography.

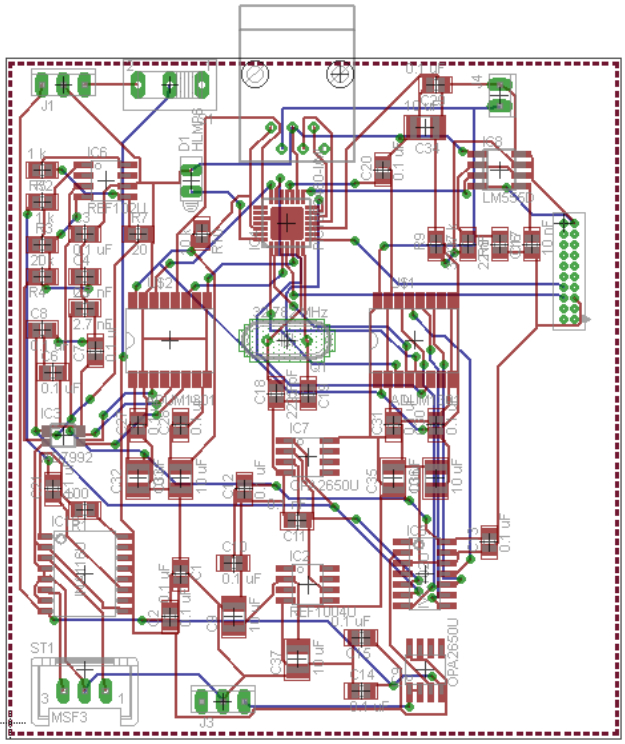

Dimensions: 7,5 cm x 7 cm